SANDIA REPORT

SAND2005-4657
Unlimited Release
Printed August 2005

Dipole Radiation From a Cylindrical Hole in the Earth

Lorena I. Basilio, Larry K. Warne, and William A. Johnson

Prepared by
Sandia National Laboratories
Albuquerque, New Mexico 87185 and Livermore, California 94550

Sandia is a multiprogram laboratory operated by Sandia Corporation,
a Lockheed Martin Company, for the United States Department of Energy's
National Nuclear Security Administration under Contract DE-AC04-94AL85000.

Issued by Sandia National Laboratories, operated for the United States Department of Energy by Sandia Corporation.

Available to DOE and DOE contractors from
U.S. Department of Energy
Office of Scientific and Technical Information
P.O. Box 62
Oak Ridge, TN 37831

Telephone: (865)576-8401
Facsimile: (865)576-5728
E-Mail: reports@adonis.osti.gov
Online ordering: http://www.osti.gov/bridge

Available to the public from
U.S. Department of Commerce
National Technical Information Service
5285 Port Royal Rd
Springfield, VA 22161

Telephone: (800)553-6847
Facsimile: (703)605-6900
E-Mail: orders@ntis.fedworld.gov
Online order: http://www.ntis.gov/help/ordermethods.asp?loc=7-4-0#online

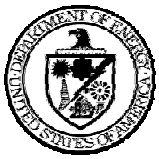

SAND2005-4657
Unlimited Release
Printed August 2005

Dipole Radiation from a Cylindrical Hole in the Earth

L.I. Basilio, L.K. Warne, W.A. Johnson

Electromagnetics and Plasma Physics Analysis Dept.

Sandia National Laboratories
P. O. Box 5800
Albuquerque, NM 87185-1152

Abstract

This report examines the problem of an antenna radiating from a cylindrical hole in the earth and the subsequent far-zone field produced in the upper air half space. The approach used for this analysis was to first examine propagation characteristics along the hole for surrounding geologic material properties. Three cases of sand with various levels of moisture content were considered as the surrounding material to the hole. For the hole diameters and sand cases examined, the radiation through the earth medium was found to be the dominant contribution to the radiation transmitted through to the upper half-space. In the analysis presented, the radiation from a vertical and a horizontal dipole source within the hole is used to determine a closed-form expression for the radiation in the earth medium which represents a modified element factor for the source and hole combination. As the final step, the well-known results for a dipole below a half space, in conjunction with the use of Snell's law to transform the modified element factor to the upper half space, determine closed-form expressions for the far-zone radiated fields in the air region above the earth.

Intentionally Left Blank

Contents

Figures

Intentionally Left Blank

1 EXECUTIVE SUMMARY

In this report we examine the radiation characteristics of a dipole antenna when oriented either vertically or horizontally within a hole in the earth. The problem geometry is shown below.

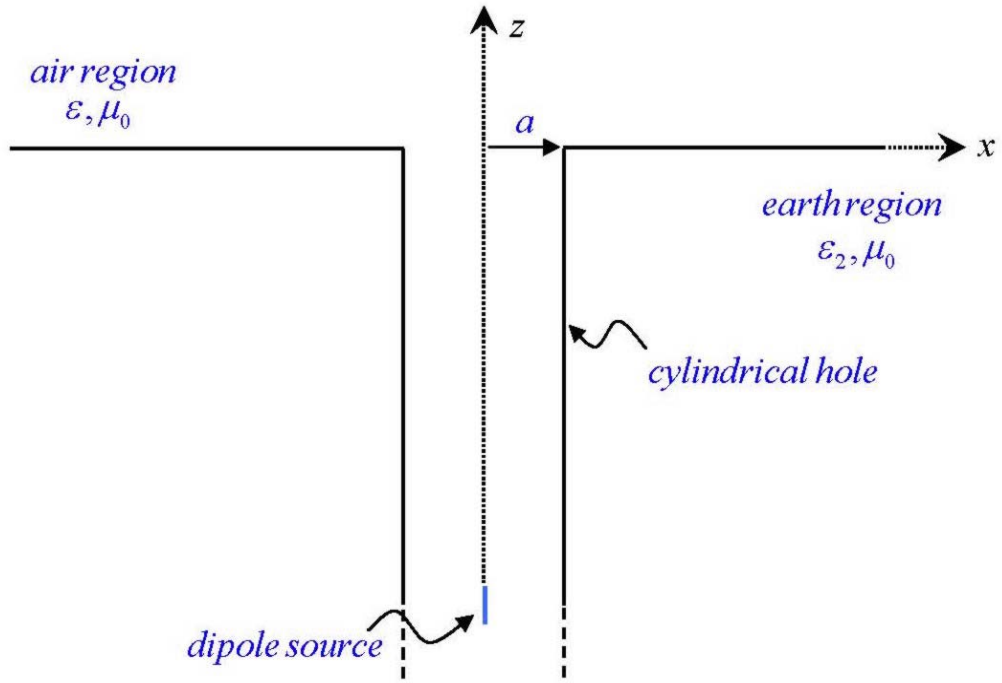

Problem geometry (shown for a vertical dipole).

In order to first understand the waveguiding characteristics of the hole, the radial (k_ρ) and axial (k_z) propagation constants are determined using a boundary-condition analysis of the hole. The modal equation governing the propagation constants is established by enforcing the continuity of the tangential components of the electric and magnetic field at the hole radius $\rho = a$.

1.1 Vertical Dipole

In the case of the vertically-polarized dipole, the modal equation is given by

$$\varepsilon k_{2\rho} J_1(k_\rho a) H_0^{(2)}(k_{2\rho} a) = \varepsilon_2 k_\rho J_0(k_\rho a) H_1^{(2)}(k_{2\rho} a)$$

Here the parameters $\varepsilon, \varepsilon_2, a, k_{2\rho}$ correspond to the permittivity of the material within the hole (in this report, ε is assumed to be the free-space permittivity, $\varepsilon_0 = 8.8542\ pF/m$), the permittivity of the earth, the hole radius, and the radial propagation constant in the earth medium. It is important to note that in the boundary-condition analysis the hole is assumed to be infinite (i.e. for the purposes of determining the propagation constants, the air-earth interface can be ignored) and therefore $k_{2\rho} = \sqrt{k_2^2 - k_{2z}^2} = \sqrt{k_2^2 - k_z^2}$, where k_2 is the wavenumber in the earth material.

One manner in which the solutions to this transcendental equation are found is by using a complex

zero-finding routine based on the complex argument principle [2]. The complex nature of the propagation constants is associated with the phase variation and attenuation in either the radial (for k_ρ) or axial direction (for k_z). Here it was necessary to carefully define the branches of the square root terms and Bessel functions and to avoid these branch cuts in the selected zero-finding regions (*Appendix A*). With knowledge of the branch cut locations, it was possible to ensure that zeros on the improper Riemann sheet were being rejected or, equivalently, that only solutions corresponding to outward propagating waves with decay were being selected.

For the purposes of characterizing the propagation within the hole, dry sand and sand of 2.18%, 3.88%, and 16.8% moisture were considered as the surrounding material to the hole. Examining a hole radius of 0.04 m at a frequency of 300 MHz, the imaginary parts of the axial propagation constants were found to be very large compared to the imaginary part of the k_2 branch point. Thus, instead of propagation along the hole direction, the energy is being transmitted into the surrounding material to the hole. For 3.0 GHz and the same hole size, it is observed that the loss due to the cutoff frequency is smaller relative to the loss values at the lower frequency, but the loss is still large compared to the direct propagation in k_2. In considering 300 MHz and a hole of radius 0.1 m, there is little change in k_z as the moisture content increases, except in the 16.8% moisture case where the imaginary part goes from approximately $-10.66k$ to $-3.68k$ (k is the free-space wavenumber). Despite this decrease however, the energy in all cases is still significantly attenuated within the hole. At 3.0 GHz, we find an overall decrease in the imaginary part of k_z ($\mathrm{Im}\,(k_z)$) for all four sand cases, but particularly for the 16.8% moisture case where the $\mathrm{Im}\,(k_z)$ becomes less than the imaginary part of the k_2 wavenumber. Thus, in increasing the radius electrically (ka has increased), k_z is approaching k and the TM_{01} (the first mode of propagation) is near its cutoff frequency. It is important to note however that, even in this case, the attenuation is still significant where for a distance of 10 m, the energy is decreased by approximately 200 dB ($\mathrm{Im}\,(k_z) \approx -0.038k$). (Plots of the k_z solutions for each of these cases are given in Figs. 3-6.)

For the purposes of design, it is also useful to reduce the transcendental expression governing the propagation constant into an equation that can be easily used to determine the approximate wavenumbers for a particular hole size, frequency, and surrounding medium characteristics. With a transverse-resonance method [3], a transcendental equation that is normalized with respect to impedance is used to develop a relatively simple closed-form expression for the propagation constants in some limiting cases.

Supposing that k_2 is large and that $k_z = O(k)$, the input impedance seen looking into the outer medium to the hole in the radial direction then becomes

$$Z_{in}^{\rho} = \frac{k_{2\rho}}{\omega\varepsilon_2} \approx \frac{k_2}{\omega\varepsilon_2} = \eta_2$$

$\left(\eta_2 = \sqrt{\mu_0/\varepsilon_2}\right)$ while looking into the interior of the hole we have

$$Z_{in}^{-\rho} = \left.\frac{E_z}{H_\varphi}\right|_{\rho=a-0} \approx -j\frac{k_\rho}{\omega\varepsilon}\frac{J_0(k_\rho a)}{J_1(k_\rho a)}$$

(The derivation of the field quantities E_z and H_φ can be found in the body of the report.) In the limit of large radius, we can asymptotically evaluate the Bessel functions to obtain

$$Z_{in}^{-\rho} \approx -j\frac{k_\rho}{\omega\varepsilon}\cot\left(k_\rho a - \frac{\pi}{4}\right)$$

At the resonant frequency and just to the interior of the $\rho = a$ boundary, we know

$$Z_{in}^{\rho} + Z_{in}^{-\rho} = 0$$

so that

$$\frac{\eta_2}{\eta} = j\frac{1}{\omega\varepsilon\eta a}\left[k_\rho a\cot\left(k_\rho a - \frac{\pi}{4}\right)\right]$$

where we have normalized the equation by $\eta = \sqrt{\mu_0/\varepsilon}$. Setting up a bilinear solution to fit the perfect-electric conducting (PEC) and perfect-magnetic conducting (PMC) boundary limits, we obtain

$$k_\rho^{app} a \approx \frac{p\pi}{4} + \frac{j\alpha}{\frac{p\pi}{4} + j\alpha\frac{2}{\pi}} = \frac{p\pi}{4} + \frac{jka\left(\eta_2/\eta\right)}{\frac{p\pi}{4} + jka\left(\eta_2/\eta\right)\frac{2}{\pi}}$$

where $p = 3, 7, 11, ...4q - 1$.

Below we show a plot of the approximate $k_\rho a$ expression, for the modes corresponding to $p = 3$ and $p = 7$, as the values of $\alpha = ka\left(\eta_2/\eta\right)$ are varied from zero to infinity. It should be noted that, although the $k_\rho a$ curves have been calculated assuming real values of η_2/η, there was found to be virtually no change in the curves when complex impedances were considered (loss tangents on the order of 0.1 were assumed). Also shown are the values of $k_\rho a$ found using the complex root-finding routine [2] and the exact transcendental equation (as opposed to the asymptotic transverse resonance equation) in the sand cases of 16.8%, 3.88%, and 2.18% moisture content [1]. For a frequency of 3 GHz and a hole radius of 0.1 m, the corresponding values of α go from 1.4, 3.0, to 4.0 as the moisture content decreases (free-space has been assumed for the inner hole medium). In order to create a high α sample point to be used with the root-finding code, the 2.18% moisture sand was considered at 3 GHz with a 0.25 m hole (this yields an $\alpha = 9.0$). Thus, we observe good agreement between the approximate values and those produced by the root-finding routine, with the approximate $k_\rho a$ curves slightly underestimating the code values near the peaks. Since the setting of $k_{2\rho}$ to k_2 and the approximation of the Bessel functions was found to lead to negligible errors, it is important to note that the errors here can be attributed to the bilinear approximation of the transcendental equation.

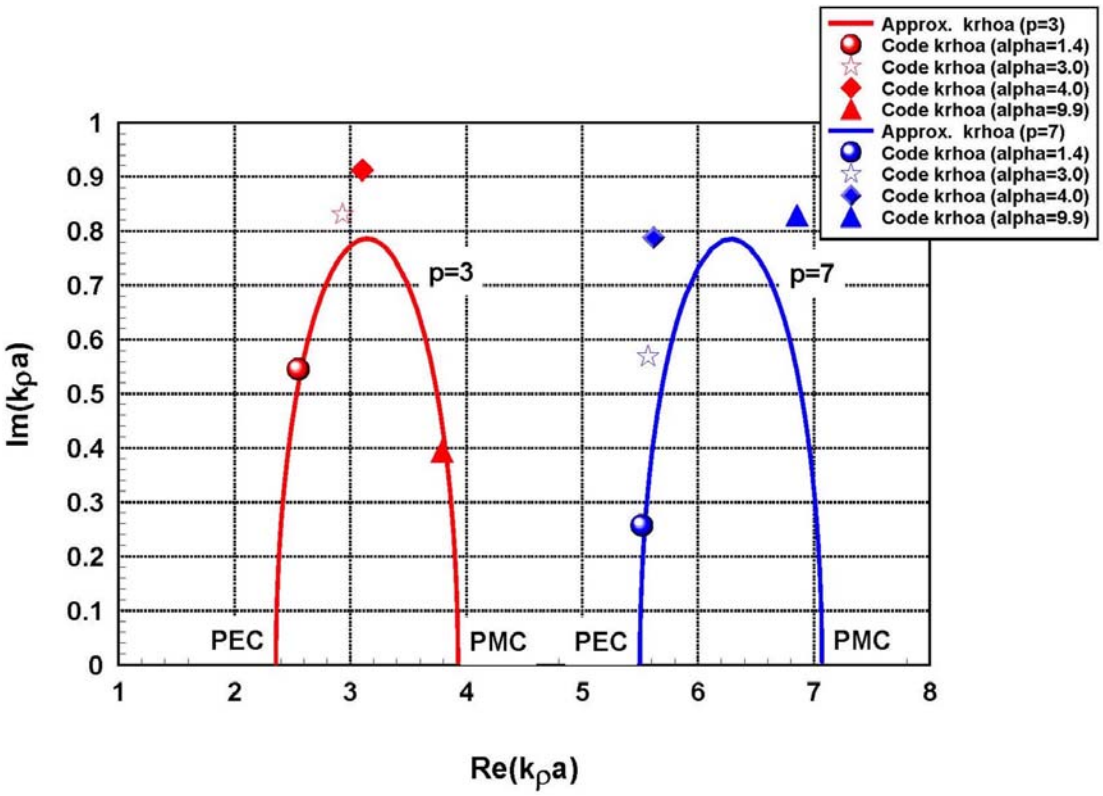

Approximate complex $k_\rho a$ values as the $\alpha = ka\eta_2/\eta$ is varied from the PEC limit to the PMC limit .

Using the approximate expression for $k_\rho a$, we can next determine an approximate expression for $k_z a$. From the separation equation, we can write

$$k_z a = \sqrt{k^2 a^2 - k_\rho^2 a^2}$$

so that substituting in, we obtain

$$k_z^{app} a = \sqrt{k^2 a^2 - \left[\frac{p\pi}{4} + \frac{jka\,(\eta_2/\eta)}{\frac{p\pi}{4} + jka\,(\eta_2/\eta)\,\frac{2}{\pi}}\right]^2}$$

Below the approximate values for k_z^{app} are compared to the values of k_z that are based on the exact transcendental equation (as opposed to the asymptotic transverse resonance equation) and the complex-root finding code [2]. A hole radius of $a = 0.1\ m$ and a frequency of 3.0 GHz are assumed for these calculations and the same three cases of varying moisture content are examined as above.

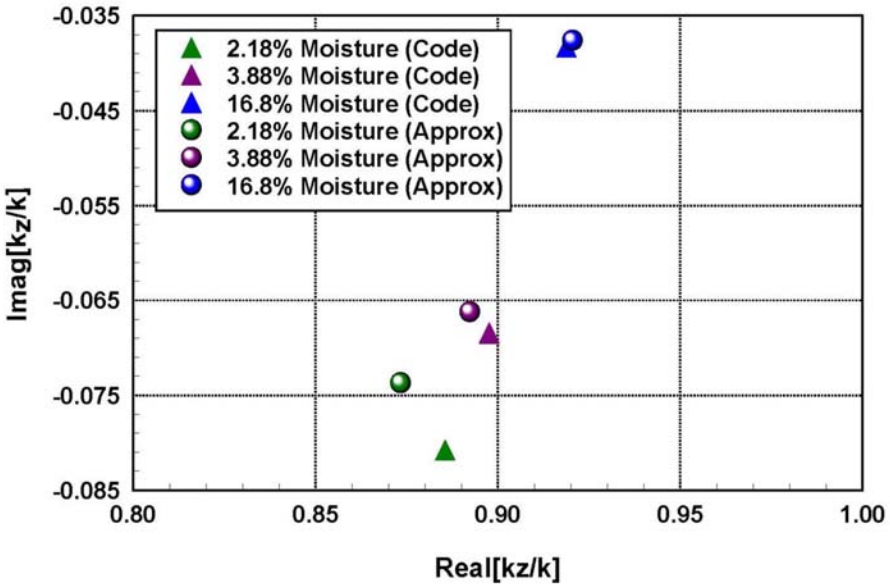

Comparing axial wavenumbers in the case of a 0.1 m radius hole and a frequency of 3.0 GHz.

Thus, for all three cases of sand considered we observe good agreement between the exact and approximate values of k_z. The approximate solution improves as the moisture content of the sand increases, with the differences in the real and imaginary parts of k_z reducing to -0.19% and 1.77% respectively at a moisture level of 16.8%. It should be noted, however, that even in the 2.18% moisture case, the approximate expression is still fairly useful in obtaining an idea of the k_z root location. In this case, the percent differences between the real and imaginary part of the approximate and exact solution are 1.38% and 8.82%, respectively.

As a means of ultimately determining the radiation due to the dipole in the upper-half space, a boundary-condition analysis for the air-earth interface followed by a saddle-point evaluation of the potential integral representations was first used to determine the field quantities in the lower-half space region. With the details presented in the body of the report, the far-zone magnetic field associated with the vertical dipole is given by

$$H_{\varphi}^{lower} \sim -\frac{j2}{\pi}\frac{k_\rho \varepsilon_2}{k_{2\rho}^s a}\left[\frac{1}{\varepsilon k_{2\rho} J_1\left(k_\rho a\right) H_0^{(2)}\left(k_{2\rho}^s a\right) - \varepsilon_2 k_\rho J_0\left(k_\rho a\right) H_1^{(2)}\left(k_{2\rho}^s a\right)}\right]\left[\frac{jk_2}{4\pi r}\left(I_0 \ell\right) e^{-jk_2 r}\sin\theta_2\right]$$

where

$$k_z^s = k_2\cos\theta_2 = k_2\frac{z}{r}$$

$$k_{2\rho}^s = k_2\sin\theta_2 = k_2\frac{\rho}{r}$$

and

$$k_\rho = \sqrt{k^2 - \left(k_z^s\right)^2}$$

Thus, the lower-half space radiation can be identified as the product of the element pattern associated with a vertical dipole in a homogeneous k_2 medium and a saddle-point coefficient accounting for the effects

of the hole on the overall radiation. In the limits of an electrically small hole, we recognize that the saddle point coefficient

$$C_v^{'}\left(k_z^s, k_{2\rho}^s\right) = \frac{-j2}{\pi}\frac{k_\rho \varepsilon_2}{k_{2\rho}^s a}\left[\frac{1}{\varepsilon k_{2\rho} J_1\left(k_\rho a\right) H_0^{(2)}\left(k_{2\rho}^s a\right) - \varepsilon_2 k_\rho J_0\left(k_\rho a\right) H_1^{(2)}\left(k_{2\rho}^s a\right)}\right]$$

goes to one.

In order to relate the field in the lower-half space to the upper-half field, we assume that the antenna source is located far away from the air-earth interface so that a multipole representation can be used to model the effects of the hole. In this case, it is shown rigorously that the overall radiation pattern in the air region is a product of the lower-half space radiation and a term associated with ray transmission through the interface. In other words, the upper-half space H_φ radiation can be written as

$$H_\varphi^{upper} \sim H_\varphi^{lower}\left[\frac{2ke^{-jh\sqrt{k_2^2 - k^2\sin^2\theta}}\varepsilon_0\cos\theta}{\varepsilon_2 k\cos\theta + \varepsilon_0\sqrt{k_2^2 - k^2\sin^2\theta}}\right]$$

or

$$H_\varphi \sim C_v^{'}\left(k_z^s, k_{2\rho}^s\right)\left[\frac{jk\left(I_0\ell\right)}{4\pi r}e^{-jkr}\sin\theta\right]\left[\frac{2ke^{-jh\sqrt{k_2^2 - k^2\sin^2\theta}}\varepsilon_0\cos\theta}{\varepsilon_2 k\cos\theta + \varepsilon_0\sqrt{k_2^2 - k^2\sin^2\theta}}\right]$$

where by Snell's Law

$$k_2\sin\theta_2 = k\sin\theta$$

It should be noted that, in the limit of a small hole ($ka \to 0$), this expression (derived using asymptotic representation of the potentials in the upper-half space region) agrees with that given in [6]. The normalized pattern given by

$$H_\varphi^{norm} = \frac{4\pi r}{\left(I_o\ell\right)e^{-jkr}}H_\varphi$$

at 300 MHz and 3.0 GHz is shown below, in the case that sand with a 2.18% moisture content is the surrounding material to the hole.

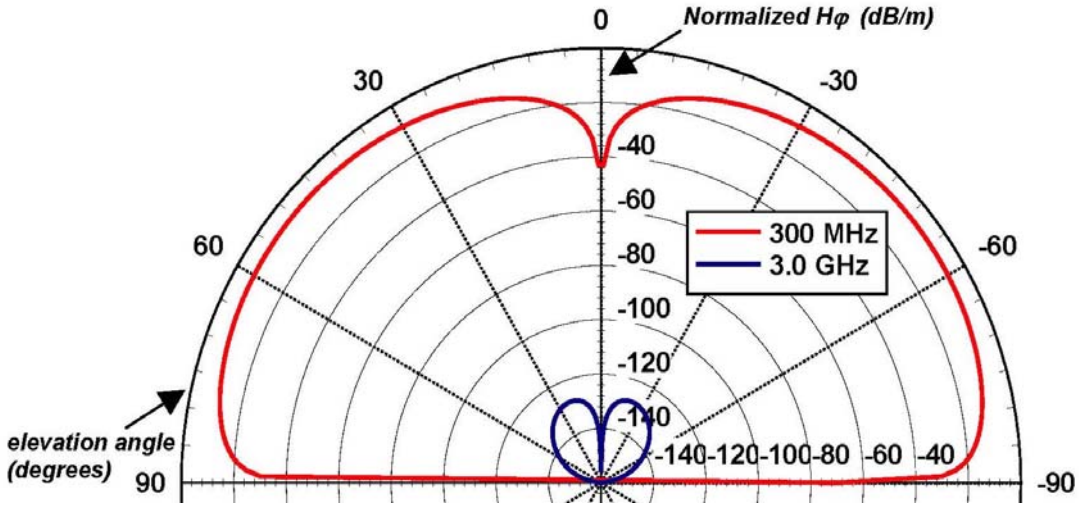

Far-field H_φ in the upper-half space for the sand case of 2.18% moisture ($h = 10\ m, a = 0.04\ m$).

From these patterns it is clear that the energy transmitted into the air region is decreased with an increase in frequency or conductive loss associated with the earth. In addition to these results, the radiation patterns associated with the dry sand, 3.88 %, and 16.8 % moisture cases are provided in the body of the report.

1.2 Horizontal Dipole

A similar procedure to that used for handling the vertical dipole is used to examine the radiation characteristics of a horizontally-oriented dipole (the dipole is assumed to lie along the $x-$direction) However, since this polarization leads to a coupled set of $E-$ and $H-$modes, the details of the analysis are much more complicated than the previous case. For this reason, only the upper-half space radiation results are presented in this section, with the details contained in the body of report.

As in the case of the vertical dipole, the radiation pattern in the lower-half space is found to be a product of the radiation pattern characterizing a horizontal dipole in a homogeneous k_2 medium and a saddle-point coefficient that is dependent on the elevation angle in the lower-half space region (θ_2). Since the pattern behavior captured by the saddle-point coefficient can be represented using a multipole representation (under the restriction that the source is concentrated at a depth h and does not interact with the interface) then it is rigorously shown that this same radiation pattern is translated up into upper-half space. Thus, the total patterns in the air region are given by the lower-half-space patterns, modulated by a term associated with the transmission of the fields from the earth region into the upper-half space. Thus, accounting for the effects of the hole and transmission through the interface, we have in the upper-half space

$$E_\varphi^{upper} \sim E_\varphi^{lower} \left[\frac{2ke^{-jh\sqrt{k_2^2 - k^2 \sin^2\theta}}}{k\cos\theta + \sqrt{k_2^2 - k^2\sin^2\theta}} \cos\theta \right]$$

or

$$E_{\varphi}^{upper} \sim C_{h,e}^{'}\left(k_z^s\right)\left[\frac{j\omega\mu_0 I_0\ell}{4\pi r}e^{-jkr}\sin\varphi\right]\left[\frac{2ke^{-jh\sqrt{k_2^2-k^2\sin^2\theta}}}{k\cos\theta+\sqrt{k_2^2-k^2\sin^2\theta}}\cos\theta\right]$$

and

$$H_{\varphi}^{upper} \sim H_{\varphi}^{lower}\left[\frac{2k^2e^{-jh\sqrt{k_2^2-k^2\sin^2\theta}}\cos\theta}{k\sqrt{k_2^2-k^2\sin^2\theta}+k_2^2\cos\theta}\right]$$

$$H_{\varphi}^{upper} \sim C_{h,h}^{'}\left(k_z^s\right)\left[-\frac{j\left(I_0\ell\right)k_2}{4\pi r}e^{-jkr}\cos\theta_2\cos\varphi\right]\left[\frac{2k^2e^{-jh\sqrt{k_2^2-k^2\sin^2\theta}}\cos\theta}{k\sqrt{k_2^2-k^2\sin^2\theta}+k_2^2\cos\theta}\right]$$

Due to the tedious nature of the saddle-point coefficients $C_{h,e}^{'}\left(k_z^s\right)$ and $C_{h,h}^{'}\left(k_z^s\right)$, they are suppressed here but can be found from the asymptotic analysis in the lower-half space region presented in a subsequent section of the report. With these two independent polarizations, the remaining far-field quantities can be determined using

$$\frac{E_{\varphi}}{H_{\theta}} = -\eta$$

and

$$\frac{E_{\theta}}{H_{\varphi}} = \eta$$

where $\eta = \sqrt{\mu_0/\varepsilon}$. Below are plots of the radiation patterns corresponding to the situation when the horizontal dipole is positioned within a hole surrounded by sand with a 2.18% moisture content. For these results, the normalizations

$$E_{\varphi}^{norm} = \frac{4\pi r}{\left(I_o\ell\right)e^{-jkr}}E_{\varphi}$$

and

$$H_{\varphi}^{norm} = \frac{4\pi r}{\left(I_o\ell\right)e^{-jkr}}\eta H_{\varphi}$$

were used. In the body of the report, radiation patterns associated with the dry sand, 3.88 %, and 16.8 % moisture cases are also included.

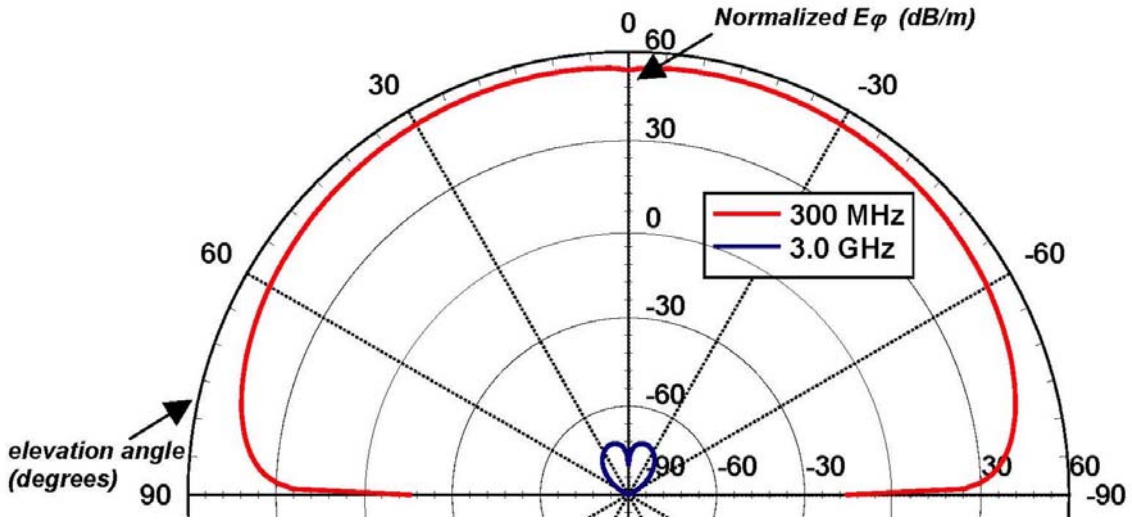

Far-zone E_φ patterns in the upper-half space for the sand case of 2.18% moisture ($h = 10\ m,\ a = 0.04\ m$).

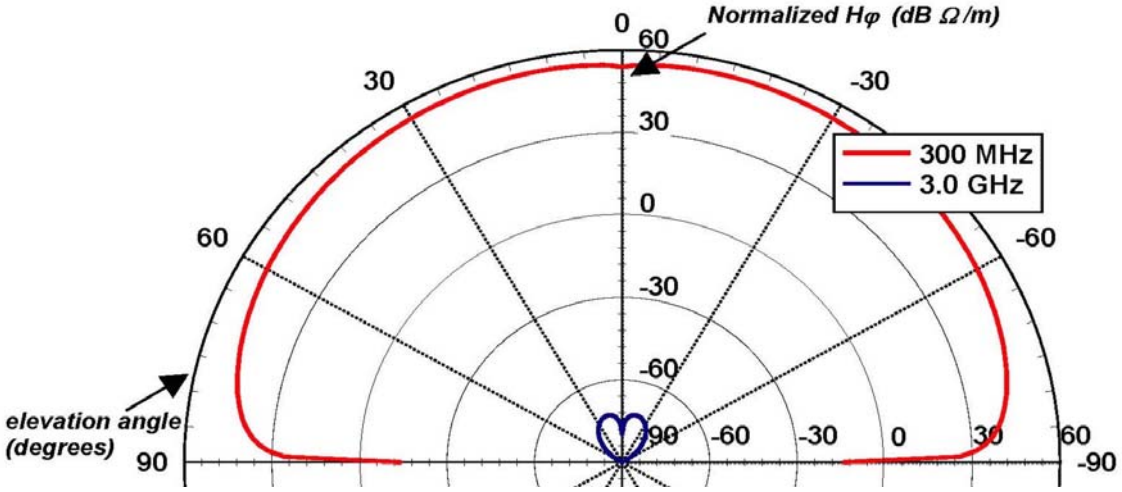

Far-zone H_φ patterns in the upper-half space for the sand case of 2.18% moisture ($h = 10\ m,\ a = 0.04\ m$).

1.3 Conclusions

We have found that for the same waveguiding mode of propagation, the diameter of a hole within the earth must be increased to obtain reasonable signal levels at the top of the hole, relative to a perfectly-electrically conducting waveguide. This was determined by using a complex-zero finding routine to solve the transcendental modal equation for the axial propagation constant (and radial) when sands with varying moisture levels (loss tangents on the order of 0.1) where taken as the surrounding material to the hole. It was also determined that, for the same signal level, the increase in the hole diameter must increase as the permittivity of the soil decreases or, equivalently, as the moisture content of the soil decreases. Thus, in general, a hole in the earth with a radius less than a wavelength does not act as a good waveguiding structure. In the case that sand with a 16.8% moisture content surrounds the hole, a hole with a 0.1 m radius and a 3.0 GHz vertical dipole source was found to be characterized by approximately 200 dB of attenuation after propagating a distance 10 m.

Due to the high losses associated with propagation through the earth at high frequencies, one solution to decreasing the levels of attenuation experienced by the signal (and consequently, obtain measurable signals at the top of the hole) would be to use higher frequencies (e.g. millimeter band frequencies) and, correspondingly, a highly directive beam. In this way, the number of reflections off the wall boundary are minimized, less energy is dissipated into the lossy soil, and reasonable signal levels could be measured at the interface. However, we note that this is only a valid solution if no backfill is introduced into the cylindrical hole during the measurement. The case of backfill would lead to extremely large attenuation at these very high frequencies (a much more severe case than when dealing with wavelengths on the order of the hole diameter).

However, instead of relying on the hole as a waveguiding structure, perhaps a better solution would be to use lower frequencies and direct radiation through the earth. In this situation, the electrical dimensions of the hole become negligible and consequently the entire problem can be treated as if the hole does not exist. Here it may be appropriate to use magnetic dipoles or loop antennas for efficiency reasons. As done in this analysis, the magnetic dipoles in the earth-air half space problem can be easily represented by an integral transform solution (which also applies to vertically layered media), which can then be asymptotically evaluated to find the far-zone fields in the air region.

2 INTRODUCTION

This report examines the problem of a dipole antenna (both vertically and horizontally oriented) radiating from a cylindrical hole in the earth and the subsequent far-zone field produced in the upper air half-space. The problem geometry is shown in Figure 1. In addition to providing guidance in the overall system design, the purpose of this analysis was to examine the important features of the radiation into the upper-half space region and also provide estimates that could be used as checks on further numerical simulations.

The approach used for this analysis was to first consider the radiation characteristics in the lower half-space with various geological materials located exterior to the hole. In particular, a hole of radius $a = 0.04\ m$ was examined and three cases of sand with varying levels of moisture content were considered as the surrounding material to the hole [1]. (The corresponding material properties are shown in Table 1.) After applying asymptotic methods to determine closed-form expressions for the radiation in the lower half-space region, the goal was next to determine analytic representations for the far-zone fields in the upper half-space (the air region) and ultimately determine the effects of the hole on the overall dipole radiation.

Table 1.Sand material properties.

	$\varepsilon_r^{300\ MHz}$	$\varepsilon_r^{3.0\ GHz}$
Dry Sand	$2.55\,(1 - j0.01)$	$2.55\,(1 - j0.0062)$
2.18% Moisture	$2.55\,(1 - j0.026)$	$2.55\,(1 - j0.03)$
3.88% Moisture	$4.5\,(1 - j0.03)$	$4.4\,(1 - j0.046)$
16.8% Moisture	$20.0\,(1 - j0.03)$	$20.0\,(1 - j0.13)$

3 HOLE-PROPAGATING CHARACTERISTICS

Waveguiding characteristics of metal tubes are a result of the nearly perfect reflectivity of the high conductivity walls. Similarly, waveguiding characteristics of optical fibers are set up by the total internal reflection occurring at the wall of the inner dielectric caused by the higher propagation velocity of the

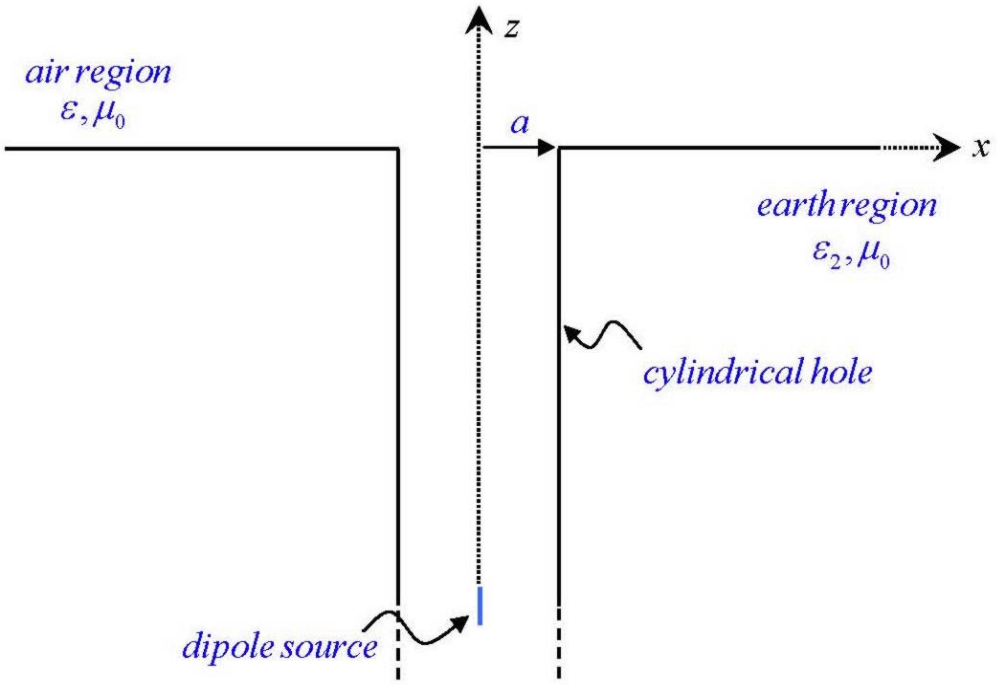

Figure 1. Problem geometry (shown for a vertical dipole).

outer medium or cladding layer (this corresponds to the fiber having a larger dielectric constant than the surrounding medium). In the case of a hole in geological media, the conductivity of the surrounding medium is not sufficiently high (the loss tangents of the geological media being less than one at high frequencies) to produce high levels of reflection, nor is it less optically dense than the interior to produce total internal reflection. In fact, Snell's law indicates that rays leaving the interior are bent toward the normal, effectively reducing the energy radiated toward the surface. Hence, in the case of a hole within the earth, we expect these guided modes to be damped, in some cases to an even greater degree than the direct radiation through the earth media. It is also clear from the decay length in the earth (determined from the permittivity characteristics of the geological media), that for these materials and radii (and frequencies near the hole cutoff frequency) most of the energy of the guided mode resides in the surrounding medium. A schematic for the ray paths in the cases of a metal waveguide, an optical fiber, and a hole within the earth are shown in Figure 2.

3.1 Propagating Characteristics for a Hole of $a = 0.04\ m$

In addition to Snell's law and the decay lengths associated with the earth, the propagation along the length of the cylindrical hole can also be understood by examining the zeros of the modal equation corresponding to a cylindrical hole in lossy media. To this end, a program was set up which uses a global complex zero-finding routine based on the complex argument principle [2] and, for this particular problem, on a transcendental equation related to the complex Bessel functions associated with the circular hole geometry. The complex-zero solutions to the transcendental function determine the propagation constants in the radial and axial directions, giving both the phase variation and attenuation along the two directions. Here it was necessary to carefully define the branches of the square root terms and Bessel functions (associated with the zeros of the wavenumbers in the radial directions) and to avoid these branch cuts in the selected zero-finding regions (more on this is discussed in *Appendix A*). With knowledge of the branch cut locations, it was possible to ensure that zeros on the improper Riemann sheet were being rejected or, equivalently, that only solutions corresponding to outward propagating waves with decay were being selected. Although the details of the transcendental equation are suppressed here, they are presented below for both a vertically and horizontally-positioned dipole.

To demonstrate the lack of wave propagation along a cylindrical hole of radius 0.04 m , the axial propagation constants k_z found closest to the real axis (using the zero-finding routine [2]) are shown in Figures 3 and 4. Here the results are shown for the case of a vertical dipole operating at 300 MHz and 3.0 GHz and the wavenumbers have been normalized to the free-space wavenumber k. (The propagation behavior for a hole of 0.1 m radius is considered in the next section.) For comparison, the wavenumbers k_2 in the various geological media are also shown, with the material properties at these frequencies (given in Table 1) being obtained from [1]. Thus, because the imaginary parts of the propagation constants were found to be very large compared to the imaginary part of the k_2 branch point, instead of propagation along the hole direction, the energy is being transmitted into the surrounding material to the hole. At 3.0 GHz, it is seen that the loss due to the cutoff frequency is smaller relative to the loss values at the lower frequency, but the loss is still large compared to the direct propagation in k_2. It is important to note that, although only the results of the vertically-oriented dipole are being shown here, the zeros associated with the horizontally-oriented dipole were also examined and found to demonstrate similar behavior.

3.2 Propagating Characteristics for a Hole of $a = 0.1\ m$

In Figures 5 and 6 we examine the propagation behavior when the radius of the hole is increased from 0.04 m to 0.1 m. In considering 300 MHz, there is little change in the location of the zeros from the $a = 0.04\ m$ case, except in the 16.8% moisture case where the normalized level of the imaginary part goes from approximately -10.66 (Figure 3) to -3.68 (Figure 5). At 3.0 GHz, we find an overall decrease in the

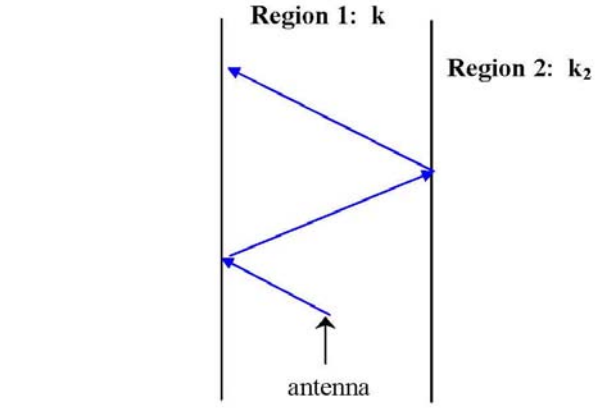

a.) Case I. $k_2<k$
Case II. $k_2 \rightarrow \infty$ (metal)

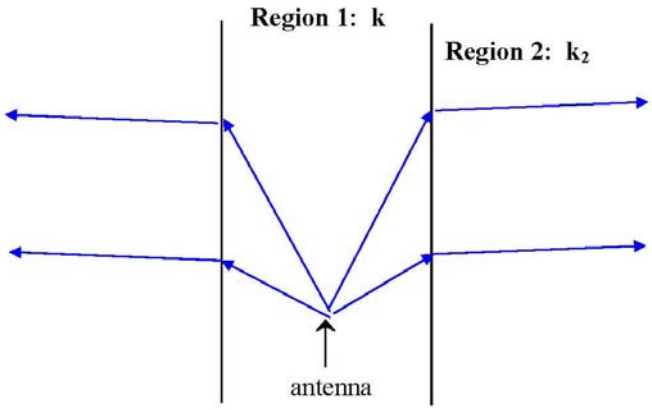

b.) Case III. $k_2>k$

Figure 2. The ray path behavior for the cases of a.) a metal waveguide and an optical fiber and b.) a hole within the earth.

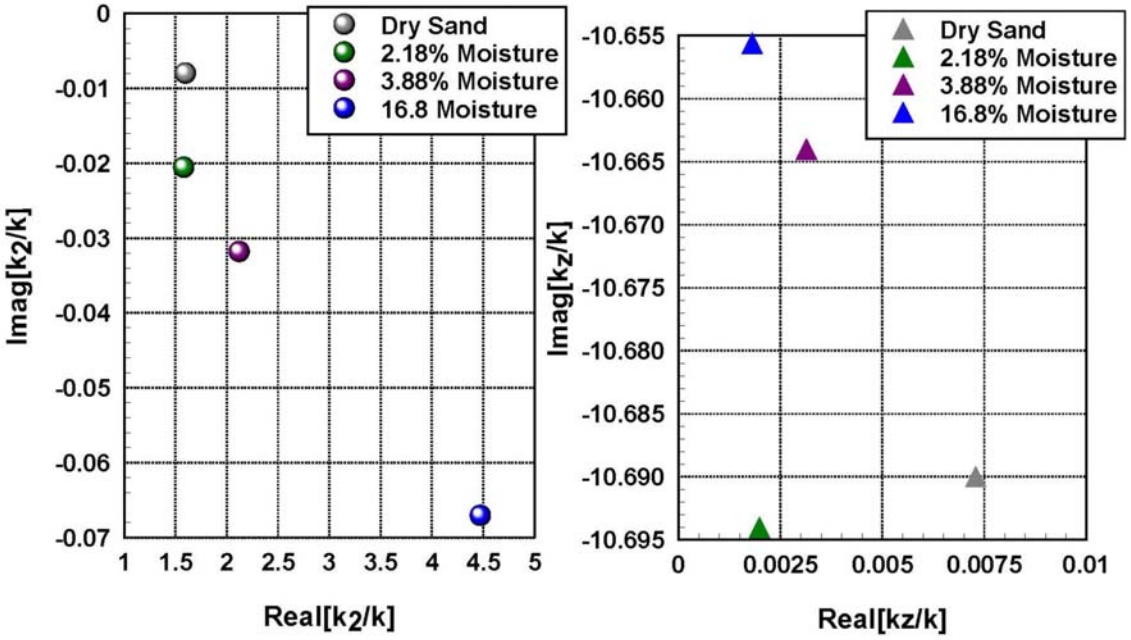

Figure 3. Normalized branch point wavenumbers and axial propagation constants for a hole of radius 0.04 m and various geological media at 300 MHz.

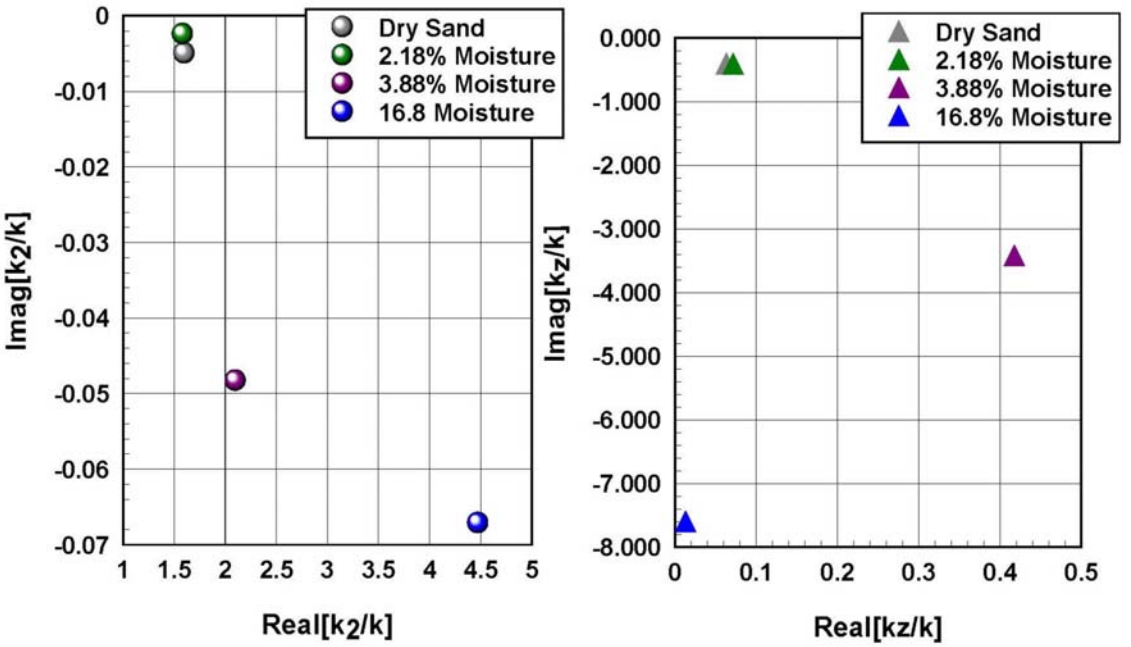

Figure 4. Normalized branch point wavenumbers and axial propagation constants for a hole of radius 0.04 m and various geological media at 3.0 GHz.

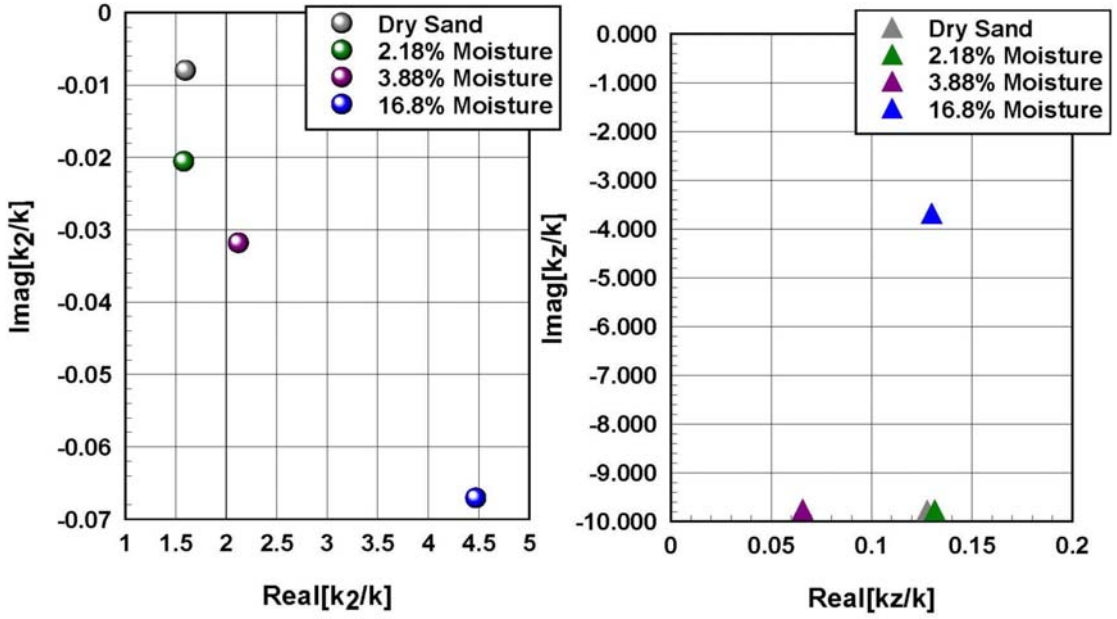

Figure 5. Normalized branch point wavenumbers and axial propagation constants for a hole of radius 0.1 m and various geological media at 300 MHz.

imaginary part of k_z ($\mathrm{Im}\,(k_z)$) for all four sand cases, but particularly for the 16.8% moisture case where the $\mathrm{Im}\,(k_z)$ becomes less than the imaginary part of the k_2 wavenumber. Thus, in increasing the radius electrically (ka has increased), k_z is approaching k and the TM_{01} (the first mode of propagation) is near its cutoff frequency.

4 VERTICAL-DIPOLE ENGINEERING FORMULAS

4.1 Radial Propagation Constant

For the purposes of design, it is useful to reduce the transcendental equation governing the propagation constant into a simple equation that can be used to determine an approximate propagation constant for a particular hole size, frequency, and surrounding medium characteristics. Although a derivation of the transcendental equation based on a boundary-condition analysis is presented in a later section, here we present an alternative formulation based on a transverse-resonance method [3]. With this method, the transcendental equation is normalized in terms of impedance and we are able to proceed to develop a relatively simple closed-form expression for the wavenumber in the axial direction (k_z) for some limiting cases. It should be noted that a similar simplification can be performed for the case of the horizontal dipole, though this is not done in this paper and is left for future work.

Looking into the outer medium to the hole in the radial direction, we can write the input impedance as

$$Z_{in}^{\rho} = \frac{k_{2\rho}}{\omega\varepsilon_2}$$

which, if we suppose that k_2 is large and that $k_z = O\,(k)$, becomes

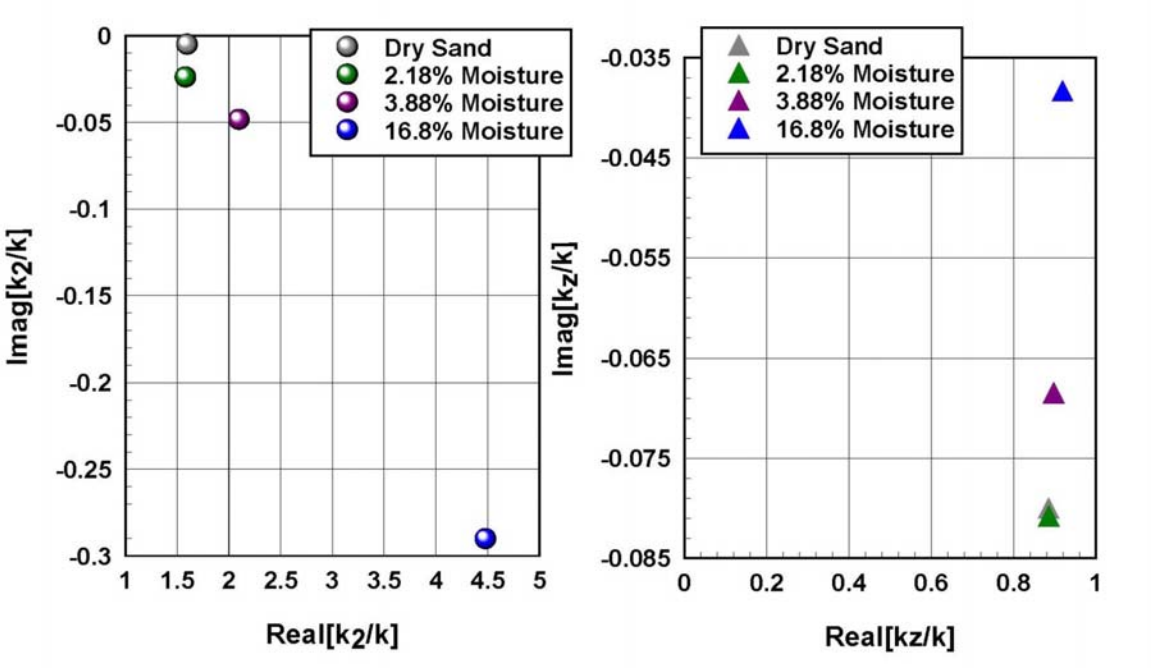

Figure 6. Normalized branch point wavenumbers and axial propagation constants for a hole of radius 0.1 m and various geological media at 3.0 GHz.

$$Z_{in}^{\rho} = \frac{k_2}{\omega\varepsilon_2} = \eta_2$$

$\left(\eta_2 = \sqrt{\mu/\varepsilon_2}\right)$. By next looking into the interior medium of the hole, the input impedance can be written as

$$Z_{in}^{-\rho} = \left.\frac{E_z}{H_\varphi}\right|_{\rho=a-0}$$

where referring to the boundary-condition analysis presented below, we have

$$Z_{in}^{-\rho} \approx -j\frac{k_\rho}{\omega\varepsilon}\frac{J_0\left(k_\rho a\right)}{J_1\left(k_\rho a\right)}$$

In the limit of large radius, we note that

$$J_0\left(k_\rho a\right) \sim \sqrt{\frac{2}{\pi k_\rho a}}\cos\left(k_\rho a - \frac{\pi}{4}\right)$$

and

$$J_1\left(k_\rho a\right) \sim \sqrt{\frac{2}{\pi k_\rho a}}\cos\left(k_\rho a - \frac{3\pi}{4}\right)$$

so that

$$\frac{J_0\left(k_\rho a\right)}{J_1\left(k_\rho a\right)} \approx \frac{\cos\left(k_\rho a - \frac{\pi}{4}\right)}{\cos\left(k_\rho a - \frac{3\pi}{4}\right)}$$

or

$$\frac{J_0\left(k_\rho a\right)}{J_1\left(k_\rho a\right)} \approx \frac{\cos\left(k_\rho a - \frac{\pi}{4}\right)}{\sin\left(k_\rho a - \frac{\pi}{4}\right)} = \cot\left(k_\rho a - \frac{\pi}{4}\right)$$

Substituting back into the input impedance seen looking into the interior of the hole, we have

$$Z_{in}^{-\rho} \approx -j\frac{k_\rho}{\omega\varepsilon}\cot\left(k_\rho a - \frac{\pi}{4}\right)$$

Here we note that $Z_{in}^{-\rho}$ is described by a perfect magnetic conductor boundary (PMC) condition shifted by an electrical distance of $\pi/4$ from the origin (as shown in Figure 7), but more will be said about this later.

The impedance transcendental equation governing the circular hole boundary is then given by

$$Z_{in}^{\rho} = -Z_{in}^{-\rho}\big|_{\rho=a-0}$$

or

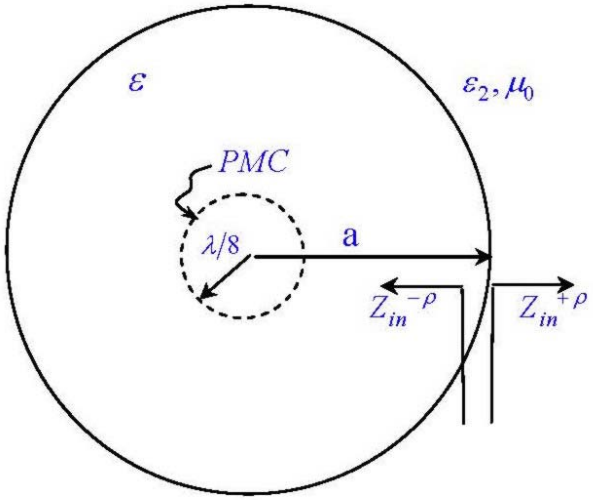

Figure 7. Input impedance seen looking into the interior and exterior of the cylindrical hole.

$$\eta_2 = j\frac{k_\rho}{\omega\varepsilon}\cot\left(k_\rho a - \frac{\pi}{4}\right)$$

Normalizing the transcendental equation by the intrinsic impedance of free-space $\left(\eta = \sqrt{\mu/\varepsilon}\right)$, we obtain

$$\frac{\eta_2}{\eta} = j\frac{k_\rho}{\omega\varepsilon\eta}\cot\left(k_\rho a - \frac{\pi}{4}\right)$$

For convenience, this equation can also be written as

$$\frac{\eta_2}{\eta} = j\frac{1}{\omega\varepsilon\eta a}\left[k_\rho a\cot\left(k_\rho a - \frac{\pi}{4}\right)\right]$$

We now note that given an expression

$$\alpha = jx\cot\left(x - \frac{\pi}{4}\right)$$

where

$$\alpha = \eta_2\omega\varepsilon a = ka\left(\eta_2/\eta\right)$$

is small, we can approximate the values of x by

$$x \approx \frac{p\pi}{4} + j\epsilon$$

where ϵ is a small number and $p = 3, 7, 11, ...4q - 1, ...$ Substituting into the expression for α, we find that

$$\alpha = j\left(\frac{p\pi}{4} + j\epsilon\right)\cot\left(q\pi - \frac{\pi}{2} + j\epsilon\right) = -j\left(\frac{p\pi}{4} + j\epsilon\right)\tan\left(j\epsilon\right)$$

or approximately

$$j\alpha \sim \left(\frac{p\pi}{4} + j\epsilon\right)j\epsilon$$

Thus, to a first-order approximation, the values of x become

$$x \approx \frac{p\pi}{4} + \frac{j\alpha}{\frac{p\pi}{4} + j\epsilon}$$

The choice of ϵ in the denominator does not affect the leading two terms of x in the $\alpha \to 0$ limit as long as $\epsilon \to 0$ in the same limit. We are thus free to choose it so that another limit is satisfied and by constraining $\epsilon = O\left(\alpha\right)$. Choosing the perfect magnetic conductor (PMC) limiting case where $\alpha \to \infty$, we

know that the solution must equal $\frac{n\pi}{4}$ where $n = 5, 9, 13, ...4q + 1, ...$, so therefore we take

$$\epsilon = \frac{2}{\pi}\alpha$$

where correspondingly,

$$k_\rho^{app} a \approx \frac{p\pi}{4} + \frac{j\alpha}{\frac{p\pi}{4} + j\alpha\frac{2}{\pi}} = \frac{p\pi}{4} + \frac{jka\,(\eta_2/\eta)}{\frac{p\pi}{4} + jka\,(\eta_2/\eta)\,\frac{2}{\pi}}$$

Thus, with this form for $k_\rho a$, we obtain the solutions for the two limiting cases of a PEC and PMC boundary condition at $\rho = a$. We note that as $\alpha \to 0$, we have a cavity formed by a PMC inner boundary and a PEC outer boundary (as shown in Figure 7) where the boundary conditions are satisfied at a frequency corresponding to $\lambda/4$. Alternatively, when the outer boundary tends towards a PMC limit, the boundary conditions are satisfied at $\lambda/2$. Thus, it is to be expected that the cutoff frequencies for a given mode are lower for the PEC cases than the PMC cases, as described in the $k_\rho^{app} a$ formula.

In Figure 8 we show a plot of the approximate $k_\rho a$ expression, for the modes corresponding to $p = 3$ and $p = 7$, as the values of $\alpha = ka\,(\eta_2/\eta)$ are varied from zero to infinity. It should be noted that, although the $k_\rho a$ curves have been calculated assuming real values of η_2/η, there was found to be virtually no change in the curves when complex impedances were considered (loss tangents on the order of 0.1 were assumed). Also shown in Figure 8 are the values of $k_\rho a$ found using the complex root-finding routine and the exact transcendental equation (as opposed to the asymptotic transverse resonance equation derived in this section) in the sand cases of 16.8%, 3.88%, and 2.18% moisture content [1]. For a frequency of 3 GHz and a hole radius of 0.1 m, the corresponding values of α go from 1.4, 3.0, to 4.0 as the moisture content decreases (free-space has been assumed for the inner hole medium). In order to create a high α sample point to be used with the root-finding code, the 2.18% moisture sand was considered at 3 GHz with a 0.25 m hole (this yields an $\alpha = 9.0$). Thus, we observe good agreement between the approximate values and those produced by the root-finding routine, with the approximate $k_\rho a$ curves slightly underestimating the code values near the peaks. Since the setting of $k_{2\rho}$ to k_2 and the approximation of the Bessel functions was found to lead to negligible errors, it is important to note that the errors here can be attributed to the bilinear approximation of the transcendental equation.

4.2 Axial Propagation Constant

Using this approximate expression for $k_\rho a$, we can next determine an approximate expression for $k_z a$. From the separation equation, we can write

$$k_z a = \sqrt{k^2 a^2 - k_\rho^2 a^2}$$

where, substituting in, we obtain

$$k_z^{app} a = \sqrt{k^2 a^2 - \left[\frac{p\pi}{4} + \frac{jka\,(\eta_2/\eta)}{\frac{p\pi}{4} + jka\,(\eta_2/\eta)\,\frac{2}{\pi}}\right]^2}$$

In Fig. 9 the approximate values for k_z^{app} are compared to the values of k_z which are based on the exact transcendental equation (as opposed to the asymptotic transverse resonance equation derived in this section) and the complex-root finding code discussed in the previous section. A hole radius of $a = 0.1$ m and a frequency of 3.0 GHz are assumed for these calculations and the same three cases of varying moisture content are examined as above. (The exact results shown here are identical to those in Fig. 6 and are

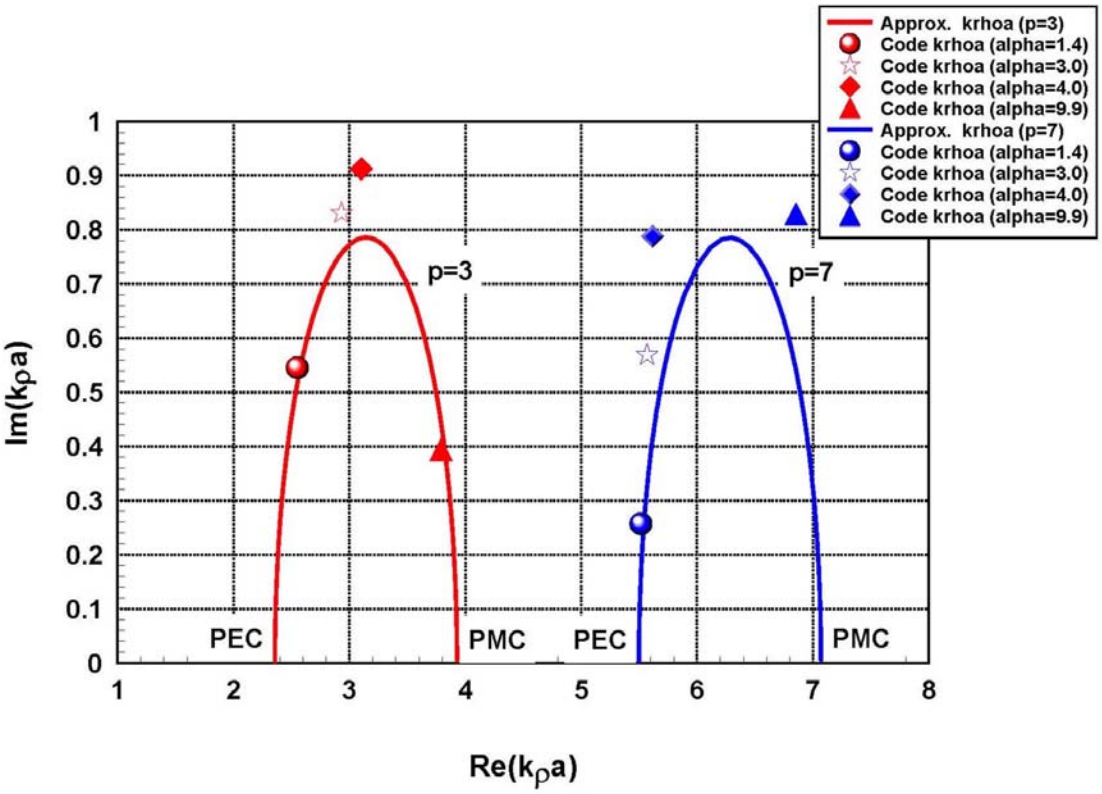

Figure 8. Approximate complex $k_\rho a$ values as the $\alpha = ka\eta_2/\eta$ is varied from the PEC limit ($\alpha = 0$) to the PMC limit ($\alpha \to \infty$). The values of $k_\rho a$ corresponding to the $p = 3$ and $p = 7$ are shown.

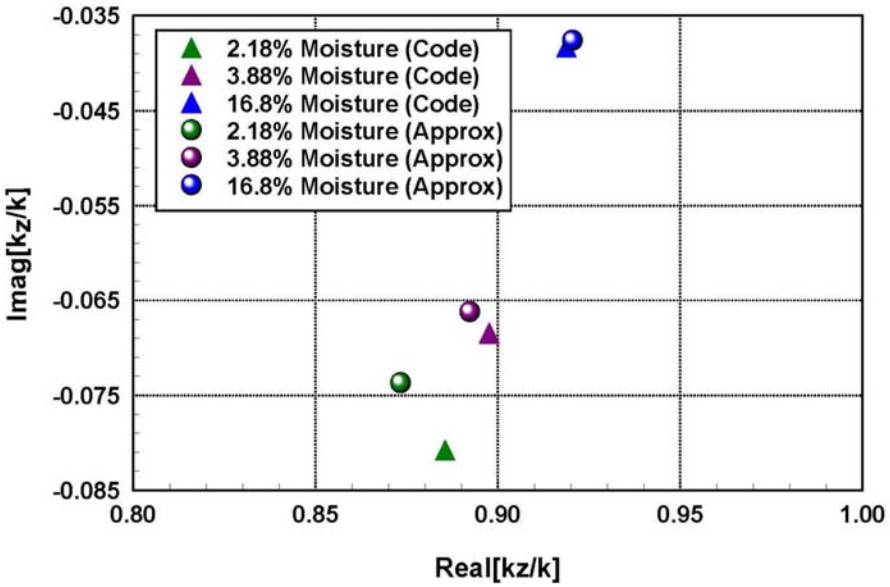

Figure 9. Comparing the exact and approximate axial wavenumbers in the case of a 0.1 m radius hole and a frequency of 3.0 GHz.

included here for comparison purposes to the approximate values.)

Thus, for all three cases of sand considered we observe good agreement between the exact and approximate values of k_z. The approximate solution improves as the moisture content of the sand increases, with the differences in the real and imaginary parts of k_z reducing to -0.19% and 1.77%, respectively at a moisture level of 16.8%. It should be noted, however, that even in the 2.18% moisture case, the approximate expression is still fairly useful in obtaining an idea of the k_z root location. In this case, the percent differences between the real and imaginary part of the approximate and exact solution are 1.38% and 8.82%, respectively.

4.3 Axial Attenuation Constant

Thus far, we have obtained an expression for the axial propagation constant k_z that yields accurate results for both the real and imaginary components. However, in order to realize a simple engineering design formula for the attenuation constant, we first take $p\pi/4$ to be the dominant part of the bracketed term above so that we have

$$k_z a \approx \sqrt{k^2a^2 - \left(\frac{p\pi}{4}\right)^2 - j2ka\,(\eta_2/\eta)}$$

For operation above the cutoff frequency (since near and below cutoff leads to larger attenuations), we will simplify by taking k^2a^2 to be the dominant real part of the square root but retain the imaginary leading term (we are also assuming the loss tangent in the material is much smaller than unity). Thus, approximating the square root function we obtain

$$k_z \approx k\left[1 - j\frac{1}{ka}\,\mathrm{Re}\,(\eta_2/\eta)\right]$$

A simple engineering formula for the attenuation of the modes within the hole, after travelling a distance of h, is then

$$\alpha_{ac}^{app} h \approx \left(\frac{h}{a}\right)\mathrm{Re}\,(\eta_2/\eta)$$

or in units of decibels,

$$\alpha_{ac}^{app} h\ dB = 20\log e^{-\alpha_{ac}^{app} h}$$

We now tabulate some attenuation values using this expression and compare them to the values found using the exact zero-finding routine (assuming $h = 10\ m$).

Table 2.Exact and approximate attenuation values.

$a\ [m]$	ε_{r2}	$\lvert\alpha\rvert = \lvert ka\,(\eta_2/\eta)\rvert$	$\alpha_{ac}^{app}\ [Np/m]$	$P_o/P_t]_{\alpha_{ac}^{app}}$	$P_o/P_t]_{k_z^{exact}}$	$\Delta\,(P_o/P_t)$
0.10	$20\,(1-j0.13)$	1.4	2.23	$-193.0\ dB$	$-209.2\ dB$	7.7%
0.194	$20\,(1-j0.13)$	2.7	1.15	$-99.5\ dB$	$-96.2\ dB$	-3.4%
0.25	$20\,(1-j0.13)$	3.5	0.891	$-77.2\ dB$	$-87.5\ dB$	11.8%

Thus, with a maximum absolute error of only 11.8% occurring in the case of $\alpha = 3.5$, the simple expression for α_{ac}^{app} is shown to yield an approximated location associated with the k_z root for moderate values of α's also (the approximations made in obtaining the simple form of the attenuation constant have assumed small values of α). In general however, the expression for k_z^{app}can always be used to obtain the attenuation constant, although the expression is much more complicated.

Table 2 also indicates that at 3.0 GHz and 16.8% moisture sand, reasonable signal levels for $h = 10m$ (corresponding to the first mode of propagation) can only be measured when the hole radius is increased beyond about $0.2m$. This situation can be compared to the case of a PEC waveguide where the cutoff frequency for a radius of 0.04 m is approximately 2.8 GHz.

5 VERTICAL-DIPOLE RADIATION CHARACTERISTICS

We first consider the case of a vertically-oriented dipole (positioned along the z-axis, Figure 1). This dipole orientation is examined before considering the horizontally-oriented dipole, since it results only in $E-$modes along the hole and hence can be reduced to a simple scalar problem. (Another scalar problem that would be of interest is a loop antenna, but it is not considered at this time.) Furthermore, because this analysis is relatively simple compared to the case of the horizontal dipole, the vertical dipole is included to provide an overall understanding of the general antenna propagation characteristics through the earth when the hole is taken into account. The case of a horizontal dipole is considered in a subsequent section of the report. It is important to note that a time dependence of $e^{j\omega t}$ is assumed and suppressed throughout this report.

5.1 Boundary-Condition Analysis

As stated previously, the vertical dipole is relatively simple because it leads to only $E-$modes along the hole and, in this case, the axial component of the magnetic vector potential can be used exclusively. The

source term satisfies

$$\left(\nabla^2 + k^2\right) A_z = \left[\frac{1}{\rho}\frac{\partial}{\partial\rho}\left(\rho\frac{\partial}{\partial\rho}\right) + \frac{\partial^2}{\partial z^2} + k^2\right] A_z = -\mu_0 J_z = -\mu_0 I_0 \ell\delta\left(\underline{r}\right) = -\mu_0 I_0 \ell\delta\left(z\right)\frac{\delta\left(\rho\right)}{2\pi\rho}$$

where the solution is

$$A_z^s = \mu_0 I_0 \ell\frac{e^{-jkr}}{4\pi r}$$

The integral representation can be found as

$$A_z^s = \frac{1}{2\pi}\int_{-\infty}^{\infty} A\left(k_z\right) H_0^{(2)}\left(k_\rho\rho\right) e^{-jk_z z} dk_z$$

where

$$k_\rho = \sqrt{k^2 - k_z^2}$$

and

$$\mathrm{Im}\left(k_\rho\right) \leq 0$$

Inserting the representation and inverting the Fourier transform gives

$$A\left(k_z\right)\left[\frac{\partial}{\partial\rho}\left(\rho\frac{\partial}{\partial\rho}\right) + \rho k_\rho^2\right] H_0^{(2)}\left(k_\rho\rho\right) = -\mu_0 I_0 \ell\frac{\delta\left(\rho\right)}{2\pi}\int_{-\infty}^{\infty}\delta\left(z\right) e^{jk_z z} dz = -\mu_0 I_0 \ell\frac{\delta\left(\rho\right)}{2\pi}$$

where next integration with respect to ρ yields

$$-A\left(k_z\right) k_\rho\rho H_1^{(2)}\left(k_\rho\rho\right) \sim -\frac{2j}{\pi} A\left(k_z\right) = -\mu_0 I_0 \ell\frac{1}{2\pi}$$

or

$$A\left(k_z\right) = -\frac{j}{4}\mu_0 I_0 \ell$$

Thus, the dipole source solution (existing in the interior of the hole) becomes

$$A_z^s = -\frac{j}{8\pi}\mu_0 I_0 \ell\int_{-\infty}^{\infty} H_0^{(2)}\left(k_\rho\rho\right) e^{-jk_z z} dk_z\,,\ 0 < \rho < a$$

where the source-free potentials are given by

$$A_z = \frac{1}{2\pi}\int_{-\infty}^{\infty} B\left(k_z\right) J_0\left(k_\rho\rho\right) e^{-jk_z z} dk_z\,,\ 0 < \rho < a$$

$$= \frac{1}{2\pi}\int_{-\infty}^{\infty} C\left(k_z\right) H_0^{(2)}\left(k_{2\rho}\rho\right) e^{-jk_z z} dk_z\,,\ \rho > a$$

and

$$k_{2\rho} = \sqrt{k_2^2 - k_z^2}$$

Enforcing the continuity of $E_z\,(\rho = a)$

$$E_z = \frac{-j}{\omega\mu_0\varepsilon}\left(\frac{\partial^2}{\partial z^2} + k^2\right) A_z$$

gives

$$-\frac{j}{4}\mu_0 I_0 \ell H_0^{(2)}\left(k_\rho a\right) + B\left(k_z\right) J_0\left(k_\rho a\right) = \frac{k_{2\rho}^2\varepsilon}{k_\rho^2\varepsilon_2} C\left(k_z\right) H_0^{(2)}\left(k_{2\rho} a\right)$$

while the continuity of $H_\varphi\,(\rho = a)$

$$\mu_0 H_\varphi = -\frac{\partial}{\partial\rho} A_z$$

yields

$$-\frac{j}{4}\mu_0 I_0 \ell k_\rho H_1^{(2)}\left(k_\rho a\right) + B\left(k_z\right) k_\rho J_1\left(k_\rho a\right) = C\left(k_z\right) k_{2\rho} H_1^{(2)}\left(k_{2\rho} a\right)$$

We next eliminate $C\left(k_z\right)$ to obtain

$$-\frac{j}{4}\mu_0 I_0 \ell H_0^{(2)}\left(k_\rho a\right) H_1^{(2)}\left(k_{2\rho} a\right) + B\left(k_z\right) J_0\left(k_\rho a\right) H_1^{(2)}\left(k_{2\rho} a\right) =$$

$$\left[-\frac{j}{4}\mu_0 I_0 \ell\left(k_\rho / k_{2\rho}\right) H_1^{(2)}\left(k_\rho a\right) H_0^{(2)}\left(k_{2\rho} a\right) + B\left(k_z\right)\left(k_\rho / k_{2\rho}\right) J_1\left(k_\rho a\right) H_0^{(2)}\left(k_{2\rho} a\right)\right] \frac{k_{2\rho}^2\varepsilon}{k_\rho^2\varepsilon_2}$$

or

$$B\left(k_z\right) = \frac{j}{4}\mu_0 I_0 \ell \frac{\varepsilon k_{2\rho} H_1^{(2)}\left(k_\rho a\right) H_0^{(2)}\left(k_{2\rho} a\right) - \varepsilon_2 k_\rho H_0^{(2)}\left(k_\rho a\right) H_1^{(2)}\left(k_{2\rho} a\right)}{\varepsilon k_{2\rho} J_1\left(k_\rho a\right) H_0^{(2)}\left(k_{2\rho} a\right) - \varepsilon_2 k_\rho J_0\left(k_\rho a\right) H_1^{(2)}\left(k_{2\rho} a\right)}$$

$$= \frac{j}{4}\mu_0 I_0 \ell\left[1 - j\frac{\varepsilon k_{2\rho} Y_1\left(k_\rho a\right) H_0^{(2)}\left(k_{2\rho} a\right) - \varepsilon_2 k_\rho Y_0\left(k_\rho a\right) H_1^{(2)}\left(k_{2\rho} a\right)}{\varepsilon k_{2\rho} J_1\left(k_\rho a\right) H_0^{(2)}\left(k_{2\rho} a\right) - \varepsilon_2 k_\rho J_0\left(k_\rho a\right) H_1^{(2)}\left(k_{2\rho} a\right)}\right]$$

Here the poles are found from the equation

$$\varepsilon k_{2\rho} J_1\left(k_\rho a\right) H_0^{(2)}\left(k_{2\rho} a\right) = \varepsilon_2 k_\rho J_0\left(k_\rho a\right) H_1^{(2)}\left(k_{2\rho} a\right)$$

provided that

$$\varepsilon k_{2\rho} H_1^{(2)}\left(k_\rho a\right) H_0^{(2)}\left(k_{2\rho} a\right) \neq \varepsilon_2 k_\rho H_0^{(2)}\left(k_\rho a\right) H_1^{(2)}\left(k_{2\rho} a\right)$$

Thus, using this expression in the root-finding code we find that the poles having high rates of decay do not contribute significantly to the potential integral A_z (the corresponding results have been presented in Figures 3 and 4.)

Adding the source and scattered parts of the potential together gives

$$A_z^{tot} = \frac{1}{8\pi}\mu_0 I_0 \ell \int_{-\infty}^{\infty} \left[\frac{\varepsilon k_{2\rho} Y_1(k_\rho a) H_0^{(2)}(k_{2\rho} a) - \varepsilon_2 k_\rho Y_0(k_\rho a) H_1^{(2)}(k_{2\rho} a)}{\varepsilon k_{2\rho} J_1(k_\rho a) H_0^{(2)}(k_{2\rho} a) - \varepsilon_2 k_\rho J_0(k_\rho a) H_1^{(2)}(k_{2\rho} a)}\right] J_0(k_\rho \rho) e^{-jk_z z} dk_z$$
$$-\frac{1}{8\pi}\mu_0 I_0 \ell \int_{-\infty}^{\infty} Y_0(k_\rho \rho) e^{-jk_z z} dk_z \,,\ 0 < \rho < a$$

or

$$A_z^{tot} = \frac{1}{8\pi}\mu_0 I_0 \ell \int_{-\infty}^{\infty} \left[\frac{\varepsilon k_{2\rho} Y_1(k_\rho a) H_0^{(2)}(k_{2\rho} a) - \varepsilon_2 k_\rho Y_0(k_\rho a) H_1^{(2)}(k_{2\rho} a)}{\varepsilon k_{2\rho} J_1(k_\rho a) H_0^{(2)}(k_{2\rho} a) - \varepsilon_2 k_\rho J_0(k_\rho a) H_1^{(2)}(k_{2\rho} a)}\right] J_0(k_\rho \rho) e^{-jk_z z} dk_z$$
$$+\mu_0 I_0 \ell \frac{\cos(kr)}{4\pi r} \,,\ 0 < \rho < a$$

We next focus on the branch cut contributions to the integral, where if we rotate k_z around the branch point k_2 and use the identities [4]

$$H_0^{(2)}\left(ze^{j\pi}\right) = 2H_0^{(2)}(z) + H_0^{(1)}(z)$$

$$H_1^{(2)}\left(ze^{j\pi}\right) = -2H_1^{(2)}(z) - H_1^{(1)}(z)$$

we find

$$\varepsilon e^{i\pi} k_{2\rho} J_1(k_\rho a) H_0^{(2)}\left(k_{2\rho} e^{i\pi} a\right) = \varepsilon_2 k_\rho J_0(k_\rho a) H_1^{(2)}\left(k_{2\rho} e^{i\pi} a\right)$$

and

$$-\varepsilon k_{2\rho} J_1(k_\rho a)\left[2H_0^{(2)}(k_{2\rho} a) + H_0^{(1)}(k_{2\rho} a)\right] = -\varepsilon_2 k_\rho J_0(k_\rho a)\left[2H_1^{(2)}(k_{2\rho} a) + H_1^{(1)}(k_{2\rho} a)\right]$$

Separating real and imaginary parts for real medium parameters yields

$$\varepsilon k_{2\rho} J_1(k_\rho a) J_0(k_{2\rho} a) = \varepsilon_2 k_\rho J_0(k_\rho a) J_1(k_{2\rho} a)$$

and

$$\varepsilon k_{2\rho} J_1(k_\rho a) Y_0(k_{2\rho} a) = \varepsilon_2 k_\rho J_0(k_\rho a) Y_1(k_{2\rho} a)$$

which are identical to the results obtained before the rotation. With the equations remaining the same, the integrand ratio becomes

$$B\left(k_z, k_{2\rho} e^{i\pi}\right) = \frac{j}{4}\mu_0 I_0 \ell \frac{\varepsilon k_{2\rho} e^{i\pi} H_1^{(2)}(k_\rho a) H_0^{(2)}\left(k_{2\rho} a e^{i\pi}\right) - \varepsilon_2 k_\rho H_0^{(2)}(k_\rho a) H_1^{(2)}\left(k_{2\rho} a e^{i\pi}\right)}{\varepsilon k_{2\rho} e^{i\pi} J_1(k_\rho a) H_0^{(2)}(k_{2\rho} a e^{i\pi}) - \varepsilon_2 k_\rho J_0(k_\rho a) H_1^{(2)}(k_{2\rho} a e^{i\pi})}$$

$$= \frac{j}{4}\mu_0 I_0 \ell \frac{\varepsilon k_{2\rho} H_1^{(2)}(k_\rho a)\left[2H_0^{(2)}(k_{2\rho}a) + H_0^{(1)}(k_{2\rho}a)\right] - \varepsilon_2 k_\rho H_0^{(2)}(k_\rho a)\left[2H_1^{(2)}(k_{2\rho}a) + H_1^{(1)}(k_{2\rho}a)\right]}{\varepsilon k_{2\rho} J_1(k_\rho a)\left[2H_0^{(2)}(k_{2\rho}a) + H_0^{(1)}(k_{2\rho}a)\right] - \varepsilon_2 k_\rho J_0(k_\rho a)\left[2H_1^{(2)}(k_{2\rho}a) + H_1^{(1)}(k_{2\rho}a)\right]}$$

$$= \frac{j}{4}\mu_0 I_0 \ell \frac{\varepsilon k_{2\rho} H_1^{(2)}(k_\rho a)\left[H_0^{(2)}(k_{2\rho}a) + 2J_0(k_{2\rho}a)\right] - \varepsilon_2 k_\rho H_0^{(2)}(k_\rho a)\left[H_1^{(2)}(k_{2\rho}a) + 2J_1(k_{2\rho}a)\right]}{\varepsilon k_{2\rho} J_1(k_\rho a)\left[H_0^{(2)}(k_{2\rho}a) + 2J_0(k_{2\rho}a)\right] - \varepsilon_2 k_\rho J_0(k_\rho a)\left[H_1^{(2)}(k_{2\rho}a) + 2J_1(k_{2\rho}a)\right]}$$

where it does not appear that the branch cut goes away. Next, if we rotate k_z around the k branch point we find

$$B\left(k_z, k_\rho e^{i\pi}\right) = \frac{j}{4}\mu_0 I_0 \ell \frac{\varepsilon k_{2\rho} H_1^{(2)}\left(k_\rho a e^{i\pi}\right) H_0^{(2)}(k_{2\rho}a) - \varepsilon_2 k_\rho e^{i\pi} H_0^{(2)}\left(k_\rho a e^{i\pi}\right) H_1^{(2)}(k_{2\rho}a)}{\varepsilon k_{2\rho} J_1\left(k_\rho a e^{i\pi}\right) H_0^{(2)}(k_{2\rho}a) - \varepsilon_2 k_\rho e^{i\pi} J_0\left(k_\rho a e^{i\pi}\right) H_1^{(2)}(k_{2\rho}a)}$$

$$= \frac{j}{4}\mu_0 I_0 \ell \frac{\varepsilon k_{2\rho}\left[2H_1^{(2)}(k_\rho a) + H_1^{(1)}(k_\rho a)\right] H_0^{(2)}(k_{2\rho}a) - \varepsilon_2 k_\rho\left[2H_0^{(2)}(k_\rho a) + H_0^{(1)}(k_\rho a)\right] H_1^{(2)}(k_{2\rho}a)}{\varepsilon k_{2\rho} J_1(k_\rho a) H_0^{(2)}(k_{2\rho}a) - \varepsilon_2 k_\rho J_0(k_\rho a) H_1^{(2)}(k_{2\rho}a)}$$

$$= \frac{j}{4}\mu_0 I_0 \ell \frac{\varepsilon k_{2\rho}\left[H_1^{(2)}(k_\rho a) + 2J_1(k_\rho a)\right] H_0^{(2)}(k_{2\rho}a) - \varepsilon_2 k_\rho\left[H_0^{(2)}(k_\rho a) + 2J_0(k_\rho a)\right] H_1^{(2)}(k_{2\rho}a)}{\varepsilon k_{2\rho} J_1(k_\rho a) H_0^{(2)}(k_{2\rho}a) - \varepsilon_2 k_\rho J_0(k_\rho a) H_1^{(2)}(k_{2\rho}a)}$$

$$= B(k_z) + \frac{j}{2}\mu_0 I_0 \ell$$

Now for $z > 0$ we can close the contour downward and obtain

$$A_z^s = -\frac{j}{8\pi}\mu_0 I_0 \ell \int_{C_k}\left[H_0^{(2)}(k_\rho \rho) - H_0^{(2)}\left(k_\rho \rho e^{i\pi}\right)\right] e^{-jk_z z} dk_z\,,\ 0 < \rho < a$$

$$= \frac{j}{8\pi}\mu_0 I_0 \ell \int_{C_k}\left[H_0^{(2)}(k_\rho \rho) + H_0^{(1)}(k_\rho \rho)\right] e^{-jk_z z} dk_z\,,\ 0 < \rho < a$$

$$= \frac{j}{4\pi}\mu_0 I_0 \ell \int_{C_k} J_0(k_\rho \rho)\, e^{-jk_z z} dk_z\,,\ 0 < \rho < a$$

where the contour C_k is along the right side of the branch cut about k from k to infinity. Using the preceding relation for the rotation of $B(k_z)$ about k we find

$$A_z = \frac{1}{2\pi}\int_{C_k}\left[B(k_z) - B\left(k_z, k_\rho e^{i\pi}\right)\right] J_0(k_\rho \rho)\, e^{-jk_z z} dk_z\,,\ 0 < \rho < a$$

$$= -\frac{j}{4\pi}\mu_0 I_0 \ell \int_{C_k} J_0(k_\rho \rho)\, e^{-jk_z z} dk_z\,,\ 0 < \rho < a$$

Thus, the source contribution exactly cancels the contribution of the scattered part of the potential on the k branch cut integral ($\rho < a$).

We now consider $\rho > a$, where the k_2 branch cut contributes. The constant $C(k_z)$ is

$$C(k_z) = -\frac{j}{4}\mu_0 I_0 \ell \frac{k_\rho^2 \varepsilon_2}{k_{2\rho}^2 \varepsilon} \frac{H_0^{(2)}(k_\rho a)}{H_0^{(2)}(k_{2\rho} a)} + B(k_z) \frac{k_\rho^2 \varepsilon_2 J_0(k_\rho a)}{k_{2\rho}^2 \varepsilon H_0^{(2)}(k_{2\rho} a)}$$

$$= -\frac{j}{4}\mu_0 I_0 \ell \frac{k_\rho^2 \varepsilon_2}{k_{2\rho}^2 \varepsilon} \frac{H_0^{(2)}(k_\rho a)}{H_0^{(2)}(k_{2\rho} a)} \left[1 - \frac{\varepsilon k_{2\rho} H_1^{(2)}(k_\rho a) H_0^{(2)}(k_{2\rho} a) - \varepsilon_2 k_\rho H_0^{(2)}(k_\rho a) H_1^{(2)}(k_{2\rho} a)}{\varepsilon k_{2\rho} J_1(k_\rho a) H_0^{(2)}(k_{2\rho} a) - \varepsilon_2 k_\rho J_0(k_\rho a) H_1^{(2)}(k_{2\rho} a)} \frac{J_0(k_\rho a)}{H_0^{(2)}(k_\rho a)}\right]$$

$$= -\frac{j}{4}\mu_0 I_0 \ell \frac{k_\rho^2 \varepsilon_2}{k_{2\rho}^2 \varepsilon} \frac{H_0^{(2)}(k_\rho a)}{H_0^{(2)}(k_{2\rho} a)} \left[\frac{\varepsilon k_{2\rho} \left\{J_1(k_\rho a) H_0^{(2)}(k_\rho a) - H_1^{(2)}(k_\rho a) J_0(k_\rho a)\right\} H_0^{(2)}(k_{2\rho} a)}{\left\{\varepsilon k_{2\rho} J_1(k_\rho a) H_0^{(2)}(k_{2\rho} a) - \varepsilon_2 k_\rho J_0(k_\rho a) H_1^{(2)}(k_{2\rho} a)\right\} H_0^{(2)}(k_\rho a)}\right]$$

$$= -\frac{1}{4}\mu_0 I_0 \ell \frac{k_\rho^2 \varepsilon_2}{k_{2\rho}} \left[\frac{J_1(k_\rho a) Y_0(k_\rho a) - Y_1(k_\rho a) J_0(k_\rho a)}{\varepsilon k_{2\rho} J_1(k_\rho a) H_0^{(2)}(k_{2\rho} a) - \varepsilon_2 k_\rho J_0(k_\rho a) H_1^{(2)}(k_{2\rho} a)}\right]$$

$$= -\frac{1}{2\pi}\mu_0 I_0 \ell \frac{k_\rho \varepsilon_2}{k_{2\rho} a} \left[\frac{1}{\varepsilon k_{2\rho} J_1(k_\rho a) H_0^{(2)}(k_{2\rho} a) - \varepsilon_2 k_\rho J_0(k_\rho a) H_1^{(2)}(k_{2\rho} a)}\right]$$

where rotating about the k branch point gives

$$C\left(k_z, k_\rho e^{j\pi}\right) = -\frac{j}{4}\mu_0 I_0 \ell \frac{k_\rho^2 \varepsilon_2}{k_{2\rho}^2 \varepsilon} \frac{H_0^{(2)}\left(k_\rho a e^{i\pi}\right)}{H_0^{(2)}(k_{2\rho} a)} + B\left(k_z, k_\rho e^{j\pi}\right) \frac{k_\rho^2 \varepsilon_2 J_0(k_\rho a)}{k_{2\rho}^2 \varepsilon H_0^{(2)}(k_{2\rho} a)}$$

$$= -\frac{j}{4}\mu_0 I_0 \ell \frac{k_\rho^2 \varepsilon_2}{k_{2\rho}^2 \varepsilon} \frac{2H_0^{(2)}(k_\rho a) + H_0^{(1)}(k_\rho a)}{H_0^{(2)}(k_{2\rho} a)} + \left\{B(k_z) + \frac{j}{2}\mu_0 I_0 \ell\right\} \frac{k_\rho^2 \varepsilon_2 J_0(k_\rho a)}{k_{2\rho}^2 \varepsilon H_0^{(2)}(k_{2\rho} a)}$$

Thus, as expected, there is no k branch point contribution,

$$C(k_z, k_\rho) - C\left(k_z, k_\rho e^{j\pi}\right) = 0$$

Rotation about the k_2 branch point gives

$$C\left(k_z, k_{2\rho} e^{j\pi}\right) = -\frac{1}{2\pi}\mu_0 I_0 \ell \frac{k_\rho \varepsilon_2}{k_{2\rho} a} \cdot$$

$$\left[\frac{1}{\varepsilon k_{2\rho} J_1(k_\rho a)\left\{H_0^{(2)}(k_{2\rho} a) + 2J_0(k_{2\rho} a)\right\} + \varepsilon_2 k_\rho J_0(k_\rho a)\left\{H_1^{(2)}(k_{2\rho} a) + 2J_1(k_{2\rho} a)\right\}}\right]$$

where using the Hankel function identity for $H_0^{(2)}\left(ze^{i\pi}\right)$ above [4]

$$H_0^{(2)}\left(k_{2\rho}\rho e^{j\pi}\right) = H_0^{(2)}\left(k_{2\rho}\rho\right) + 2J_0\left(k_{2\rho}\rho\right)$$

Thus, recalling that

$$A_z = \frac{1}{2\pi}\int_{-\infty}^{\infty} C\left(k_z\right) H_0^{(2)}\left(k_{2\rho}\rho\right) e^{-jk_z z} dk_z\,,\ \rho > a$$

we can also write

$$A_z = \frac{1}{2\pi}\int_{C_{k_2}} \left[C\left(k_z, k_{2\rho}\right) H_0^{(2)}\left(k_{2\rho}\rho\right) - C\left(k_z, k_{2\rho}e^{j\pi}\right) H_0^{(2)}\left(k_{2\rho}\rho e^{j\pi}\right)\right] e^{-jk_z z} dk_z\,,\ \rho > a$$

5.2 Radiation in the Lower Half-Space

In this section we compare the results from an asymptotic evaluation of the fields in the lower half-space to those resulting from the exact numerical integration. The far-zone magnetic field is examined, where in the particular case of a vertical dipole, only an azimuthal component is present. With the asymptotic analysis, the effects of the hole on the radiation can be easily identified in terms of a scaling coefficient associated with the saddle-point in the lower region, thereby producing an *effective dipole source*. The saddle-point coefficient is then used to determine the radiation in the upper-half space.

5.2.1 Magnetic Vector Potential: Dipole Approximation

We first want to compare A_z for large $z >> a$ with the approximate form of a dipole sitting in an infinite k_2 space,

$$A_z^{app} = \mu_0 I_0 \ell \frac{e^{-jk_2 r}}{4\pi r}$$

If we approximate the branch cut integral for large z and thus the integrand for $k_{2\rho}a \to 0$ and $k_\rho \to k_{02} = \sqrt{k^2 - k_2^2}$ (where $-2\pi < \arg\left(k - k_2\right) < -\pi$ and $-\pi/2 < \arg\left(k + k_2\right) < 0$), we obtain

$$B\left(k_z\right) \sim \frac{j}{4}\mu_0 I_0 \ell \frac{H_0^{(2)}\left(k_{02}a\right)}{J_0\left(k_{02}a\right)}$$

and

$$C\left(k_z, k_{2\rho}\right) \sim \frac{-\frac{j}{4}\mu_0 I_0 \ell}{J_0\left(k_{02}a\right)} \sim C\left(k_z, k_{2\rho}e^{j\pi}\right)$$

so that

$$A_z \sim \frac{1}{2\pi}\frac{\frac{j}{2}\mu_0 I_0 \ell}{J_0\left(k_{02}a\right)}\int_{C_{k_2}} J_0\left(k_{2\rho}\rho\right) e^{-jk_z z} dk_z\,,\ \rho > a\,,\ z >> a$$

Next using the relationship

$$\mu_0 I_0 \ell \frac{e^{-jkr}}{4\pi r} = \frac{j}{4\pi}\mu_0 I_0 \ell \int_{C_k} J_0\left(k_\rho \rho\right) e^{-jk_z z} dk_z$$

we obtain

$$A_z \sim \frac{1}{J_0\left(k_{02} a\right)}\mu_0 I_0 \ell \frac{e^{-jk_2 r}}{4\pi r}\,,\ \rho > a\,,\ z >> a$$

In a subsequent section, this form of the magnetic vector potential will be used to evaluate the field in the upper half space.

5.2.2 Magnetic Vector Potential: Saddle-Point Evaluation

If the Hankel function is expanded for large ρ, the combined exponential function can then be used to define the phase function $\psi\left(k_z\right)$. The resulting function is then differentiated to determine the location of the saddle point [5]. We recall that A_z in the outside region of the hole $(\rho > a)$ is given by

$$A_z = \frac{1}{2\pi}\int_{-\infty}^{\infty} C\left(k_z\right) H_0^{(2)}\left(k_{2\rho}\rho\right) e^{-jk_z z} dk_z\,,\ \rho > a$$

where, for convenience in evaluating the final integral, this can also be written as

$$A_z = -\frac{j}{8\pi}\mu_0 I_0 \ell \int_{-\infty}^{\infty} C_v^{'}\left(k_z\right) H_0^{(2)}\left(k_{2\rho}\rho\right) e^{-jk_z z} dk_z\,,\ \rho > a$$

Here

$$C_v^{'}\left(k_z\right) = \left(-\frac{4}{j\mu_0 I_0 \ell}\right) C\left(k_z\right)$$

and $C\left(k_z\right)$ is given above. Evaluating this integral asymptotically, A_z becomes

$$A_z \sim -\frac{j}{8\pi}\mu_0 I_0 \ell \int_{-\infty}^{\infty} C_v^{'}\left(k_z\right)\sqrt{\frac{2}{\pi k_{2\rho}\rho}} e^{-jk_z z - j\left(k_{2\rho}\rho - \pi/4\right)} dk_z$$

or

$$A_z \sim -\frac{j}{8\pi}\mu_0 I_0 \ell \int_{-\infty}^{\infty} C_v^{'}\left(k_z\right) e^{j\pi/4}\sqrt{\frac{2}{\pi k_{2\rho}\rho}} e^{-j\psi(k_z)} dk_z$$

where

$$\psi\left(k_z\right) = k_z z + k_{2\rho}\rho = k_z z + \sqrt{k_2^2 - k_z^2}\,\rho$$

Differentiating with respect to k_z to determine the saddle-point, we have

$$\psi'\left(k_z\right) = z - \frac{k_z}{\sqrt{k_2^2 - k_z^2}}\rho = 0$$

or

$$\frac{k_z}{\sqrt{k_2^2 - k_z^2}} = z/\rho = \cot\theta_2$$

where, consequently,

$$k_z^s = k_2 \cos\theta_2 = k_2 \frac{z}{r}$$

$$k_{2\rho}^s = k_2 \sin\theta_2 = k_2 \frac{\rho}{r}$$

It is interesting to note that if we average the value of k_z, we obtain the same result as the saddle point. That is,

$$\langle k_z \rangle = \frac{-\frac{j}{8\pi}\int_{-\infty}^{\infty} k_z H_0^{(2)}(k_{2\rho}\rho)\, e^{-jk_z z} dk_z}{-\frac{j}{8\pi}\int_{-\infty}^{\infty} H_0^{(2)}(k_{2\rho}\rho)\, e^{-jk_z z} dk_z} = \frac{j\frac{\partial}{\partial z}\left(\frac{e^{-jk_2 r}}{4\pi r}\right)}{\left(\frac{e^{-jk_2 r}}{4\pi r}\right)}$$

$$= j\cos\theta \frac{\frac{\partial}{\partial r}\left(\frac{e^{-jk_2 r}}{4\pi r}\right)}{\left(\frac{e^{-jk_2 r}}{4\pi r}\right)} = \frac{z}{r}\left(k_2 - \frac{1}{r}\right) \sim k_2 \frac{z}{r}$$

(In a similar manner, averaging $k_{2\rho}$ yields the same result as $k_{2\rho}^s$.) By next using the dipole source relationship,

$$-\frac{j}{8\pi}\mu_0 I_0 \ell \int_{-\infty}^{\infty} H_0^{(2)}(k_{2\rho}\rho)\, e^{-jk_z z} dk_z = \mu_0 I_0 \ell \frac{e^{-jk_2 r}}{4\pi r}$$

the evaluation of A_z at the saddle point becomes

$$A_z \sim C_v'\left(k_z^s, k_{2\rho}^s\right) \mu_0 I_0 \ell \frac{e^{-jk_2 r}}{4\pi r}$$

where

$$C_v'\left(k_z^s, k_{2\rho}^s\right) = \frac{-j2}{\pi}\frac{k_\rho \varepsilon_2}{k_{2\rho}^s a}\left[\frac{1}{\varepsilon k_{2\rho} J_1(k_\rho a)\, H_0^{(2)}\left(k_{2\rho}^s a\right) - \varepsilon_2 k_\rho J_0(k_\rho a)\, H_1^{(2)}\left(k_{2\rho}^s a\right)}\right]$$

and k_ρ is evaluated within the hole as

$$k_\rho = \sqrt{k^2 - \left(k_z^s\right)^2}$$

As with the dipole approximation to the magnetic vector potential, the field results corresponding to the saddle point evaluation of A_z will be examined in the next section and compared to the exact numerical integration of the potential integral. It is important to note that here, unlike the previous approximation, the coefficient $C_v'\left(k_z^s, k_{2\rho}^s\right)$ is not a constant but rather, a function of $z/r, \rho/r$, or θ. This is a consequence

of the modifications to the radiation pattern resulting from the local hole effect on the source.

5.2.3 Numerical and Asymptotic Evaluations of H_φ

In the case of the vertical dipole, we found the asymptotic form of the magnetic vector potential to be given by

$$A_z \sim C^a\left(k_z, k_{2\rho}\right)\frac{e^{-jk_2 r}}{4\pi r}\,,\ \rho > a\,,\ z >> a$$

where, approximating the potential as that of a dipole source in a homogenous medium,

$$C^a\left(k_z, k_{2\rho}\right) = \frac{1}{J_0\left(k_{02}a\right)}\mu_0 I_0 \ell \tag{1}$$

(as stated previously, here the scaling factor $C^a\left(k_z, k_{2\rho}\right)$ is a constant or independent of the observation point and is strictly a dipole field). On the other hand, using a saddle-point evaluation of the asymptotic integral,

$$C^a\left(k_z, k_{2\rho}\right) = C_v^{'}\left(k_z^s, k_{2\rho}^s\right)$$

$$= -\mu_0 I_0 \ell \frac{j2}{\pi}\frac{k_\rho \varepsilon_2}{k_{2\rho}^s a}\left[\frac{1}{\varepsilon k_{2\rho} J_1\left(k_\rho a\right) H_0^{(2)}\left(k_{2\rho}^s a\right) - \varepsilon_2 k_\rho J_0\left(k_\rho a\right) H_1^{(2)}\left(k_{2\rho}^s a\right)}\right] \tag{2}$$

Here $\varepsilon_{2,} k_2$ are the permittivity and wavenumber characterizing the medium surrounding the hole. Using these forms of the magnetic vector potential, the asymptotic field component H_φ can then be written as

$$\mu_0 H_\varphi = -\frac{\partial}{\partial \rho} A_z$$

$$H_\varphi^{asym} \sim -\frac{1}{\mu_0} C^a\left(k_z, k_{2\rho}\right)\frac{\partial}{\partial \rho}\frac{e^{-jk_2\sqrt{\rho^2+z^2}}}{4\pi\sqrt{\rho^2+z^2}}$$

$$H_\varphi^{asym} \sim -\frac{1}{\mu_0} C^a\left(k_z, k_{2\rho}\right)\left(-\frac{\rho e^{-jk_2 r}}{4\pi r^2}\right)\left(jk_2\right),\ \rho > a\,,\ z >> a \tag{3}$$

Alternatively, the integral representation of A_z is given by

$$A_z = \frac{1}{2\pi}\int_{-\infty}^{\infty} C\left(k_z\right) H_0^{(2)}\left(k_{2\rho}\rho\right) e^{-jk_z z} dk_z\,,\ \rho > a$$

where

$$C\left(k_z\right) = -\frac{1}{2\pi}\mu_0 I_0 \ell \frac{k_\rho \varepsilon_2}{k_{2\rho} a}\left[\frac{1}{\varepsilon k_{2\rho} J_1\left(k_\rho a\right) H_0^{(2)}\left(k_{2\rho} a\right) - \varepsilon_2 k_\rho J_0\left(k_\rho a\right) H_1^{(2)}\left(k_{2\rho} a\right)}\right]$$

so that

$$\mu_0 H_\varphi^{num} = -\frac{1}{2\pi}\int_{-\infty}^{\infty} C\left(k_z\right)\frac{\partial}{\partial\rho}H_0^{(2)}\left(k_{2\rho}\rho\right)e^{-jk_z z}dk_z$$

$$\mu_0 H_\varphi^{num} = -\frac{1}{2\pi}\int_{-\infty}^{\infty} C\left(k_z\right)k_{2\rho}H_0^{(2)'}\left(k_{2\rho}\rho\right)e^{-jk_z z}dk_z$$

$$H_\varphi^{num} = \frac{1}{2\pi\mu_0}\int_{-\infty}^{\infty} C\left(k_z\right)k_{2\rho}H_1^{(2)}\left(k_{2\rho}\rho\right)e^{-jk_z z}dk_z$$

Note that, due to the even nature of the integrand with respect to the integration variable k_z over the range $(-\infty,\infty)$, this can also be written

$$H_\varphi^{num} = \frac{1}{\pi\mu_0}\int_{0}^{\infty} C\left(k_z\right)k_{2\rho}H_1^{(2)}\left(k_{2\rho}\rho\right)\cos\left(k_z z\right)dk_z \tag{4}$$

5.2.4 Results

The asymptotic evaluations of H_φ at the interface between an air and dry-sand medium, as well as the numerical evaluation of the field, are shown in Figure 10. It is important to note here that the asymptotic results correspond to a dipole in a homogeneous region approximation and also, the saddle-point evaluation of the asymptotic integral for A_z. The results are presented as a function of radial distance ρ from the hole and at a frequency of 300 MHz. The source is assumed to be located a distance of 10 m from the interface and the sand properties at this frequency are assumed to be $\varepsilon_r = 2.55\left(1 - j0.01\right)$ [1]. (In these results and those that follow, a unit-strength dipole moment is assumed $(I_0\ell = 1\ A\cdot m)$).

Thus, in this relatively low frequency case, it is observed that the hole has little effect on the radiated field and the field can most simply be taken as the field produced by a dipole positioned in a homogeneous medium with an amplitude weighted by 1. While the numerical calculation of H_φ best captures the null behavior in the radiation directly above the hole, the three sets of results are virtually indistinguishable as the radial distance from the hole increases.

Increasing the frequency to 3.0 GHz and using a sand permittivity of $\varepsilon_r = 2.55\left(1 - j0.0062\right)$ [1], the results shown in Figure 11 are obtained. In this case the presence of the hole is evident in the discrepancy between the dipole-field approximation (which has a constant coefficient $C^a\left(k_z, k_{2\rho}\right)$) and the numerical calculation of the magnetic field. However, the asymptotic evaluation of the field at the saddle-point is in excellent agreement with the results obtained from the numerical evaluation of the integral.

Thus, by examining the asymptotic form the fields in the lower half-space, we recognize that to an excellent approximation, the fields associated with a vertical dipole present within a cylindrical hole in the earth are, in general, the fields of a dipole located in a homogeneous medium scaled by the saddle-point coefficient $C_v^{'}\left(k_z^s, k_{2\rho}^s\right)$. Stated another way, we find here that the radiation pattern is modified from the simple dipole by the multiplicative factor $C_v^{'}\left(k_z^s, k_{2\rho}^s\right)$, which is a function of θ. (In the low-frequency case, the effect of the hole is to simply reduce the amplitude of the field produced by a dipole in a homogeneous medium by a constant independent of the observation point.) In the next section, the coefficient $C_v^{'}\left(k_z^s, k_{2\rho}^s\right)$ is used to determine the radiated fields in the upper half-space or air region.

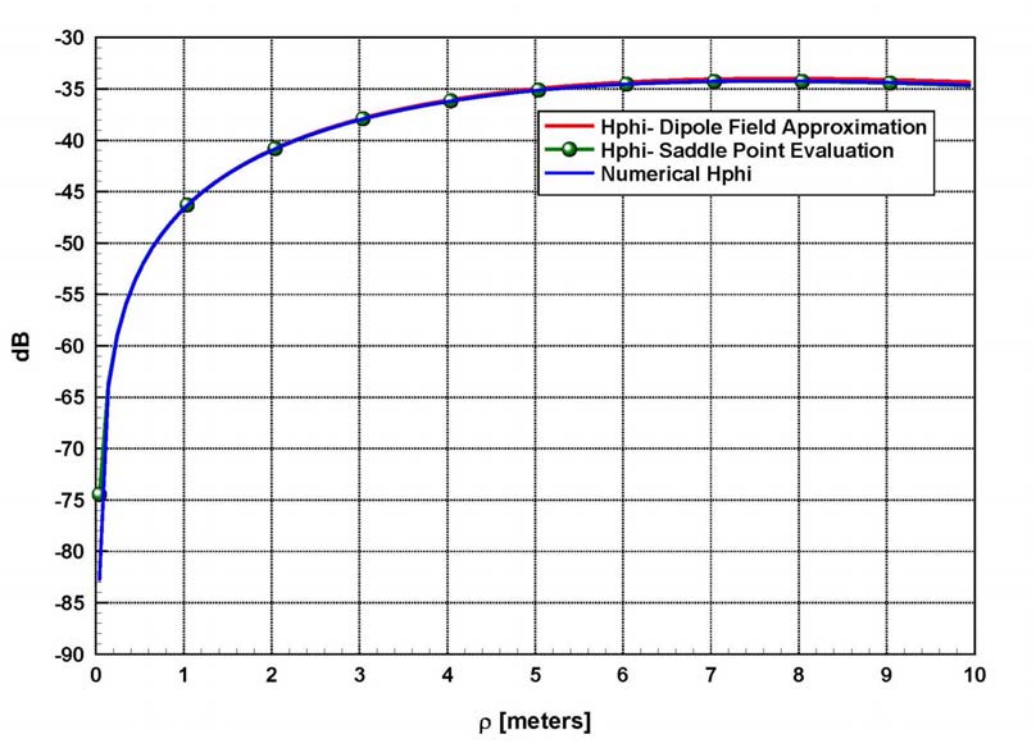

Figure 10. Azimuth magnetic field distributions along an air/dry sand interface at 300 MHz, determined using asymptotic expressions and an exact numerical evaluation.

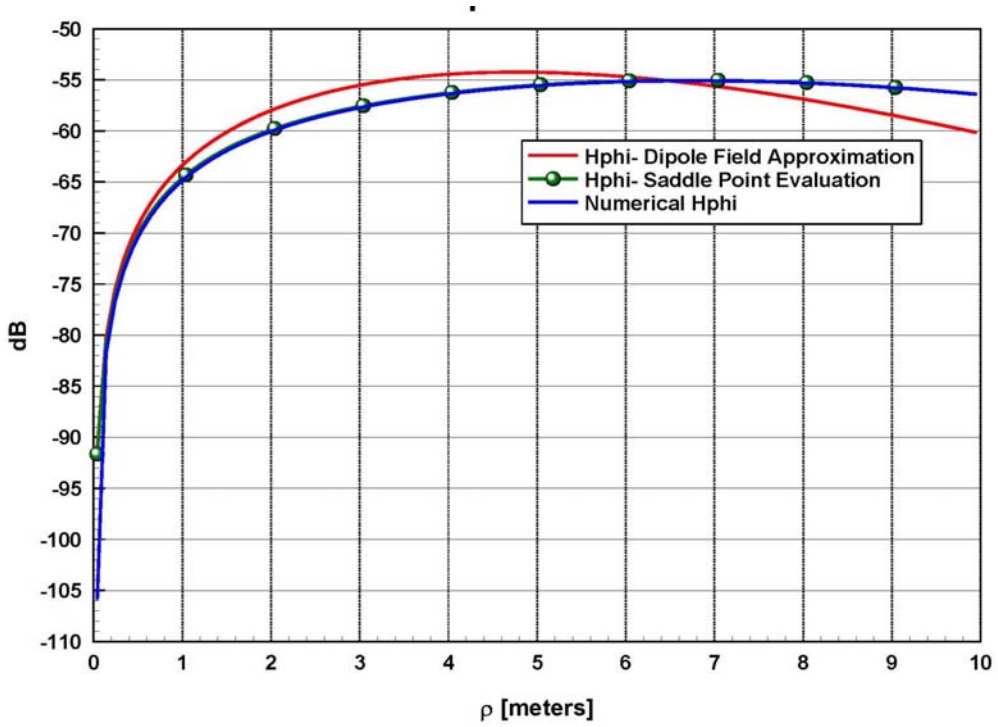

Figure 11. Azimuth magnetic field distributions along an air/dry sand interface at 3.0 GHz, determined using asymptotic expressions and an exact numerical evaluation.

5.3 Radiation in the Upper Half-Space

In this section, we use the saddle-point method of the potential-integral representation to evaluate the upper-half space radiation associated with a vertical dipole placed in a cylindrical hole. As a means of obtaining the final results, we first consider a vertical dipole positioned in a half-space with no hole present (homogeneous media). In this case, the saddle-point method is shown to yield identical far-zone results to those found in [6],[7], and [8]. By next assuming that the source is positioned far from the interface and, consequently, that a multipole representation can be used to model the hole effects, the field in the upper half-space is then shown to be a product of the multipole element pattern (determined from the lower-half space analysis presented above) and a pattern associated with ray transmission through the interface. Here it is important to note that the earth region was considered homogenous, although it could have been taken as a layered medium. In addition, we note that, although not done so in the case of the vertical dipole (due to the null in the radiation pattern along the hole direction), a small contribution to the radiation resulting from the hole intersection with the interface (corresponding to an electric-field discontinuity) can be added to assess the error associated with ignoring the hole intersection with the upper-half space..

5.3.1 Half-Space Problem: No Hole

The formulation of a dipole interacting with a half space can be found in [9]. In addition, the case where the dipole is in the conducting half space along with many expansions of the field can be found in [6] and more recent expansions can be found in [7] and [8]. Here we give far-zone expansions in the upper half-space by a saddle point treatment of the potential integrals, which can be shown to produce equivalent fields to the previously cited results.

In the case of a vertical dipole in the conductive half space, the source term is

$$A_z^s = \mu_0 I_0 \ell \frac{e^{-jk_2 r}}{4\pi r}$$

Note that for a triangular current distribution, we can take $I_0 = I(0)$ (the current at the center of the dipole), and ℓ as the physical half height of the antenna. We can expand the Green's function as

$$A_z^s = \mu_0 I_0 \ell \int_0^\infty D(k_\rho) J_0(k_\rho \rho) e^{-jk_{2z}|z|} k_\rho dk_\rho$$

where

$$k_{2z} = \sqrt{k_2^2 - k_\rho^2}$$

and

$$\mathrm{Im}(k_{2z}) \leq 0$$

To solve for the coefficient $D(k_\rho)$ we write

$$\left(\nabla^2 + k_2^2\right) A_z^s = \left[\frac{1}{\rho}\frac{\partial}{\partial \rho}\left(\rho \frac{\partial A_z^s}{\partial \rho}\right) + \frac{\partial^2}{\partial z^2} + k_2^2\right] A_z^s = -\mu_0 I_0 \ell \frac{\delta(\rho)}{2\pi\rho}\delta(z)$$

so that

$$\int_0^\infty \left[\frac{1}{\rho}\frac{\partial}{\partial\rho}\left(\rho\frac{\partial}{\partial\rho}\right)+\frac{\partial^2}{\partial z^2}+k_2^2\right] D\left(k_\rho\right) J_0\left(k_\rho\rho\right) e^{-jk_{2z}|z|} k_\rho dk_\rho = -\frac{\delta\left(z\right)\delta\left(\rho\right)}{2\pi\rho}$$

$$= \int_0^\infty D\left(k_\rho\right) J_0\left(k_\rho\rho\right)\left(\frac{\partial^2}{\partial z^2}+k_2^2-k_\rho^2\right) e^{-jk_{2z}|z|} k_\rho dk_\rho$$

Inverting the Hankel transform gives

$$D\left(k_\rho\right)\left(\frac{\partial^2}{\partial z^2}+k_2^2-k_\rho^2\right) e^{-jk_{2z}|z|} = -\frac{\delta\left(z\right)}{2\pi}\int_0^\infty J_0\left(k_\rho\rho\right)\delta\left(\rho\right) d\rho = -\frac{\delta\left(z\right)}{2\pi}$$

where integration with respect to z yields

$$D\left(k_\rho\right) = -\frac{j}{4\pi k_{2z}}$$

Now we take as the source potential

$$A_z^s = -\frac{j}{4\pi}\mu_0 I_0 \ell \int_0^\infty J_0\left(k_\rho\rho\right) e^{-jk_{2z}|z+h|}\frac{k_\rho dk_\rho}{k_{2z}}$$

with the source-free potentials given by

$$A_z = \mu_0 I_0 \ell \int_0^\infty E\left(k_\rho\right) J_0\left(k_\rho\rho\right) e^{-jk_z z} k_\rho dk_\rho\,,\ z>0$$

$$= \mu_0 I_0 \ell \int_0^\infty F\left(k_\rho\right) J_0\left(k_\rho\rho\right) e^{jk_{2z}z} k_\rho dk_\rho\,,\ z<0$$

$$k_z = \sqrt{k^2-k_\rho^2}$$

and enforce the boundary conditions at $z=0$ using

$$H_\varphi = -\frac{1}{\mu_0}\frac{\partial}{\partial\rho}A_z$$

and

$$E_\rho = \frac{-j}{\omega\mu_0\varepsilon}\frac{\partial^2}{\partial\rho\partial z}A_z$$

Thus, enforcing continuity along the air-earth interface, we have

$$E\left(k_\rho\right) = -\frac{j}{4\pi k_{2z}} e^{-jk_{2z}h} + F\left(k_\rho\right)$$

and

$$-\frac{j}{4\pi k_{2z}}e^{-jk_{2z}h} - F\left(k_\rho\right) = \frac{\varepsilon_2 k_z}{\varepsilon_0 k_{2z}}E\left(k_\rho\right)$$

The coefficient for the potential in the upper-half space region then becomes

$$-\frac{j}{2\pi}\frac{\varepsilon_0}{\varepsilon_2 k_z + \varepsilon_0 k_{2z}}e^{-jk_{2z}h} = E\left(k_\rho\right)$$

so that

$$A_z = -\frac{j}{2\pi}\mu_0 I_0 \ell \int_0^\infty \frac{\varepsilon_0}{\varepsilon_2 k_z + \varepsilon_0 k_{2z}}e^{-jk_{2z}h}J_0\left(k_\rho\rho\right)e^{-jk_z z}k_\rho dk_\rho$$

We can also write this potential integral as

$$A_z = -\frac{j}{4\pi}\mu_0 I_0 \ell \int_0^\infty \frac{\varepsilon_0}{\varepsilon_2 k_z + \varepsilon_0 k_{2z}}e^{-jk_{2z}h}\left[H_0^{(2)}\left(k_\rho\rho\right) + H_0^{(1)}\left(k_\rho\rho\right)\right]e^{-jk_z z}k_\rho dk_\rho$$

or

$$A_z = -\frac{j}{4\pi}\mu_0 I_0 \ell \int_0^\infty \frac{\varepsilon_0}{\varepsilon_2 k_z + \varepsilon_0 k_{2z}}e^{-jk_{2z}h}H_0^{(2)}\left(k_\rho\rho\right)e^{-jk_z z}k_\rho dk_\rho$$

$$-\frac{j}{4\pi}\mu_0 I_0 \ell \int_0^\infty \frac{\varepsilon_0}{\varepsilon_2 k_z + \varepsilon_0 k_{2z}}e^{-jk_{2z}h}H_0^{(1)}\left(k_\rho\rho\right)e^{-jk_z z}k_\rho dk_\rho$$

Using a change of variables for the second integral contribution,

$$k_\rho = k_\rho^{'}e^{j\pi}$$

A_z becomes

$$A_z = -\frac{j}{4\pi}\mu_0 I_0 \ell \int_0^\infty \frac{\varepsilon_0}{\varepsilon_2 k_z + \varepsilon_0 k_{2z}}e^{-jk_{2z}h}H_0^{(2)}\left(k_\rho\rho\right)e^{-jk_z z}k_\rho dk_\rho$$

$$-\frac{j}{4\pi}\mu_0 I_0 \ell \int_0^{-\infty} \frac{\varepsilon_0}{\varepsilon_2 k_z + \varepsilon_0 k_{2z}}e^{-jk_{2z}h}H_0^{(1)}\left(k_\rho^{'}e^{j\pi}\rho\right)e^{-jk_z z}k_\rho^{'}dk_\rho^{'}$$

or

$$A_z = -\frac{j}{4\pi}\mu_0 I_0 \ell \int_0^\infty \frac{\varepsilon_0}{\varepsilon_2 k_z + \varepsilon_0 k_{2z}}e^{-jk_{2z}h}H_0^{(2)}\left(k_\rho\rho\right)e^{-jk_z z}k_\rho\ dk_\rho$$

$$-\frac{j}{4\pi}\mu_0 I_0 \ell \int_{-\infty}^0 \frac{\varepsilon_0}{\varepsilon_2 k_z + \varepsilon_0 k_{2z}}e^{-jk_{2z}h}H_0^{(2)}\left(k_\rho\rho\right)e^{-jk_z z}k_\rho\ dk_\rho$$

if we use the analytic continuation of the Hankel function [4]

$$H_0^{(1)}\left(ze^{j\pi}\right) = -H_0^{(2)}\left(z\right)$$

and the fact that k_z is an even function of k_ρ. Thus,

$$A_z = -\frac{j}{4\pi}\mu_0 I_0 \ell \int_{-\infty}^{\infty} \frac{\varepsilon_0}{\varepsilon_2 k_z + \varepsilon_0 k_{2z}} e^{-jk_{2z}h} H_0^{(2)}\left(k_\rho \rho\right) e^{-jk_z z} k_\rho \, dk_\rho$$

Here we note that there are branch points at k_ρ equal to k and k_2. An additional branch point is introduced in the Hankel functions at $k_\rho = 0$ (we can choose the original contour either above or below this point because it is not a branch point of $J_0\left(k_\rho \rho\right)$). Since we do not want to include this branch cut for $z > 0$, we choose the original contour below the origin and note that poles occur if

$$\varepsilon_2 k_z + \varepsilon_0 k_{2z} = \varepsilon_2 \sqrt{k^2 - k_\rho^2} + \varepsilon_0 \sqrt{k_2^2 - k_\rho^2} = 0$$

We assume we can deform the contour for each term through a saddle point for which $|k_\rho|\,\rho >> 1$ (we leave out the overhead point $\rho \to 0$, as well as the approach to the surface $z = 0$, for the time being). Thus, for large arguments we can expand the Hankel function as

$$H_0^{(2)}\left(k_\rho \rho\right) \sim \sqrt{\frac{2}{\pi k_\rho \rho}} e^{-jk_\rho \rho + j\pi/4}$$

We take $\rho = r\sin\theta$ and $z = r\cos\theta$ with $0 < \theta < \pi/2$ and let $kr \to \infty$. The large argument exponential phase function then takes the form

$$\exp\left[-j\left(k_z z + k_\rho \rho\right)\right] = \exp\left[-jkr\psi\left(\tau\right)\right]$$

where $k_\rho = k\tau$ and $k_z = k\sqrt{1-\tau^2}$

$$\psi\left(\tau\right) = \tau\sin\theta + \sqrt{1-\tau^2}\cos\theta$$

The saddle points are at

$$\psi'\left(\tau_s\right) = \sin\theta - \frac{\tau}{\sqrt{1-\tau^2}}\cos\theta = 0$$

or

$$\tau_s = \sin\theta$$

where

$$\psi\left(\tau_s\right) = 1$$

The steepest descent contours are defined by

$$\mathrm{Re}\left[\psi\left(\tau\right) - \psi\left(\tau_s\right)\right] = \mathrm{Re}\left[\tau\sin\theta + \sqrt{1-\tau^2}\cos\theta - 1\right] = 0$$

If we approximate near τ_s by letting $\tau = \tau_s + \delta$ we have

$$\mathrm{Re}\left[(\sin\theta+\delta)\sin\theta+\sqrt{1-(\sin\theta+\delta)^2}\cos\theta\right]=1$$

$$=\mathrm{Re}\left[(\sin\theta+\delta)\sin\theta+\sqrt{1-2\delta\sin\theta/\cos^2\theta-\delta^2/\cos^2\theta}\cos^2\theta\right]$$

$$=\mathrm{Re}\left[(\sin\theta+\delta)\sin\theta+\left\{1-\delta\sin\theta/\cos^2\theta-\frac{1}{2}\delta^2/\cos^2\theta-\frac{1}{2}\delta^2\sin^2\theta/\cos^4\theta\right\}\cos^2\theta\right]$$

$$=\mathrm{Re}\left[-\frac{1}{2}\delta^2-\frac{1}{2}\delta^2\sin^2\theta/\cos^2\theta\right]+1$$

or

$$-\frac{1}{2}\sec^2\theta\,\mathrm{Re}\left(\delta^2\right)=-\frac{1}{2}\left(\delta'^2-\delta''^2\right)\sec^2\theta=0$$
$$\delta'^2=\delta''^2$$

where $\delta=\delta'+j\delta''$. Noting that

$$-\frac{1}{2}\sec^2\theta\,\mathrm{Im}\left(\delta^2\right)=-\delta'\delta''\sec^2\theta$$

we see that

$$-j\psi\left(\tau\right)=-j\psi\left(\tau_s+\delta\right)\sim-j+j\frac{1}{2}\delta^2\sec^2\theta$$

and on the constant phase contours that

$$-j\psi\left(\tau\right)\sim-j-\delta'\delta''\sec^2\theta$$

Thus, from these expression, it is evident that $\delta'>0$ and $\delta''>0$ or $\delta'<0$ and $\delta''<0$ lead to descent on both sides of each saddle point. Letting

$$\delta=ve^{j\pi/4}$$

with $k_\rho=k\tau=k\tau_s+k\delta$ we see that

$$dk_\rho=kd\tau=ke^{j\pi/4}dv$$

$$k_\rho\sim k\sin\theta$$
$$k_z\sim k\cos\theta$$

$$-j\psi\left(\tau\right)\sim-j-\frac{1}{2}v^2\sec^2\theta$$

Using the saddle point contributions alone we have

$$A_z \sim -\frac{j}{4\pi}\mu_0 I_0 \ell \sqrt{\frac{2}{\pi\rho}} \int_{-\infty}^{\infty} \frac{\varepsilon_0 \sqrt{k_\rho}}{\varepsilon_2 k_z + \varepsilon_0 k_{2z}} e^{-jk_{2z}h + j\pi/4} e^{-jk_\rho \rho} e^{-jk_z z} dk_\rho$$

$$\sim -\frac{j}{4\pi}\mu_0 I_0 \ell \sqrt{\frac{2}{\pi\rho}} \frac{\varepsilon_0 \sqrt{k_\rho^s}}{\varepsilon_2 k_z^s + \varepsilon_0 k_{2z}^s} e^{-jk_{2z}^+ h + j\pi/4 - jkr} \int_{-\infty}^{\infty} e^{-\frac{1}{2}krv^2 \sec^2\theta} k e^{j\pi/4} dv$$

$$\sim \frac{e^{-jk_{2z}^s h - jkr}}{4\pi r}\mu_0 I_0 \ell \sqrt{\frac{2}{\pi \sin\theta}} \frac{\varepsilon_0 \sqrt{k \sin\theta}}{\varepsilon_2 k_z^s + \varepsilon_0 k_{2z}^s} \cos\theta \sqrt{2\pi k}$$

$$\sim \frac{k e^{-jk_{2z}^s h - jkr}}{2\pi r}\mu_0 I_0 \ell \frac{\varepsilon_0}{\varepsilon_2 k_z^s + \varepsilon_0 k_{2z}^s} \cos\theta$$

Finally because

$$k_z^s = k\cos\theta$$

$$k_{2z}^s = \sqrt{k_2^2 - k^2 \sin^2\theta}$$

we have

$$A_z \sim \frac{k e^{-jh\sqrt{k_2^2 - k^2\sin^2\theta} - jkr}}{2\pi r}\mu_0 I_0 \ell \frac{\varepsilon_0}{\varepsilon_2 k\cos\theta + \varepsilon_0 \sqrt{k_2^2 - k^2\sin^2\theta}} \cos\theta$$

To now transform the magnetic vector potential to spherical coordinates, we use the unit-vector relation

$$\underline{e}_z = \underline{e}_r \cos\theta - \underline{e}_\theta \sin\theta$$

and find

$$A_r \sim \frac{k e^{-jh\sqrt{k_2^2 - k^2\sin^2\theta} - jkr}}{2\pi r}\mu_0 I_0 \ell \frac{\varepsilon_0}{\varepsilon_2 k\cos\theta + \varepsilon_0 \sqrt{k_2^2 - k^2\sin^2\theta}} \cos^2\theta$$

$$A_\theta \sim -\frac{k e^{-jh\sqrt{k_2^2 - k^2\sin^2\theta} - jkr}}{2\pi r}\mu_0 I_0 \ell \frac{\varepsilon_0}{\varepsilon_2 k\cos\theta + \varepsilon_0 \sqrt{k_2^2 - k^2\sin^2\theta}} \sin\theta\cos\theta$$

Next using

$$H_\varphi = \frac{1}{\mu_0}\frac{1}{r}\left[\frac{\partial}{\partial r}(rA_\theta) - \frac{\partial A_r}{\partial\theta}\right]$$

we obtain, in the far zone,

$$H_\varphi \sim -j\frac{k}{\mu_0}A_\theta \sim j\frac{k^2 e^{-jh\sqrt{k_2^2 - k^2\sin^2\theta} - jkr}}{2\pi r} I_0 \ell \frac{\varepsilon_0}{\varepsilon_2 k\cos\theta + \varepsilon_0 \sqrt{k_2^2 - k^2\sin^2\theta}} \sin\theta\cos\theta$$

$$\sim I_0 \ell \frac{e^{-jkr}}{4\pi r} e^{-jh\sqrt{k_2^2 - k^2 \sin^2\theta}} \frac{jk \sin(2\theta)}{(\varepsilon_2/\varepsilon_0)\cos\theta + \sqrt{(\varepsilon_2/\varepsilon_0) - \sin^2\theta}} \tag{5}$$

which is identical to the series of formulas: (1.18) p. 7, (2.104) p. 43, (2.147) p. 53, and the leading term of the result (6.37) p. 180 in [6]. The far-zone electric field is then

$$E_\theta \sim H_\varphi / \eta_0$$

For convenience in determining the far-zone magnetic field when the hole is considered, H_φ can be rewritten as

$$H_\varphi \sim \left[\frac{jk\,(I_0\ell)}{4\pi r} e^{-jkr} \sin\theta\right] \left[\frac{2ke^{-jh\sqrt{k_2^2 - k^2\sin^2\theta}}\varepsilon_0 \cos\theta}{\varepsilon_2 k \cos\theta + \varepsilon_0\sqrt{k_2^2 - k^2\sin^2\theta}}\right]$$

where the first term in brackets is the far-field pattern of the vertical dipole antenna and the second term is associated with the rays transmitted through the interface and arriving at the observation angle θ.

5.3.2 Half-Space Problem: Including Hole

Comparing the radiated field by a vertical dipole in a lower-half space k_2 medium to the field radiated in the upper half-space by the same dipole (positioned in the lower half-space), we find that the field is modified only by a term related to ray transmission through the material interface. The purpose of this section is to demonstrate that the same relationship between the lower-half space radiation associated with the dipole within a hole in the earth and the radiation in the upper-half space holds; that is, the upper-half space pattern is the lower-half space pattern scaled by a transmission term. Since we are assuming that the source is located far from the earth-air interface, and, consequently, that any radiated field can be represented in terms of multipoles, here we demonstrate this relationship for any general multipole expansion.

Thus, for the purposes of determining the upper-half space radiation accounting for the presence of the hole, we first examine the forms of the lower and upper half-space patterns in the case of a homogeneous lower-half space region. In the lower-half space, the dipole far-field radiation is given by

$$H_\varphi^{L,dipole} = \left[\frac{jk_2}{4\pi r}(I_0\ell)\, e^{-jk_2 r} \sin\theta_2\right]$$

where, in general, the radiation associated with additional multipoles ($n = 0$ corresponding to a dipole) can be found as

$$H_\varphi^{L,n} = \frac{\partial}{\partial z} H_\varphi^{L,(n-1)}$$

or

$$H_\varphi^{L,n} = j\frac{k_2}{4\pi r}(I_0\ell)\, e^{-jk_2 r} \sin\theta_2 \,(-jk_2\cos\theta_2)^n$$

Using a power-series expansion, the total field accounting for all multipoles can, by superposition, then be written as

$$\frac{H_{\varphi}^{L}\left(\theta_{2}\right)}{\sin\theta_{2}}=\sum_{n=0}^{n=\infty}l_{n}\left(-jk_{2}\cos\theta_{2}\right)^{n}$$

where l_n are the multipole coefficients. Now, referring to the derivation presented above (the result which was verified with [6]), we have

$$H_{\varphi}\sim\left[\frac{jk\left(I_{0}\ell\right)}{4\pi r}e^{-jkr}\sin\theta\right]\left[\frac{2ke^{-jh\sqrt{k_{2}^{2}-k^{2}\sin^{2}\theta}}\varepsilon_{0}\cos\theta}{\varepsilon_{2}k\cos\theta+\varepsilon_{0}\sqrt{k_{2}^{2}-k^{2}\sin^{2}\theta}}\right]$$

for the upper-half space radiation associated with a dipole. In this case, to account for higher-order multipoles, we differentiate with respect to the parameter h to obtain

$$H_{\varphi}^{U,n}=\left(-jk_{2}\cos\theta_{2}\right)^{n}\left[\frac{jk\left(I_{0}\ell\right)}{4\pi r}e^{-jkr}\sin\theta\right]\left[\frac{2ke^{-jhk_{2}\cos\theta_{2}}\varepsilon_{0}\cos\theta}{\varepsilon_{2}k\cos\theta+\varepsilon_{0}k_{2}\cos\theta_{2}}\right]$$

where n is the order of the multipole moment. Using Snell's Law, this can also be written as

$$H_{\varphi}^{U,n}=\left(-jk_{2}\cos\theta_{2}\right)^{n}\left[\frac{jk_{2}\left(I_{0}\ell\right)}{4\pi r}e^{-jkr}\sin\theta_{2}\right]\left[\frac{2ke^{-jhk_{2}\cos\theta_{2}}\varepsilon_{0}\cos\theta}{\varepsilon_{2}k\cos\theta+\varepsilon_{0}k_{2}\cos\theta_{2}}\right]$$

where the pattern can be interpreted as a product of the element pattern of a $n-pole$ antenna with a term associated with ray transmission through the interface. Written in terms of a power series expansion in θ_2, the element pattern associated with each individual multipole,

$$e^{U,n}\left(\theta_{2}\right)=\left(-jk_{2}\cos\theta_{2}\right)^{n}\left[\frac{jk_{2}\left(I_{0}\ell\right)}{4\pi r}e^{-jkr}\sin\theta_{2}\right]$$

can be summed to form the element pattern associated with the entire system of multipoles. That is, we would have

$$e_{n}^{U}\left(\theta_{2}\right)=\frac{e^{U}\left(\theta_{2}\right)}{\sin\theta_{2}}=\sum u_{n}\left(-jk_{2}\cos\theta_{2}\right)^{n}$$

and, comparing this to the lower-half space element pattern, we find that the element pattern remains the same in both the lower and upper-half space field representations. Here u_n are the multipole coefficients characterizing the upper half-space radiation. Therefore, in terms of the power-series expansions,

$$l_{n}=u_{n}$$

If we assume that the antenna source is located far away from the interface then, based on this result, the multipole representation of the field can be used to model the effects of the hole on the overall radiation pattern, in *both* the lower and half-space regions. We recall that from the saddle-point analysis for the fields in the k_2 medium, the azimuthal component of the magnetic field was found to be

$$H_{\varphi}^{asym} \sim \frac{1}{\mu_0} C^a\left(k_z, k_{2\rho}\right)\left(\frac{e^{-jk_2 r}}{4\pi r}\right)\left(jk_2 \sin\theta_2\right)$$

(we use the angle θ_2 since we are examining a field in the k_2 region) where

$$C^a\left(k_z, k_{2\rho}\right) = -\mu_0 I_0 \ell \frac{j2}{\pi}\frac{k_\rho \varepsilon_2}{k_{2\rho}^s a}\left[\frac{1}{\varepsilon k_{2\rho} J_1\left(k_\rho a\right) H_0^{(2)}\left(k_{2\rho}^s a\right) - \varepsilon_2 k_\rho J_0\left(k_\rho a\right) H_1^{(2)}\left(k_{2\rho}^s a\right)}\right]$$

Thus, given that the hole effect contained in $C^a\left(k_z, k_{2\rho}\right)$ can be modeled with a multipole expansion, the radiation pattern in the upper half-space region including the effects of the hole can very simply be written as

$$H_\varphi \sim C_v^{'}\left(k_z^s, k_{2\rho}^s\right)\left[\frac{jk\left(I_0\ell\right)}{4\pi r} e^{-jkr}\sin\theta\right]\left[\frac{2ke^{-jh\sqrt{k_2^2 - k^2\sin^2\theta}}\varepsilon_0\cos\theta}{\varepsilon_2 k\cos\theta + \varepsilon_0\sqrt{k_2^2 - k^2\sin^2\theta}}\right]$$

where

$$C_v^{'}\left(k_z^s, k_{2\rho}^s\right) = -\frac{j2}{\pi}\frac{k_\rho \varepsilon_2}{k_{2\rho}^s a}\left[\frac{1}{\varepsilon k_{2\rho} J_1\left(k_\rho a\right) H_0^{(2)}\left(k_{2\rho}^s a\right) - \varepsilon_2 k_\rho J_0\left(k_\rho a\right) H_1^{(2)}\left(k_{2\rho}^s a\right)}\right] \tag{6}$$

and the saddle points $k_z^s, k_{2\rho}^s$ in the k_2 region have been defined above. It should be noted that a line-source distribution of current can also be used to model the effects of the hole. The result in this case will be the same provided that the current is concentrated at depth h, so that there is little interaction between the source and the interface.

5.3.3 Results

To demonstrate the dependence of the transmitted energy into the upper-half space region on the antenna frequency and the characteristics of the earth, dry sand and sand with a moisture content of 2.18% are considered at 3.0 GHz and 300 MHz. For the radiation patterns shown, the hole was assumed to have a radius of 0.04 m and the dipole was assumed to be located a distance of 10 m from the air-earth interface. From [1], the relative permittivities of dry sand were taken to be $2.55(1-j0.01)$ and $2.55(1-j0.0062)$, while those for the sand with a 2.18% moisture were taken as $2.5(1-j0.026)$ and $2.5(1-j0.03)$ at 300 MHz and 3.0 GHz , respectively. The normalized H_φ component of radiation for these cases are shown in Figures 12 and 13, where the normalization is given by

$$H_\varphi^{norm} = \frac{4\pi r}{\left(I_o\ell\right)e^{-jkr}} H_\varphi$$

Thus, it is clear from the patterns that the energy transmitted into the air region is decreased with an increase in frequency or conductive loss associated with the earth. Also, it is important to note that the effect due to the earth losses becomes more pronounced at higher frequencies. Figure 14 shows the normalized H_φ patterns in the air region when sand with moisture levels of 3.88% and 16.8% is considered. Here the patterns are shown only for the frequency of 300 MHz, since with the high level of conductivity at 3.0 GHz virtually all of the energy is dissipated into the sand.

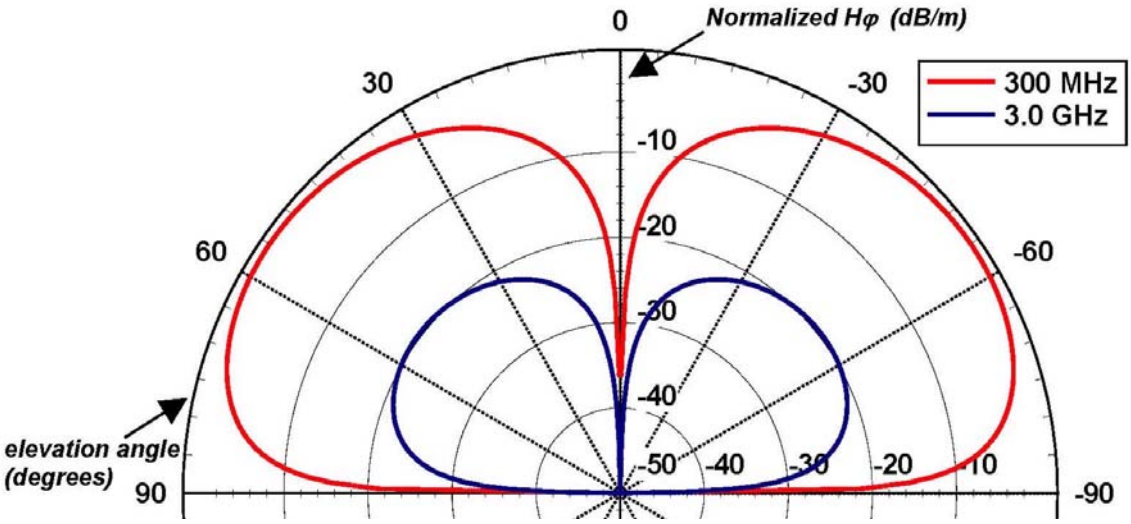

Figure 12. Far-field radiation patterns produced in the air region for a vertical dipole positioned in a hole contained in dry sand ($h = 10\ m,\ a = 0.04\ m$).

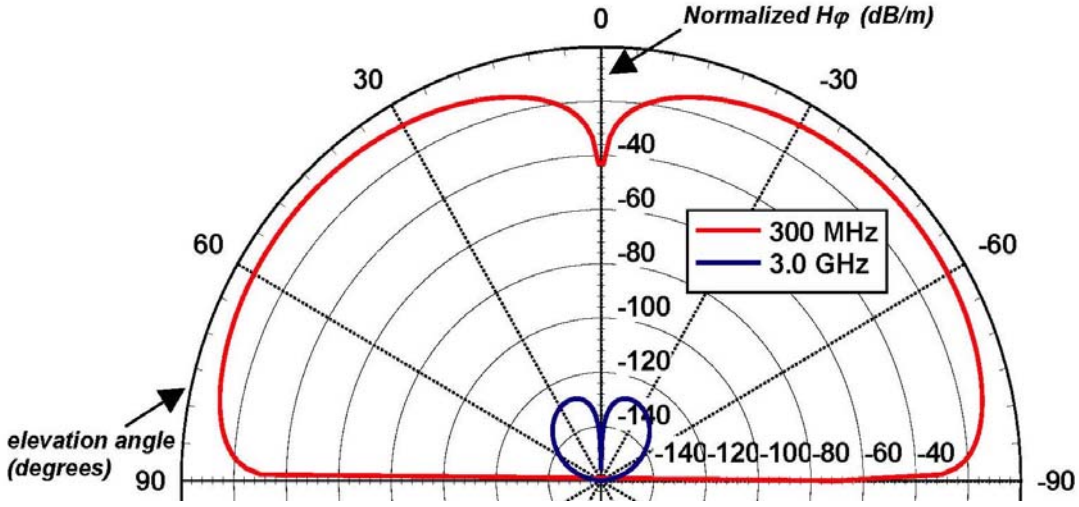

Figure 13. Far-field radiation patterns produced in the air region for a vertical dipole positioned in a hole contained in sand of 2.18% moisture content ($h = 10\ m,\ a = 0.04\ m$).

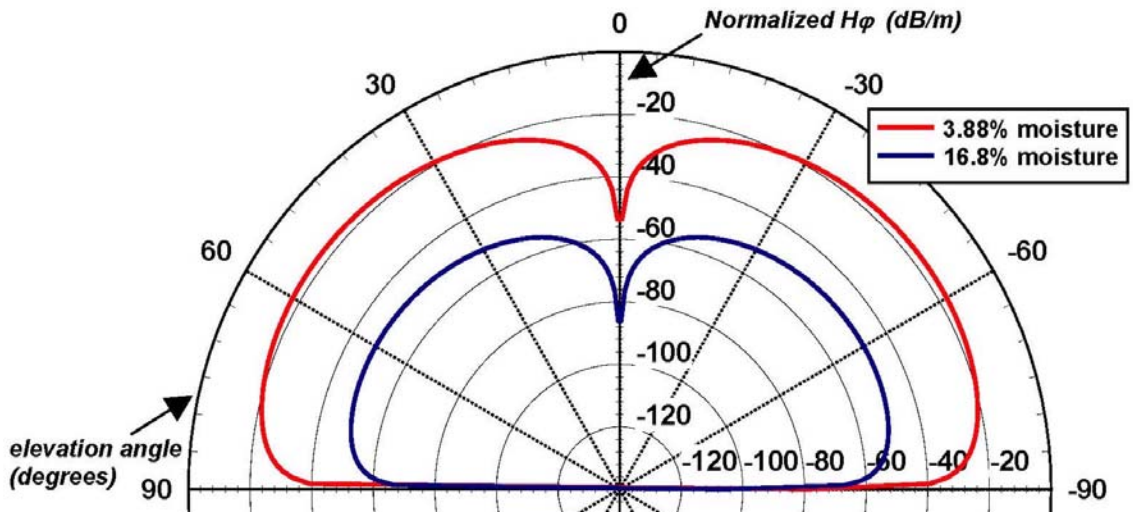

Figure 14. Far-field radiation patterns produced in the air region for a vertical dipole positioned in a hole contained in sand of various moisture contents at 300 MHz ($h = 10\ m,\ a = 0.04\ m$).

6 Horizontal-Dipole Radiation Characteristics

We next examine the radiation characteristics of a horizontally-oriented dipole positioned within a hole in the earth. The dipole is assumed to lie along the $x-$direction (Figure 1). As mentioned in the vertical-dipole section, this dipole orientation is much more complicated than the previous case since it leads to a coupled set of $E-$ and $H-$modes. We next examine the radiation characteristics of a horizontally-oriented dipole positioned within a hole in the earth. The dipole is assumed to lie along the $x-$direction (Figure 1). As mentioned in the vertical-dipole section, this dipole orientation is much more complicated than the previous case since it leads to a coupled set of $E-$ and $H-$modes.

For this case, the source potential is taken as

$$A_x^s = \mu_0 I_0 \ell \frac{e^{-jkr}}{4\pi r}$$

where the integral transform representation is

$$A_x^s = -\frac{j}{8\pi}\mu_0 I_0 \ell \int_{-\infty}^{\infty} H_0^{(2)}\left(k_\rho \rho\right) e^{-jk_z z} dk_z \, , \; 0 < \rho < a$$

Using the unit vector identity

$$\underline{e}_x = \underline{e}_\rho \cos\varphi - \underline{e}_\varphi \sin\varphi$$

this vector potential can be written in terms of the cylindrical components

$$A_\rho^s = -\frac{j}{8\pi}\mu_0 I_0 \ell \cos\varphi \int_{-\infty}^{\infty} H_0^{(2)}\left(k_\rho \rho\right) e^{-jk_z z} dk_z \, , \; 0 < \rho < a$$

$$A_\varphi^s = \frac{j}{8\pi}\mu_0 I_0 \ell \sin\varphi \int_{-\infty}^{\infty} H_0^{(2)}\left(k_\rho \rho\right) e^{-jk_z z} dk_z \, , \; 0 < \rho < a$$

Note that

$$\frac{1}{\rho}\left\{\frac{\partial}{\partial\rho}\left(\rho A_\rho^s\right) + \frac{\partial}{\partial\varphi}A_\varphi^s\right\} = \frac{j}{8\pi}\mu_0 I_0 \ell \cos\varphi \int_{-\infty}^{\infty} k_\rho H_1^{(2)}\left(k_\rho \rho\right) e^{-jk_z z} dk_z$$

In addition, we have the axial component of the magnetic vector potential ($E-$modes)

$$A_z = \cos\varphi \frac{1}{2\pi}\int_{-\infty}^{\infty} B_m\left(k_z\right) J_1\left(k_\rho \rho\right) e^{-jk_z z} dk_z \, , \; 0 < \rho < a$$

$$= \cos\varphi \frac{1}{2\pi}\int_{-\infty}^{\infty} C_m\left(k_z\right) H_1^{(2)}\left(k_{2\rho} \rho\right) e^{-jk_z z} dk_z \, , \; \rho > a$$

and the axial component of the electric vector potential ($H-$modes)

$$A_{ez} = \sin\varphi \frac{1}{2\pi} \int_{-\infty}^{\infty} B_e\left(k_z\right) J_1\left(k_\rho \rho\right) e^{-jk_z z} dk_z \,,\; 0 < \rho < a$$

$$= \sin\varphi \frac{1}{2\pi} \int_{-\infty}^{\infty} C_e\left(k_z\right) H_1^{(2)}\left(k_{2\rho} \rho\right) e^{-jk_z z} dk_z \,,\; \rho > a$$

The fields in the hole are given by

$$E_z = -\frac{j}{\omega\mu_0\varepsilon}\left[\left(\frac{\partial^2}{\partial z^2} + k^2\right) A_z + \frac{\partial}{\partial z}\frac{1}{\rho}\left\{\frac{\partial}{\partial\rho}\left(\rho A_\rho^s\right) + \frac{\partial}{\partial\varphi} A_\varphi^s\right\}\right]$$

$$E_\varphi = -\frac{j}{\omega\mu_0\varepsilon}\left[\frac{1}{\rho}\frac{\partial^2}{\partial\varphi\partial z} A_z + \frac{1}{\rho}\frac{\partial}{\partial\varphi}\frac{1}{\rho}\left\{\frac{\partial}{\partial\rho}\left(\rho A_\rho^s\right) + \frac{\partial}{\partial\varphi} A_\varphi^s\right\} + k^2 A_\varphi^s\right] + \frac{1}{\varepsilon}\frac{\partial}{\partial\rho} A_{ez}$$

$$H_z = -\frac{j}{\omega\mu_0\varepsilon}\left(\frac{\partial^2}{\partial z^2} + k^2\right) A_{ez} + \frac{1}{\mu_0}\frac{1}{\rho}\left\{\frac{\partial}{\partial\rho}\left(\rho A_\varphi^s\right) - \frac{\partial}{\partial\varphi} A_\rho^s\right\}$$

$$H_\varphi = -\frac{j}{\omega\mu_0\varepsilon}\left(\frac{1}{\rho}\frac{\partial^2}{\partial\varphi\partial z}\right) A_{ez} - \frac{1}{\mu_0}\frac{\partial}{\partial\rho} A_z + \frac{1}{\mu_0}\frac{\partial}{\partial z} A_\rho^s$$

where outside the hole they become

$$E_z = -\frac{j}{\omega\mu_0\varepsilon_2}\left(\frac{\partial^2}{\partial z^2} + k_2^2\right) A_z$$

$$E_\varphi = -\frac{j}{\omega\mu_0\varepsilon_2}\frac{1}{\rho}\frac{\partial^2}{\partial\varphi\partial z} A_z + \frac{1}{\varepsilon_2}\frac{\partial}{\partial\rho} A_{ez}$$

$$H_z = -\frac{j}{\omega\mu_0\varepsilon_2}\left(\frac{\partial^2}{\partial z^2} + k_2^2\right) A_{ez}$$

$$H_\varphi = -\frac{j}{\omega\mu_0\varepsilon_2}\left(\frac{1}{\rho}\frac{\partial^2}{\partial\varphi\partial z}\right) A_{ez} - \frac{1}{\mu_0}\frac{\partial}{\partial\rho} A_z$$

Continuity of these tangential components at the boundary of the cylindrical wall yields

$$k_\rho^2 B_m\left(k_z\right) J_1\left(k_\rho a\right) + \frac{1}{4}\mu_0 I_0 \ell k_z k_\rho H_1^{(2)}\left(k_\rho a\right) = \frac{\varepsilon}{\varepsilon_2} k_{2\rho}^2 C_m\left(k_z\right) H_1^{(2)}\left(k_{2\rho} a\right)$$

$$k_z B_m\left(k_z\right) J_1\left(k_\rho a\right) + \frac{1}{4}\mu_0 I_0 \ell\left\{k^2 a H_0^{(2)}\left(k_\rho a\right) - k_\rho H_1^{(2)}\left(k_\rho a\right)\right\} + \omega\mu_0 B_e\left(k_z\right)\left\{k_\rho a J_0\left(k_\rho a\right) - J_1\left(k_\rho a\right)\right\}$$

$$= \frac{\varepsilon}{\varepsilon_2} k_z C_m\left(k_z\right) H_1^{(2)}\left(k_{2\rho} a\right) + \frac{\varepsilon}{\varepsilon_2}\omega\mu_0 C_e\left(k_z\right)\left\{k_{2\rho} a H_0^{(2)}\left(k_{2\rho} a\right) - H_1^{(2)}\left(k_{2\rho} a\right)\right\}$$

$$k_\rho^2 B_e\left(k_z\right) J_1\left(k_\rho a\right) + \frac{\varepsilon}{4}\omega\mu_0 I_0 \ell k_\rho H_1^{(2)}\left(k_\rho a\right) = \frac{\varepsilon}{\varepsilon_2} k_{2\rho}^2 C_e\left(k_z\right) H_1^{(2)}\left(k_{2\rho} a\right)$$

$$k_z B_e\left(k_z\right) J_1\left(k_\rho a\right)+\omega\varepsilon B_m\left(k_z\right)\left\{k_\rho a J_0\left(k_\rho a\right)-J_1\left(k_\rho a\right)\right\}+\frac{a\varepsilon}{4}\omega\mu_0 I_0\ell k_z H_0^{(2)}\left(k_\rho a\right)$$

$$=\frac{\varepsilon}{\varepsilon_2}k_z C_e\left(k_z\right) H_1^{(2)}\left(k_{2\rho}a\right)+\omega\varepsilon C_m\left(k_z\right)\left\{k_{2\rho}aH_0^{(2)}\left(k_{2\rho}a\right)-H_1^{(2)}\left(k_{2\rho}a\right)\right\}$$

6.0.4

6.0.5 Developing a 2X2 System for $C_m\left(k_z\right)$ and $C_e\left(k_z\right)$

Eliminating B_m and B_e using from the system of equations given above, we obtain

$$B_m\left(k_z\right) J_1\left(k_\rho a\right)=\frac{\varepsilon}{\varepsilon_2}\frac{k_{2\rho}^2}{k_\rho^2}C_m\left(k_z\right) H_1^{(2)}\left(k_{2\rho}a\right)-\frac{1}{4k_\rho^2}\mu_0 I_0\ell k_z k_\rho H_1^{(2)}\left(k_\rho a\right)$$

$$B_e\left(k_z\right) J_1\left(k_\rho a\right)=\frac{\varepsilon}{\varepsilon_2}\frac{k_{2\rho}^2}{k_\rho^2}C_e\left(k_z\right) H_1^{(2)}\left(k_{2\rho}a\right)-\frac{\varepsilon}{4k_\rho^2}\omega\mu_0 I_0\ell k_\rho H_1^{(2)}\left(k_\rho a\right)$$

which then gives

$$k_z\left\{\frac{\varepsilon}{\varepsilon_2}\frac{k_{2\rho}^2}{k_\rho^2}C_m\left(k_z\right) H_1^{(2)}\left(k_{2\rho}a\right)-\frac{1}{4k_\rho^2}\mu_0 I_0\ell k_z k_\rho H_1^{(2)}\left(k_\rho a\right)\right\}+\frac{1}{4}\mu_0 I_0\ell\left\{k^2 aH_0^{(2)}\left(k_\rho a\right)-k_\rho H_1^{(2)}\left(k_\rho a\right)\right\}$$

$$+\omega\mu_0\left\{\frac{\varepsilon}{\varepsilon_2}\frac{k_{2\rho}^2}{k_\rho^2}C_e\left(k_z\right) H_1^{(2)}\left(k_{2\rho}a\right)-\frac{\varepsilon}{4k_\rho^2}\omega\mu_0 I_0\ell k_\rho H_1^{(2)}\left(k_\rho a\right)\right\}\left\{k_\rho a J_0\left(k_\rho a\right)/J_1\left(k_\rho a\right)-1\right\}$$

$$=\frac{\varepsilon}{\varepsilon_2}k_z C_m\left(k_z\right) H_1^{(2)}\left(k_{2\rho}a\right)+\frac{\varepsilon}{\varepsilon_2}\omega\mu_0 C_e\left(k_z\right)\left\{k_{2\rho}aH_0^{(2)}\left(k_{2\rho}a\right)-H_1^{(2)}\left(k_{2\rho}a\right)\right\}$$

and

$$k_z\left\{\frac{\varepsilon}{\varepsilon_2}\frac{k_{2\rho}^2}{k_\rho^2}C_e\left(k_z\right) H_1^{(2)}\left(k_{2\rho}a\right)-\frac{\varepsilon}{4k_\rho^2}\omega\mu_0 I_0\ell k_\rho H_1^{(2)}\left(k_\rho a\right)\right\}$$

$$+\omega\varepsilon\left\{\frac{\varepsilon}{\varepsilon_2}\frac{k_{2\rho}^2}{k_\rho^2}C_m\left(k_z\right) H_1^{(2)}\left(k_{2\rho}a\right)-\frac{1}{4k_\rho^2}\mu_0 I_0\ell k_z k_\rho H_1^{(2)}\left(k_\rho a\right)\right\}\left\{k_\rho a J_0\left(k_\rho a\right)/J_1\left(k_\rho a\right)-1\right\}$$

$$+\frac{a\varepsilon}{4}\omega\mu_0 I_0\ell k_z H_0^{(2)}\left(k_\rho a\right)=\frac{\varepsilon}{\varepsilon_2}k_z C_e\left(k_z\right) H_1^{(2)}\left(k_{2\rho}a\right)+\omega\varepsilon C_m\left(k_z\right)\left\{k_{2\rho}aH_0^{(2)}\left(k_{2\rho}a\right)-H_1^{(2)}\left(k_{2\rho}a\right)\right\}$$

Let us write this system as

$$c_{11}C_m+c_{12}C_e=f_1$$

$$c_{21}C_m + c_{22}C_e = f_2$$

where

$$c_{11} = \frac{\varepsilon}{\varepsilon_2} k_z \left(1 - k_{2\rho}^2/k_\rho^2\right) H_1^{(2)}\left(k_{2\rho}a\right) = \frac{\varepsilon}{\varepsilon_2} k_z \left(\frac{k^2 - k_2^2}{k_\rho^2}\right) H_1^{(2)}\left(k_{2\rho}a\right)$$

$$c_{12} / \left(\frac{\varepsilon}{\varepsilon_2}\omega\mu_0\right) = \frac{k_{2\rho}a}{J_1\left(k_\rho a\right)} \left[H_0^{(2)}\left(k_{2\rho}a\right) J_1\left(k_\rho a\right) - \left(k_{2\rho}/k_\rho\right) J_0\left(k_\rho a\right) H_1^{(2)}\left(k_{2\rho}a\right)\right] - \left(1 - k_{2\rho}^2/k_\rho^2\right) H_1^{(2)}\left(k_{2\rho}a\right)$$

$$f_1 = \frac{1}{4}\mu_0 I_0 \ell \frac{k^2 a}{J_1\left(k_\rho a\right)} \left[H_0^{(2)}\left(k_\rho a\right) J_1\left(k_\rho a\right) - H_1^{(2)}\left(k_\rho a\right) J_0\left(k_\rho a\right)\right]$$

$$= -\frac{j}{2\pi}\mu_0 I_0 \ell \frac{k^2/k_\rho}{J_1\left(k_\rho a\right)}$$

$$c_{21} / \left(\frac{\varepsilon}{\varepsilon_2}\omega\varepsilon\right) = \frac{k_2^2}{k^2}\left\{k_{2\rho}aH_0^{(2)}\left(k_{2\rho}a\right) - H_1^{(2)}\left(k_{2\rho}a\right)\right\} - \frac{k_{2\rho}^2}{k_\rho^2}\frac{H_1^{(2)}\left(k_{2\rho}a\right)}{J_1\left(k_\rho a\right)}\left\{k_\rho a J_0\left(k_\rho a\right) - J_1\left(k_\rho a\right)\right\}$$

$$= \frac{k_{2\rho}a}{J_1\left(k_\rho a\right)} \left[\left(k_2^2/k^2\right) H_0^{(2)}\left(k_{2\rho}a\right) J_1\left(k_\rho a\right) - \left(k_{2\rho}/k_\rho\right) H_1^{(2)}\left(k_{2\rho}a\right) J_0\left(k_\rho a\right)\right] - \left(k_2^2/k^2 - k_{2\rho}^2/k_\rho^2\right) H_1^{(2)}\left(k_{2\rho}a\right)$$

Here we note that

$$c_{21} / \left(\frac{\varepsilon}{\varepsilon_2}\omega\varepsilon\right) - c_{12} / \left(\frac{\varepsilon}{\varepsilon_2}\omega\mu_0\right) = \left(k_2^2/k^2 - 1\right) \left[k_{2\rho}aH_0^{(2)}\left(k_{2\rho}a\right) - H_1^{(2)}\left(k_{2\rho}a\right)\right]$$

$$c_{22} = \frac{\varepsilon}{\varepsilon_2} k_z \left(1 - k_{2\rho}^2/k_\rho^2\right) H_1^{(2)}\left(k_{2\rho}a\right)$$

$$f_2 = \frac{1}{4}\omega\varepsilon\mu_0 I_0 \ell \frac{k_z a}{J_1\left(k_\rho a\right)} \left[H_0^{(2)}\left(k_\rho a\right) J_1\left(k_\rho a\right) - H_1^{(2)}\left(k_\rho a\right) J_0\left(k_\rho a\right)\right]$$

$$= -\frac{j}{2\pi}\omega\varepsilon\mu_0 I_0 \ell \frac{k_z/k_\rho}{J_1\left(k_\rho a\right)} = \left(\frac{k_z}{\omega\mu_0}\right) f_1$$

Thus, the coefficients associated with the exterior of the hole (C_m and C_e) are given by

$$C_e = \frac{1}{c_{11}}\left(f_2 - c_{21}C_m\right)$$

and

$$C_m = \frac{f_1 - \frac{c_{12}}{c_{11}} f_2}{\left(c_{11} - \frac{c_{12}c_{21}}{c_{11}}\right)}$$

Note though that from above,

$$f_2 = \left(\frac{k_z}{\omega\mu_0}\right) f_1$$

so then we have

$$C_m = \frac{f_1\left[1 - \frac{c_{12}}{c_{11}}\left(\frac{k_z}{\omega\mu_0}\right)\right]}{\left(c_{11} - \frac{c_{12}c_{21}}{c_{11}}\right)}$$

6.1 Radiation in the Lower Half-Space

In a similar manner to the vertical dipole case, in this section we compare the results from an asymptotic evaluation of the fields in the lower half-space to those resulting from the exact numerical integration of the potential. The far-zone magnetic field is examined, where in this case both an azimuthal and radial component are present.

6.1.1 Asymptotic Evaluation of H_φ

Recall that

$$A_z = \cos\varphi \frac{1}{2\pi}\int_{-\infty}^{\infty} C_m\left(k_z\right) H_1^{(2)}\left(k_{2\rho}\rho\right) e^{-jk_z z} dk_z\,,\ \rho > a$$

$$A_{ez} = \sin\varphi \frac{1}{2\pi}\int_{-\infty}^{\infty} C_e\left(k_z\right) H_1^{(2)}\left(k_{2\rho}\rho\right) e^{-jk_z z} dk_z\,,\ \rho > a$$

where the coefficients $C_m\left(k_z\right)$ and $C_e\left(k_z\right)$ have been determined from the boundary conditions along the cylindrical hole. The azimuthal component of the magnetic field in the region exterior to the hole is given by

$$H_\varphi = -\frac{j}{\omega\mu_0\varepsilon_2}\left(\frac{1}{\rho}\frac{\partial^2}{\partial\varphi\partial z}\right) A_{ez} - \frac{1}{\mu_0}\frac{\partial}{\partial\rho}A_z$$

Differentiating we obtain

$$H_\varphi = -\frac{1}{2\pi\rho\mu_0}\cos\varphi\int_{-\infty}^{\infty}\left\{\frac{k_z}{\omega\varepsilon_2}C_e\left(k_z\right)H_1^{(2)}\left(k_{2\rho}\rho\right) + C_m\left(k_z\right)k_{2\rho}\rho H_1^{(2)'}\left(k_{2\rho}\rho\right)\right\} e^{-jk_z z} dk_z$$

or

$$H_\varphi = -\frac{1}{2\pi\rho\mu_0}\cos\varphi\int_{-\infty}^{\infty}\left\{\frac{k_z}{\omega\varepsilon_2}C_e\left(k_z\right)H_1^{(2)}\left(k_{2\rho}\rho\right) + C_m\left(k_z\right)\left[k_{2\rho}\rho H_0^{(2)}\left(k_{2\rho}\rho\right) - H_1^{(2)}\left(k_{2\rho}\rho\right)\right]\right\} e^{-jk_z z} dk_z$$

where, rearranging terms, we have

$$H_\varphi = \frac{-1}{2\pi\rho\mu_0}\cos\varphi\int_{-\infty}^{\infty}\left[\left\{\frac{k_z}{\omega\varepsilon_2}C_e\left(k_z\right) - C_m\left(k_z\right)\right\}H_1^{(2)}\left(k_{2\rho}\rho\right) + C_m\left(k_z\right)k_{2\rho}\rho H_0^{(2)}\left(k_{2\rho}\rho\right)\right] e^{-jk_z z} dk_z$$

Expanding the Hankel functions for large arguments, the integral representation can be rewritten as

$$H_{\varphi}^{asym} \sim \frac{-1}{2\pi\rho\mu_0}\cos\varphi\cdot$$

$$\left\{\int_{-\infty}^{\infty}\sqrt{\frac{2}{\pi k_{2\rho}\rho}}\left[\left\{\frac{k_z}{\omega\varepsilon_2}C_e\left(k_z\right)-C_m\left(k_z\right)\right\}e^{-jk_zz-j(k_{2\rho}\rho-3\pi/4)}+C_m\left(k_z\right)k_{2\rho}\rho e^{-jk_zz-j(k_{2\rho}\rho-\pi/4)}\right]dk_z\right\}$$

or, factoring,

$$H_{\varphi}^{asym} \sim \frac{-1}{2\pi\rho\mu_0}\cos\varphi\int_{-\infty}^{\infty}\sqrt{\frac{2}{\pi k_{2\rho}\rho}}\left\{e^{j3\pi/4}\left(\frac{k_z}{\omega\varepsilon_2}C_e\left(k_z\right)-C_m\left(k_z\right)\right)+C_m\left(k_z\right)e^{j\pi/4}k_{2\rho}\rho\right\}e^{-j(k_zz+k_{2\rho}\rho)}dk_z$$

From the phase function,

$$\psi\left(k_z\right)=k_zz+k_{2\rho}\rho=k_zz+\sqrt{k_2^2-k_z^2}\rho$$

the saddle points were previously found to be (in the vertical dipole asymptotic analysis)

$$k_z^s=k_2\cos\theta_2=k_2\frac{z}{r}$$

and

$$k_{2\rho}^s=k_2\sin\theta_2=k_2\frac{\rho}{r}$$

At the saddle point, the magnetic field then becomes

$$H_{\varphi}^{asym} \sim \frac{-1}{2\pi\rho\mu_0}\left\{e^{j\pi/2}\left(\frac{k_z^s}{\omega\varepsilon_2}C_e\left(k_z^s\right)-C_m\left(k_z^s\right)\right)+C_m\left(k_z^s\right)k_{2\rho}^s\rho\right\}\cos\varphi\int_{-\infty}^{\infty}\sqrt{\frac{2}{\pi k_{2\rho}\rho}}e^{j\pi/4}e^{-j(k_zz+k_{2\rho}\rho)}dk_z$$

or, equivalently,

$$H_{\varphi}^{asym} \sim \frac{-1}{2\pi\rho\mu_0}\left\{e^{j\pi/2}\left(\frac{k_z^s}{\omega\varepsilon_2}C_e\left(k_z^s\right)-C_m\left(k_z^s\right)\right)+C_m\left(k_z^s\right)k_{2\rho}^s\rho\right\}\cos\varphi\int_{-\infty}^{\infty}H_0^{(2)}\left(k_{2\rho}\rho\right)e^{-jk_zz}dk_z$$

Using the relationship (from the source potential representation of A_x^s)

$$\int_{-\infty}^{\infty}H_0^{(2)}\left(k_{2\rho}\rho\right)e^{-jk_zz}dk_z=j\frac{2e^{-jk_2r}}{r}$$

we can write

$$H_{\varphi}^{asym} \sim \frac{-j}{\pi\rho\mu_0}\left(\frac{e^{-jk_2r}}{r}\right)\left\{e^{j\pi/2}\left(\frac{k_z^s}{\omega\varepsilon_2}C_e\left(k_z^s\right)-C_m\left(k_z^s\right)\right)+C_m\left(k_z^s\right)k_{2\rho}^s\rho\right\}\cos\varphi$$

or, recognizing that the first term is not a component of the far-zone,

$$H_{\varphi}^{asym} \sim \frac{-j}{\pi\mu_0}\left(\frac{e^{-jk_2r}}{r}\right)C_m\left(k_z^s\right)k_{2\rho}^s\cos\varphi \tag{7}$$

6.1.2 Numerical Evaluation of H_φ

From above, we have

$$H_{\varphi} = \frac{-1}{2\pi\rho\mu_0}\cos\varphi\int_{-\infty}^{\infty}\left[\left\{\frac{k_z}{\omega\varepsilon_2}C_e\left(k_z\right)-C_m\left(k_z\right)\right\}H_1^{(2)}\left(k_{2\rho}\rho\right)+C_m\left(k_z\right)k_{2\rho}\rho H_0^{(2)}\left(k_{2\rho}\rho\right)\right]e^{-jk_zz}dk_z$$

Noting that the integrand is an odd function of k_z (this can be shown numerically and with the asymptotic forms of the coefficients), we can rewrite the integral as

$$H_{\varphi}^{num} = \frac{j}{\pi\rho\mu_0}\cos\varphi\int_{0}^{\infty}\left[\left\{\frac{k_z}{\omega\varepsilon_2}C_e\left(k_z\right)-C_m\left(k_z\right)\right\}H_1^{(2)}\left(k_{2\rho}\rho\right)+C_m\left(k_z\right)k_{2\rho}\rho H_0^{(2)}\left(k_{2\rho}\rho\right)\right]\sin\left(k_zz\right)dk_z$$

which in the far-field becomes

$$H_{\varphi}^{num} = \frac{j}{\pi\mu_0}\cos\varphi\int_{0}^{\infty}C_m\left(k_z\right)k_{2\rho}H_0^{(2)}\left(k_{2\rho}\rho\right)\sin\left(k_zz\right)dk_z \tag{8}$$

6.1.3 H_φ Results

The asymptotic and numerical evaluations of H_φ at the interface between an air and dry-sand medium at 300 MHz and 3.0 GHz are shown in Figures 15 and 16. The results are presented as a function of radial distance ρ from the hole and and the source is assumed to be located a distance of 10 m from the interface. As in the case of the vertical dipole, a unit-strength dipole moment is assumed ($I_0\ell = 1\ A\cdot m$) for these and all remaining horizontal dipole results. The sand properties are assumed to be $\varepsilon_r = 2.55\left(1-j0.01\right)$ and $\varepsilon_r = 2.55\left(1-j0.0062\right)$ at 300 MHz and 3.0 GHz, respectively [1].

In both cases the saddle-point evaluation is a very good approximation to the exact numerical integration of the field. As one would expect, there is a slight discrepancy between the results when the observation point is very close to the hole. However, the results become indistinguishable as the distance from the hole increases.

6.1.4 Asymptotic Evaluation of H_ρ

For this component of the magnetic field, we have

$$H_{\rho} = \frac{1}{\mu_0}\frac{1}{\rho}\frac{\partial}{\partial\varphi}A_z - j\frac{1}{\omega\varepsilon_2\mu_0}\left(\frac{\partial^2}{\partial\rho\partial z}A_{ez}\right)$$

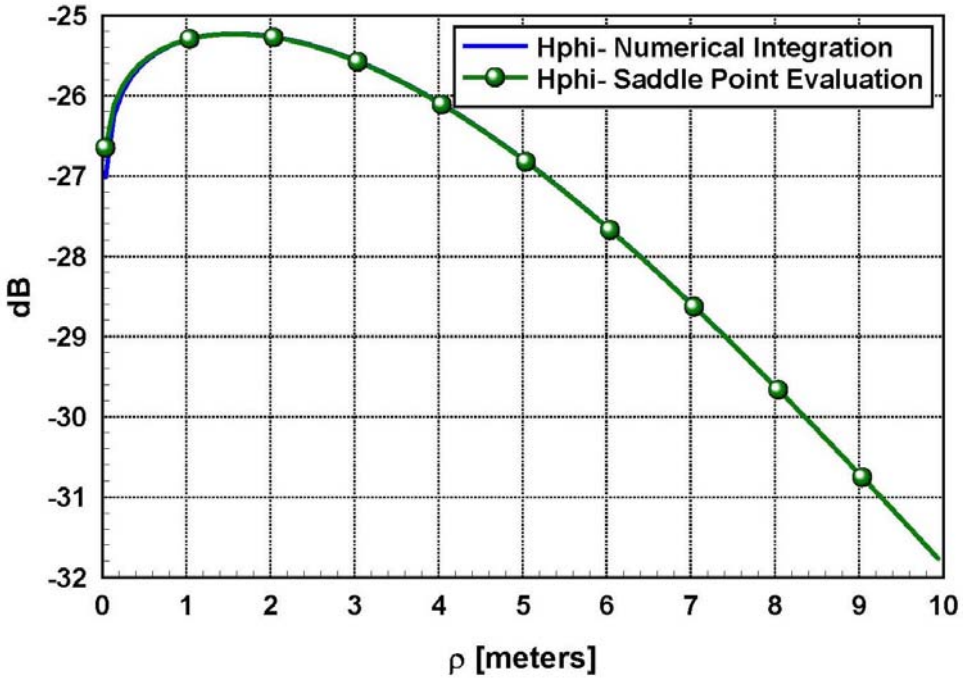

Figure 15. Azimuth magnetic field distributions along an air/dry sand interface at 300 MHz, determined using asymptotic expressions and an exact numerical evaluation ($a = 0.04\ m$).

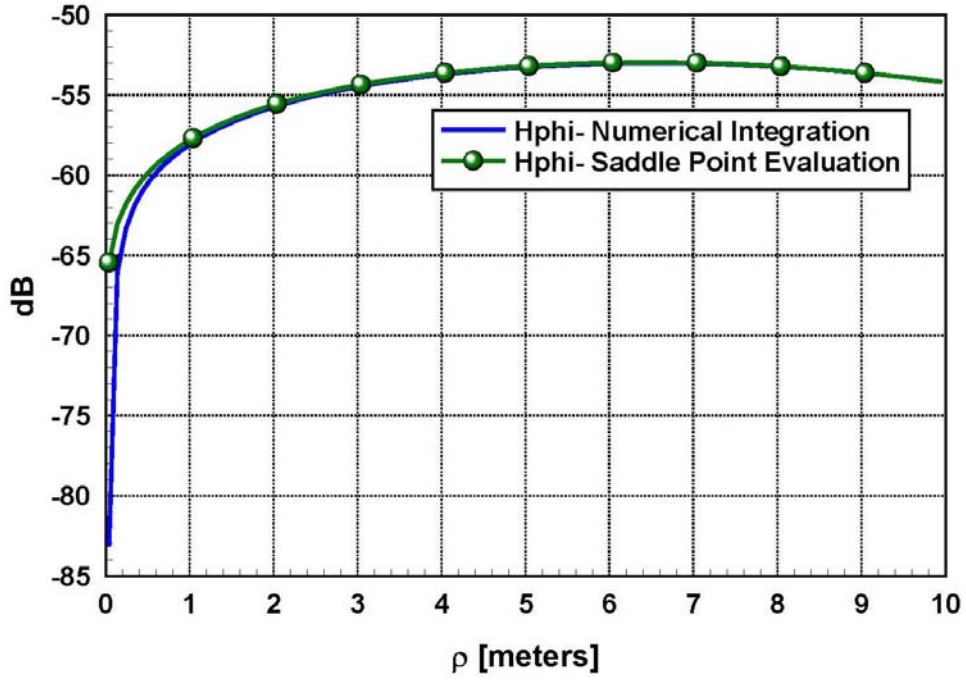

Figure 16. Azimuth magnetic field distributions along an air/dry sand interface at 3.0 GHz, determined using asymptotic expressions and an exact numerical evaluation ($a = 0.04\ m$).

so that

$$H_\rho = -\frac{1}{\mu_0}\frac{1}{\rho}\sin\varphi\frac{1}{2\pi}\int_{-\infty}^{\infty}\left[\left\{C_m\left(k_z\right) - \frac{k_z}{\omega\varepsilon_2}C_e\left(k_z\right)\right\}H_1^{(2)}\left(k_{2\rho}\rho\right) + \frac{1}{\omega\varepsilon_2}k_z C_e\left(k_z\right)k_{2\rho}\rho H_0^{(2)}\left(k_{2\rho}\rho\right)\right]e^{-jk_z z}dk_z$$

Following a similar saddle-point method as above, we obtain

$$H_\rho^{asym} \sim -\frac{1}{2\pi\rho\mu_0}\sin\varphi\left\{e^{j\pi/2}\left(C_m\left(k_z^s\right) - \frac{k_z^s}{\omega\varepsilon_2}C_e\left(k_z^s\right)\right) + \frac{1}{\omega\varepsilon_2}k_z^s C_e\left(k_z^s\right)k_{2\rho}^s\rho\right\}\cdot \left\{\int_{-\infty}^{\infty}\sqrt{\frac{2}{\pi k_{2\rho}\rho}}e^{j\pi/4}e^{-j\left(k_z z + k_{2\rho}\rho\right)}dk_z\right\}$$

which, in the far-field, becomes

$$H_\rho^{asym} \sim -\frac{j}{\pi\mu_0}\sin\varphi\left(\frac{e^{-jk_2 r}}{r}\right)\left[\frac{1}{\omega\varepsilon_2}k_z^s C_e\left(k_z^s\right)k_{2\rho}^s\right] \tag{9}$$

6.1.5 Numerical Evaluation of H_ρ

Numerically, we evaluate

$$H_\rho^{num} = -\frac{1}{\mu_0}\frac{1}{\rho}\sin\varphi\frac{1}{2\pi}\int_{-\infty}^{\infty}\left[\left\{C_m\left(k_z\right) - \frac{k_z}{\omega\varepsilon_2}C_e\left(k_z\right)\right\}H_1^{(2)}\left(k_{2\rho}\rho\right) + \frac{k_z}{\omega\varepsilon_2}C_e\left(k_z\right)k_{2\rho}\rho H_0^{(2)}\left(k_{2\rho}\rho\right)\right]e^{-jk_z z}dk_z$$

where we note that again the first part of the integrand is an odd function of k_z . Thus, the far-zone radial component of the magnetic field can be rewritten as

$$H_\rho^{num} = \frac{j}{\mu_0}\sin\varphi\frac{1}{\pi}\int_0^{\infty}\frac{k_z}{\omega\varepsilon_2}C_e\left(k_z\right)k_{2\rho}H_0^{(2)}\left(k_{2\rho}\rho\right)\sin\left(k_z z\right)dk_z \tag{10}$$

6.1.6 H_ρ Results

Figures 17 and 18 show the radial component of the magnetic field at the interface of the air and dry sand regions at 300 MHz and 3.0 GHz, respectively. As one would expect given the previous results, we again see excellent agreement between the saddle point evaluation and numerical integration of the field.

6.2 Radiation in the Upper-Half Space

To compute the fields in the upper-half space, we use an approach similar to that used for the vertical dipole. The fields in the air region, without the effects of the hole, are first determined using a saddle-point evaluation of the integral representation for the half -space problem and the results are verified against the results in [6]. In order to address the issue of the hole, a multipole expansion of the radiation is performed and shown to yield identical element patterns in both regions. Thus, assuming the source is placed far enough from the interface and the effects of the hole on the overall radiation can accurately be modeled using a multipole expansion, the radiation in the air region is shown to be a product of the multipole element pattern and a term associated with ray transmission through the interface. Again it is important to recognize that, to obtain the total field in the upper-air half space, it is possible to add the radiation

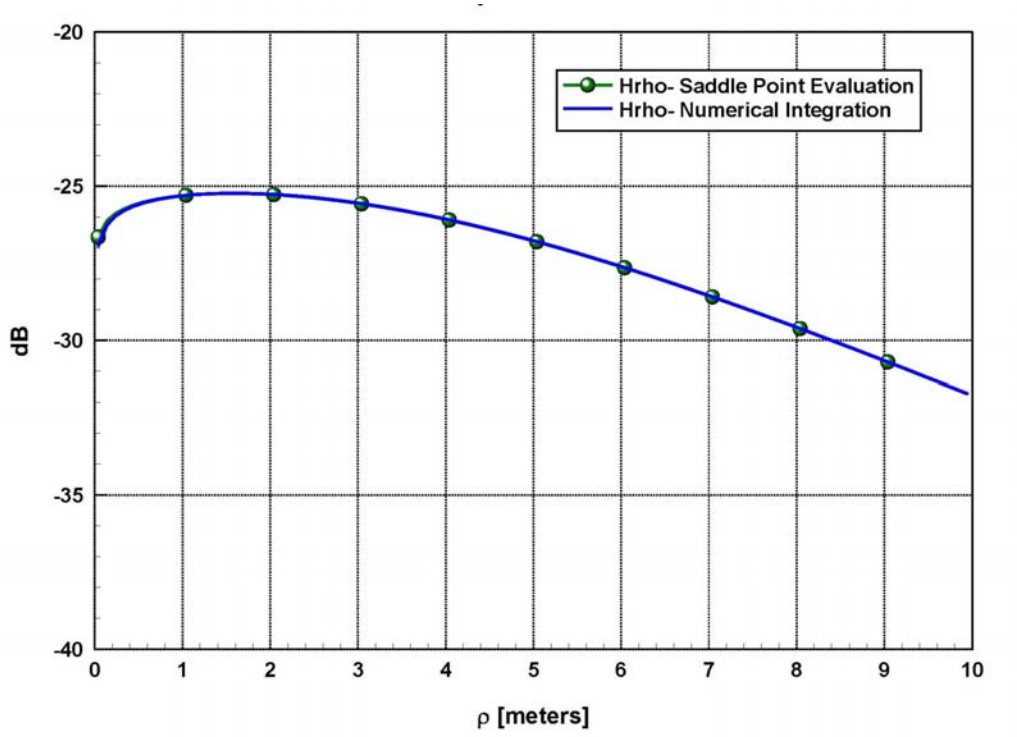

Figure 17. Radial magnetic field distributions along an air/dry sand interface at 300 MHz, determined using asymptotic expressions and an exact numerical evaluation ($a = 0.04\ m$).

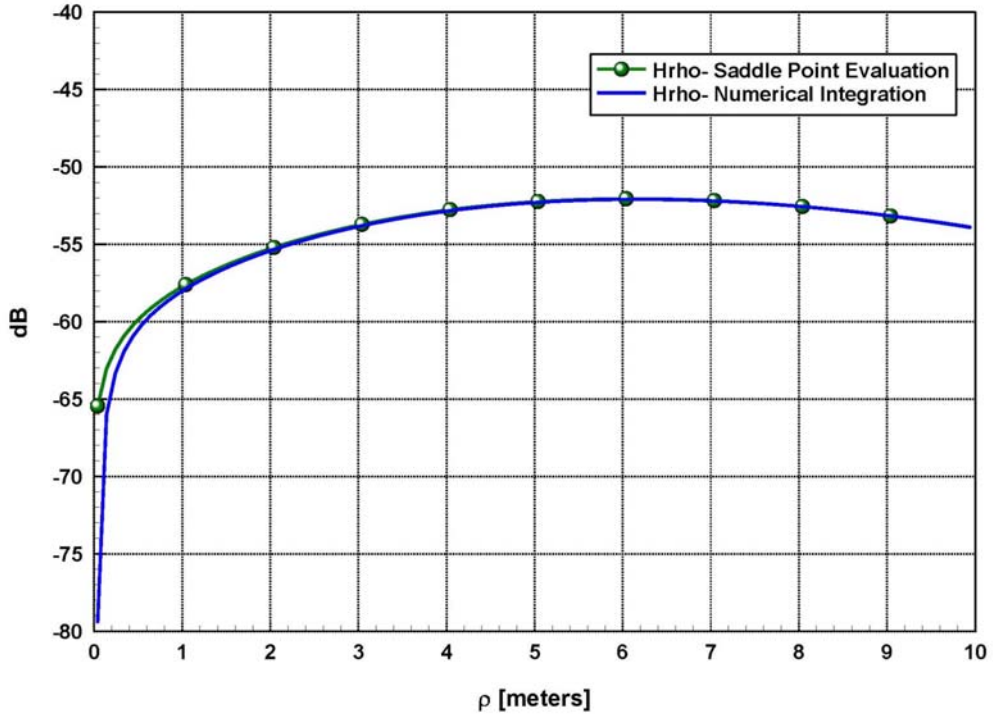

Figure 18. Radial magnetic field distributions along an air/dry sand interface at 3.0 GHz, determined using asymptotic expressions and an exact numerical evaluation ($a = 0.04\ m$).

associated with the electric-field discontinuity at the air-earth interface to the dipole radiation. Since, as expected, the contribution due to this continuity is found to be negligible, the analysis is suppressed here and presented in *Appendix B*.

6.2.1 Boundary-Condition Analysis

The source magnetic vector potential can be written as

$$A_x^s = \mu_0 I_0 \ell \frac{e^{-jk_2 r}}{4\pi r}$$

$$A_x^s = -\frac{j}{4\pi}\mu_0 I_0 \ell \int_0^\infty J_0\left(k_\rho \rho\right) e^{-jk_{2z}|z+h|} \frac{k_\rho dk_\rho}{k_{2z}}$$

which in cylindrical coordinates becomes

$$A_\rho^s = -\frac{j}{4\pi}\mu_0 I_0 \ell \cos\varphi \int_0^\infty J_0\left(k_\rho \rho\right) e^{-jk_{2z}|z+h|} \frac{k_\rho dk_\rho}{k_{2z}}$$

$$A_\varphi^s = \frac{j}{4\pi}\mu_0 I_0 \ell \sin\varphi \int_0^\infty J_0\left(k_\rho \rho\right) e^{-jk_{2z}|z+h|} \frac{k_\rho dk_\rho}{k_{2z}}$$

where the unit vector $\underline{e}_x$ is given by

$$\underline{e}_x = \underline{e}_\rho \cos\varphi - \underline{e}_\varphi \sin\varphi$$

Also, the scattered potentials (magnetic and electric) can be written as

$$A_z = \mu_0 I_0 \ell \cos\varphi \int_0^\infty E_e\left(k_\rho\right) J_1\left(k_\rho \rho\right) e^{-jk_z z} k_\rho dk_\rho\,,\ z > 0$$

$$= \mu_0 I_0 \ell \cos\varphi \int_0^\infty F_e\left(k_\rho\right) J_1\left(k_\rho \rho\right) e^{jk_{2z} z} k_\rho dk_\rho\,,\ z < 0$$

and

$$A_{ez} = \mu_0 I_0 \ell \sin\varphi \int_0^\infty E_m\left(k_\rho\right) J_1\left(k_\rho \rho\right) e^{-jk_z z} k_\rho dk_\rho\,,\ z > 0$$

$$= \mu_0 I_0 \ell \sin\varphi \int_0^\infty F_m\left(k_\rho\right) J_1\left(k_\rho \rho\right) e^{jk_{2z} z} k_\rho dk_\rho\,,\ z < 0$$

Enforcing the continuity of H_φ at $z = 0$ where

$$H_\varphi = -\frac{j}{\omega\mu_0\varepsilon}\left(\frac{1}{\rho}\frac{\partial^2}{\partial\varphi\partial z}\right) A_{ez} - \frac{1}{\mu_0}\frac{\partial}{\partial\rho} A_z + \frac{1}{\mu_0}\frac{\partial}{\partial z} A_\rho^s$$

we obtain

$$-\frac{k_z}{\omega\varepsilon}E_m\left(k_\rho\right)J_1\left(k_\rho\rho\right)-E_e\left(k_\rho\right)\left\{k_\rho\rho J_0\left(k_\rho\rho\right)-J_1\left(k_\rho\rho\right)\right\}$$

$$=\frac{k_{2z}}{\omega\varepsilon_2}F_m\left(k_\rho\right)J_1\left(k_\rho\rho\right)-F_e\left(k_\rho\right)\left\{k_\rho\rho J_0\left(k_\rho\rho\right)-J_1\left(k_\rho\rho\right)\right\}-\frac{1}{4\pi}\rho J_0\left(k_\rho\rho\right)e^{-jk_{2z}|h|}$$

Enforcing the continuity of E_φ at $z=0$ where

$$E_\varphi=-\frac{j}{\omega\mu_0\varepsilon}\left[\frac{1}{\rho}\frac{\partial^2}{\partial\varphi\partial z}A_z+\frac{1}{\rho}\frac{\partial}{\partial\varphi}\frac{1}{\rho}\left\{\frac{\partial}{\partial\rho}\left(\rho A_\rho^s\right)+\frac{\partial}{\partial\varphi}A_\varphi^s\right\}+k^2A_\varphi^s\right]+\frac{1}{\varepsilon}\frac{\partial}{\partial\rho}A_{ez}$$

we obtain

$$\frac{k_z}{\omega\varepsilon}E_e\left(k_\rho\right)J_1\left(k_\rho\rho\right)+\frac{1}{\varepsilon}\mu_0E_m\left(k_\rho\right)\left\{k_\rho\rho J_0\left(k_\rho\rho\right)-J_1\left(k_\rho\rho\right)\right\}$$

$$=-\frac{j}{\omega\varepsilon_2}\left[-jk_{2z}F_e\left(k_\rho\right)J_1\left(k_\rho\rho\right)-\frac{j}{4\pi}\left\{k_\rho J_1\left(k_\rho\rho\right)\right\}e^{-jk_{2z}|h|}\frac{1}{k_{2z}}+k_2^2\frac{j}{4\pi}\rho J_0\left(k_\rho\rho\right)e^{-jk_{2z}|h|}\frac{1}{k_{2z}}\right]$$

$$+\frac{1}{\varepsilon_2}\mu_0F_m\left(k_\rho\right)\left\{k_\rho\rho J_0\left(k_\rho\rho\right)-J_1\left(k_\rho\rho\right)\right\}$$

Note that

$$\left\{\frac{\partial}{\partial\rho}\left(\rho A_\rho^s\right)+\frac{\partial}{\partial\varphi}A_\varphi^s\right\}=\frac{j}{4\pi}\mu_0I_0\ell\cos\varphi\int_0^\infty\left\{k_\rho\rho J_1\left(k_\rho\rho\right)\right\}e^{-jk_{2z}|z+h|}\frac{k_\rho dk_\rho}{k_{2z}}$$

Enforcing the continuity of H_ρ at $z=0$ where

$$H_\rho=\frac{1}{\mu_0}\left(\frac{1}{\rho}\frac{\partial}{\partial\varphi}\right)A_z-\frac{j}{\omega\mu_0\varepsilon}\frac{\partial^2}{\partial\rho\partial z}A_{ez}-\frac{1}{\mu_0}\frac{\partial}{\partial z}A_\varphi^s$$

we obtain

$$-E_e\left(k_\rho\right)J_1\left(k_\rho\rho\right)-\frac{k_z}{\omega\varepsilon}E_m\left(k_\rho\right)\left\{k_\rho\rho J_0\left(k_\rho\rho\right)-J_1\left(k_\rho\rho\right)\right\}=$$

$$-F_e\left(k_\rho\right)J_1\left(k_\rho\rho\right)+\frac{k_{2z}}{\omega\varepsilon_2}F_m\left(k_\rho\right)\left\{k_\rho\rho J_0\left(k_\rho\rho\right)-J_1\left(k_\rho\rho\right)\right\}-\frac{1}{4\pi}\rho J_0\left(k_\rho\rho\right)e^{-jk_{2z}|h|}$$

Enforcing the continuity of E_ρ at $z=0$ where

$$E_\rho=-\frac{j}{\omega\mu_0\varepsilon}\left[\frac{\partial^2}{\partial\rho\partial z}A_z+\frac{\partial}{\partial\rho}\frac{1}{\rho}\left\{\frac{\partial}{\partial\rho}\left(\rho A_\rho^s\right)+\frac{\partial}{\partial\varphi}A_\varphi^s\right\}\right]-\frac{1}{\varepsilon}\left(\frac{1}{\rho}\frac{\partial}{\partial\varphi}\right)A_{ez}-j\omega A_\rho^s$$

we obtain

$$-\frac{k_z}{\omega\mu_0\varepsilon}E_e\left(k_\rho\right)\left\{k_\rho\rho J_0\left(k_\rho\rho\right)-J_1\left(k_\rho\rho\right)\right\}-\frac{1}{\varepsilon}E_m\left(k_\rho\right)J_1\left(k_\rho\rho\right)$$

$$= -\frac{j}{\omega\mu_0\varepsilon_2}\left[jk_{2z}F_e\left(k_\rho\right)\left\{k_\rho\rho J_0\left(k_\rho\rho\right) - J_1\left(k_\rho\rho\right)\right\} + \frac{j}{4\pi}\left\{k_\rho\rho J_0\left(k_\rho\rho\right) - J_1\left(k_\rho\rho\right)\right\}e^{-jk_{2z}|h|}\frac{k_\rho}{k_{2z}}\right]$$

$$-\frac{1}{\varepsilon_2}F_m\left(k_\rho\right)J_1\left(k_\rho\rho\right) - \frac{\omega}{4\pi}\rho J_0\left(k_\rho\rho\right)e^{-jk_{2z}|h|}\frac{1}{k_{2z}}$$

To solve for the unknown coefficients, we note that maintaining the same radial functionality on both sides of the equations, this rather complicated 4×4 system can be reduced to two redundant, but much simpler systems of 2×2 order. That is, since the boundary conditions must be satisfied for all ρ along the interface, we can use the continuity of H_φ to equate $J_0\left(k_\rho\rho\right)$ and $J_1\left(k_\rho\rho\right)$ terms on both sides of the equation. Thus, using

$$k_\rho E_e\left(k_\rho\right) - F_e\left(k_\rho\right)k_\rho = \frac{1}{4\pi}e^{-jk_{2z}|h|}$$

and

$$-E_e\left(k_\rho\right) + \frac{k_z}{\omega\varepsilon}E_m\left(k_\rho\right) + F_e\left(k_\rho\right) + \frac{k_{2z}}{\omega\varepsilon_2}F_m\left(k_\rho\right) = 0$$

we obtain expressions for the electric potential coefficients in terms of the magnetic potential coefficients given by

$$F_e\left(k_\rho\right) = E_e\left(k_\rho\right) - \frac{1}{4\pi k_\rho}e^{-jk_{2z}|h|}$$

$$F_m\left(k_\rho\right) = -\frac{k_z\varepsilon_2}{k_{2z}\varepsilon}E_m\left(k_\rho\right) + \frac{\omega\varepsilon_2}{4\pi k_\rho k_{2z}}e^{-jk_{2z}|h|}$$

Next using the continuity of E_φ, we have

$$F_m\left(k_\rho\right) = \frac{\varepsilon_2}{\varepsilon}E_m\left(k_\rho\right) - \frac{1}{4\pi\omega\mu_0}e^{-jk_{2z}|h|}\frac{k_2^2}{k_{2z}k_\rho}$$

$$F_e\left(k_\rho\right) = -\frac{k_z\varepsilon_2}{k_{2z}\varepsilon}E_e\left(k_\rho\right) + \frac{k_2^2}{4\pi k_{2z}^2 k_\rho}e^{-jk_{2z}|h|} - \frac{k_\rho}{4\pi k_{2z}^2}e^{-jk_{2z}|h|}$$

where, upon substitution, we obtain

$$E_m\left(k_\rho\right) = \frac{e^{-jk_{2z}|h|}{}_{\omega\varepsilon}}{2\pi k_\rho\left[k_{2z} + k_z\right]}$$

$$E_e\left(k_\rho\right) = \frac{e^{-jk_{2z}|h|}k_{2z}\varepsilon}{2\pi k_\rho\left[k_{2z}\varepsilon + k_z\varepsilon_2\right]}$$

We note that these coefficients can also be obtained from the continuity in the radial components of the electric and magnetic field.

6.2.2 Half-Space Problem: No Hole

We now asymptotically evaluate the fields in the upper-half space and compare the results to those obtained by [6]. Recall the magnetic potential expression in the region $z > 0$

$$A_z = \mu_0 I_0 \ell \cos\varphi \int_0^\infty E_e\left(k_\rho\right) J_1\left(k_\rho \rho\right) e^{-jk_z z} k_\rho dk_\rho$$

which can be rewritten as

$$A_z = \frac{\mu_0 I_0 \ell}{2} \cos\varphi \int_0^\infty E_e\left(k_\rho\right) \left[H_1^{(2)}\left(k_\rho \rho\right) + H_1^{(1)}\left(k_\rho \rho\right)\right] e^{-jk_z z} k_\rho dk_\rho$$

or, applying a change of variables as was done in the vertical electric dipole case when evaluating the upper-half space radiation,

$$\begin{aligned} A_z = &\frac{\mu_0 I_0 \ell}{2} \cos\varphi \int_0^\infty E_e\left(k_\rho\right) H_1^{(2)}\left(k_\rho \rho\right) e^{-jk_z z} k_\rho dk_\rho \\ &+ \frac{\mu_0 I_0 \ell}{2} \cos\varphi \int_0^{\infty e^{-j\pi}} E_e\left(k_\rho e^{j\pi}\right) H_1^{(1)}\left(k_\rho e^{j\pi} \rho\right) e^{-jk_z z} k_\rho dk_\rho \end{aligned}$$

The magnetic vector potential then becomes

$$\begin{aligned} A_z = &\frac{\mu_0 I_0 \ell}{2} \cos\varphi \int_0^\infty E_e\left(k_\rho\right) H_1^{(2)}\left(k_\rho \rho\right) e^{-jk_z z} k_\rho dk_\rho \\ &- \frac{\mu_0 I_0 \ell}{2} \cos\varphi \int_{-\infty}^0 E_e\left(k_\rho e^{j\pi}\right) H_1^{(2)}\left(k_\rho \rho\right) e^{-jk_z z} k_\rho dk_\rho \end{aligned}$$

where [4]

$$H_1^{(1)}\left(z e^{j\pi}\right) = -e^{-j\pi} H_1^{(2)}\left(z\right)$$

Next, noting that

$$E_e\left(k_\rho e^{j\pi}\right) = -E_e\left(k_\rho\right)$$

we obtain

$$A_z = \frac{\mu_0 I_0 \ell}{2} \cos\varphi \int_{-\infty}^\infty E_e\left(k_\rho\right) H_1^{(2)}\left(k_\rho \rho\right) e^{-jk_z z} k_\rho dk_\rho$$

Similarly, for the electric vector potential

$$A_{ez} = \mu_0 I_0 \ell \sin\varphi \int_0^\infty E_m\left(k_\rho\right) J_1\left(k_\rho \rho\right) e^{-jk_z z} k_\rho dk_\rho$$

or

$$A_{ez} = \frac{\mu_0 I_0 \ell}{2} \sin\varphi \int_{-\infty}^\infty E_m\left(k_\rho\right) H_1^{(2)}\left(k_\rho \rho\right) e^{-jk_z z} k_\rho dk_\rho$$

For the asymptotic evaluations, we first examine A_z and deform the contour through the saddle point for the Hankel function. Expanding the Hankel function as

$$H_1^{(2)}(k_\rho \rho) \sim \sqrt{\frac{2}{\pi k_\rho \rho}} e^{-jk_\rho \rho + j3\pi/4}$$

A_z becomes

$$A_z \sim \frac{\mu_0 I_0 \ell}{2} \sqrt{\frac{2}{\pi \rho}} \cos\varphi \int_{-\infty}^{\infty} E_e(k_\rho) \sqrt{k_\rho} e^{j3\pi/4} e^{-jk_\rho \rho} e^{-jk_z z} dk_\rho$$

Using the saddle-point results found in the case of the vertical dipole (when evaluating the magnetic vector potentials in the upper-half space), the magnetic vector potential for the horizontal dipole is given by

$$A_z \sim \frac{\mu_0 I_0 \ell}{2} \cos\varphi \sqrt{\frac{2}{\pi \rho}} E_e(k_\rho^s) \sqrt{k_\rho^s} e^{j3\pi/4 - jkr} \int_{-\infty}^{\infty} e^{-\frac{1}{2} kr v^2 \sec^2\theta} k e^{j\pi/4} dv$$

or

$$A_z \sim \frac{\mu_0 I_0 \ell}{2} \cos\varphi \sqrt{\frac{2}{\pi r \sin\theta}} E_e(k_\rho^s) \sqrt{k_\rho^s} e^{j3\pi/4 - jkr} \left(k e^{j\pi/4}\right) \frac{\sqrt{2\pi}}{\sqrt{kr \sec^2\theta}}$$

Simplifying,

$$A_z \sim \left(-\frac{k e^{-jkr}}{r} \mu_0 I_0 \ell\right) E_e(k_\rho^s) \cos\theta \cos\varphi$$

and in a similar fashion,

$$A_{ez} \sim \left(-\frac{k e^{-jkr}}{r} \mu_0 I_0 \ell\right) E_m(k_\rho^s) \cos\theta \sin\varphi$$

In spherical coordinates (again we note that $\underline{e}_z = \underline{e}_r \cos\theta - \underline{e}_\theta \sin\theta$), the magnetic potentials are given by

$$A_r \sim \left(-\frac{k e^{-jkr}}{r} \mu_0 I_0 \ell\right) E_e(k_\rho^s) \cos^2\theta \cos\varphi$$

$$A_\theta \sim \left(\frac{k e^{-jkr}}{r} \mu_0 I_0 \ell\right) E_e(k_\rho^s) \cos\theta \sin\theta \cos\varphi$$

while the electric potentials are given by

$$A_{er} \sim \left(-\frac{k e^{-jkr}}{r} \mu_0 I_0 \ell\right) E_m(k_\rho^s) \cos^2\theta \sin\varphi$$

$$A_{e\theta} \sim \left(\frac{k e^{-jkr}}{r} \mu_0 I_0 \ell\right) E_m(k_\rho^s) \cos\theta \sin\theta \sin\varphi$$

Using the principle of superposition (for both potential types), the fields in the upper half-space region

can be written as

$$E_\varphi = -j\frac{1}{\omega\varepsilon\mu_0}\frac{1}{r\sin\theta}\frac{\partial}{\partial\varphi}\left[\frac{1}{r^2}\frac{\partial}{\partial r}\left(r^2A_r\right)+\frac{1}{r\sin\theta}\frac{\partial}{\partial\theta}\left(\sin\theta A_\theta\right)\right]-\frac{1}{\varepsilon}\frac{1}{r}\left[\frac{\partial}{\partial r}\left(rA_{e\theta}\right)-\frac{\partial}{\partial\theta}A_{er}\right]$$

and

$$H_\varphi = \frac{1}{\mu_0}\frac{1}{r}\left[\frac{\partial}{\partial r}\left(rA_\theta\right)-\frac{\partial A_r}{\partial\theta}\right]-j\frac{1}{\omega\varepsilon\mu_0}\frac{1}{r\sin\theta}\frac{\partial}{\partial\varphi}\left[\frac{1}{r^2}\frac{\partial}{\partial r}\left(r^2A_{er}\right)+\frac{1}{r\sin\theta}\frac{\partial}{\partial\theta}\left(\sin\theta A_{e\theta}\right)\right]$$

We first consider the electric-field component E_φ. Substituting and retaining only far-field terms, E_φ becomes

$$E_\varphi \sim j\frac{k^2e^{-jkr}}{\varepsilon r}\mu_0 I_0\ell E_m\left(k_\rho^s\right)\cos\theta\sin\theta\sin\varphi$$

or

$$E_\varphi \sim j\omega\mu_0 I_0\ell\sin\varphi\left[\frac{k}{k\cos\theta+\sqrt{k_2^2-k^2\sin^2\theta}}\right]\frac{2\cos\theta e^{-jkr-jh\sqrt{k_2^2-k^2\sin^2\theta}}}{4\pi r} \tag{11}$$

We note that this expression is identical to the far-field contribution derived in [6].

Substituting into the magnetic field expression and again considering only the far-field contributions, we obtain

$$H_\varphi \sim \frac{1}{\mu_0}\frac{1}{r}\left[-jk^2e^{-jkr}\mu_0 I_0\ell E_e\left(k_\rho^s\right)\cos\theta\sin\theta\cos\varphi\right]$$

or

$$H_\varphi \sim -jI_0\ell\cos\varphi\frac{1}{4\pi}\left[\frac{\sqrt{k_2^2-k^2\sin^2\theta}}{k\sqrt{k_2^2-k^2\sin^2\theta}+k_2^2\cos\theta}\right]\frac{2k^2\cos\theta e^{-jkr-jh\sqrt{k_2^2-k^2\sin^2\theta}}}{r} \tag{12}$$

which can be shown to be equivalent to the far-zone magnetic field derived in [6].

6.2.3 Half-Space Problem: Including Hole

E_φ Radiation: For convenience in including the effects of the hole, the fields in the upper-half space region can be rewritten as a product of the far-field of a horizontal dipole in a homogeneous medium and the pattern associated with the rays originating from the source, being transmitted through to the air region, and arriving at the observation point. That is, in the case of the azimuthal electric field component, we can write

$$E_\varphi \sim \left[\frac{j\omega\mu_0 I_0 \ell}{4\pi r} e^{-jkr}\sin\varphi\right]\left[\frac{2ke^{-jh\sqrt{k_2^2-k^2\sin^2\theta}}}{\left\{k\cos\theta+\sqrt{k_2^2-k^2\sin^2\theta}\right\}}\cos\theta\right]$$

To determine the far-zone electric field in the upper-half space when the effects of the hole are considered, we first note that the total E_φ element pattern generated by accounting for additional multipoles has the form

$$e_n^U(\theta_2) = \sum u_n \left(-jk_2\cos\theta_2\right)^n$$

which can be shown to be identical to the lower-half space radiation when the same multipoles are considered. Thus, the element pattern translates directly from the lower-half space region into the upper-half space.

We now examine E_φ in the lower-half space,

$$E_\varphi = -\frac{j}{\omega\varepsilon_2\mu_0}\frac{1}{\rho}\frac{\partial^2}{\partial\varphi\partial z}A_z + \frac{1}{\varepsilon_2}\frac{\partial}{\partial\rho}A_{ez}$$

or, upon substitution,

$$E_\varphi = \frac{1}{\varepsilon_2}\sin\varphi\frac{1}{2\pi\rho}\int_{-\infty}^{\infty}\left\{\left[\frac{k_z}{\omega\mu_0}C_m(k_z) - C_e(k_z)\right]H_1^{(2)}(k_{2\rho}\rho) + C_e(k_z)\,k_{2\rho}\rho H_0^{(2)}(k_{2\rho}\rho)\right\}e^{-jk_z z}dk_z$$

Here we recall the potentials in the lower-half space region,

$$A_z = \cos\varphi\frac{1}{2\pi}\int_{-\infty}^{\infty} C_m(k_z)\,H_1^{(2)}(k_{2\rho}\rho)\,e^{-jk_z z}dk_z\,,\ \rho > a$$

and

$$A_{ez} = \sin\varphi\frac{1}{2\pi}\int_{-\infty}^{\infty} C_e(k_z)\,H_1^{(2)}(k_{2\rho}\rho)\,e^{-jk_z z}dk_z\,,\ \rho > a$$

Using a similar saddle-point procedure to that used to evaluate H_φ^{asym}, in the far-field this becomes

$$E_\varphi^{asym} = \frac{j}{\pi\varepsilon_2}\left(\frac{e^{-jk_2 r}}{r}\right)C_e(k_z^s)\,k_{2\rho}^s\sin\varphi$$

where since this is the field in the lower-half space, $\rho = r\sin\theta_2$. For convenience in comparing to the fields produced from a dipole in a half-space (the fields derived in the previous section), we rewrite the field in the lower region as

$$E_{\varphi}^{asym} = \left[\frac{j\omega\mu_0 I_0 \ell}{4\pi r} e^{-jk_2 r}\sin\varphi\right] C_{h,e}^{'}\left(k_z^s\right)$$

where

$$C_{h,e}^{'}\left(k_z^s\right) = \frac{4}{\omega\mu_0 I_0 \ell \varepsilon_2} C_e\left(k_z^s\right) k_{2\rho}^s$$

Since the pattern behavior captured by the saddle-point coefficient can be represented using a multipole representation (under the restriction that the source is concentrated at a depth h and does not interact with the interface) then, from what has been shown above, this same element pattern is contained in the total upper-half space radiation. Accounting for the effects of the hole and transmission through the interface, we have in the upper-half space

$$E_{\varphi} \sim C_{h,e}^{'}\left(k_z^s\right)\left[\frac{j\omega\mu_0 I_0 \ell}{4\pi r} e^{-jkr}\sin\varphi\right]\left[\frac{2ke^{-jh\sqrt{k_2^2-k^2\sin^2\theta}}}{\left\{k\cos\theta + \sqrt{k_2^2 - k^2\sin^2\theta}\right\}}\cos\theta\right] \tag{13}$$

E_{φ} Results: As was done with the dipole oriented in the vertical direction, the dependence of the transmitted energy into the upper-half space region on the antenna frequency and the characteristics of the earth is demonstrated by evaluating the radiated fields at 300 MHz and 3.0 GHz for soils of various moisture contents. As was done previously, the hole was assumed to have a radius of 0.04 m and the dipole was assumed to be located a distance of 10 m from the air-earth interface. From [1], the relative permittivities of dry sand were taken to be $2.55(1 - j0.01)$ and $2.55(1 - j0.0062)$, while those for the sand with a 2.18% moisture were taken as $2.5(1 - j0.026)$ and $2.5(1 - j0.03)$ at 300 MHz and 3.0 GHz, respectively. The normalized E_{φ} component of radiation for these cases are shown in Figures 19 and 20, where the normalization is given by

$$E_{\varphi}^{norm} = \frac{4\pi r}{(I_o \ell)\, e^{-jkr}} E_{\varphi}$$

In Figure 21, the azimuthal component of the electric field (with the same normalization) is shown for sand with moisture levels of 3.88% ($\varepsilon_r = 4.5\,(1 - j0.03)$) and 16.8% ($\varepsilon_r = 20.0\,(1 - j0.03)$) at 300 MHz [1]. It is important to note that all these radiation patterns are shown for the H-plane ($\varphi = 90°$). As in the case of the vertical dipole, the frequency 3.0 GHz is omitted since with these levels of moisture content, the conductive losses are high enough so that virtually all of the field is dissipated into the sand and very little is transmitted into the air region.

Reviewing the far-field patterns, we observe very similar behavior to what was found when the dipole was oriented vertically within the hole. As before, we find that less energy is transmitted into the air region when the frequency or the conductivity of the earth is increased, with the earth conductivity having more of an effect at higher frequencies.

H_{φ} Radiation: As was done in the evaluation of E_{φ}, we rewrite the half-space magnetic field as a product of the far-field of a horizontal dipole in a homogeneous medium and the pattern associated with the transmission of rays through the air-earth interface and arriving at the observation point. Referring to the magnetic field above, we can also write

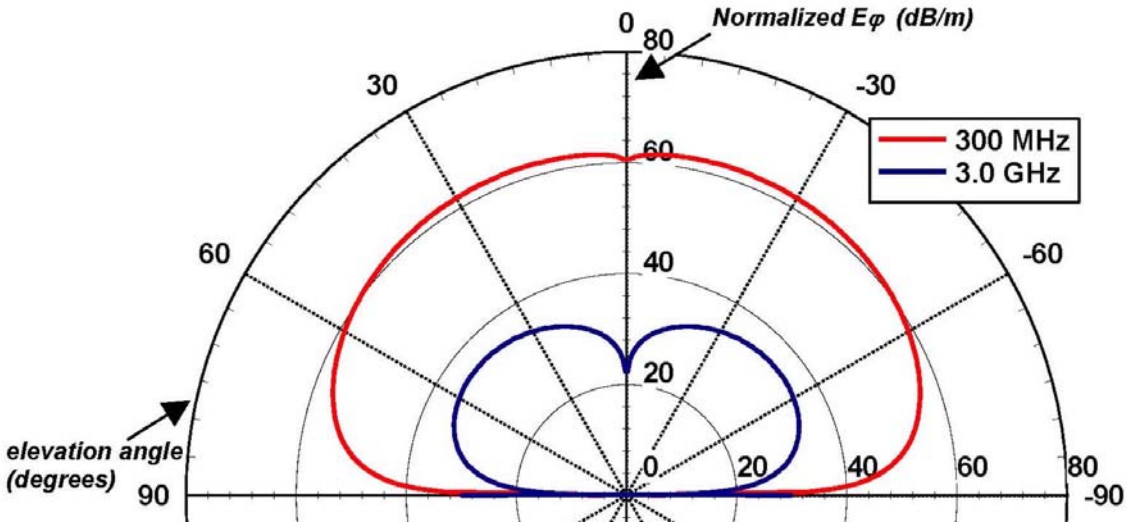

Figure 19. Far-zone H-plane electric field patterns produced in the air region by a horizontal dipole positioned in a hole contained in dry sand ($a = 0.04\ m$).

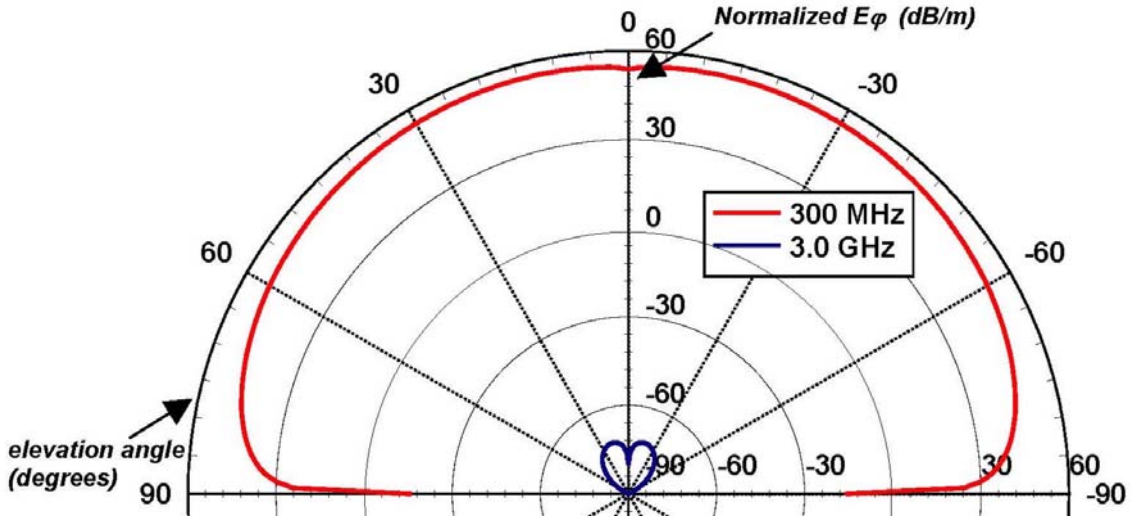

Figure 20. Far-zone H-plane electric field patterns produced in the air region for a horizontal dipole positioned in a hole contained in sand of 2.18% moisture content.

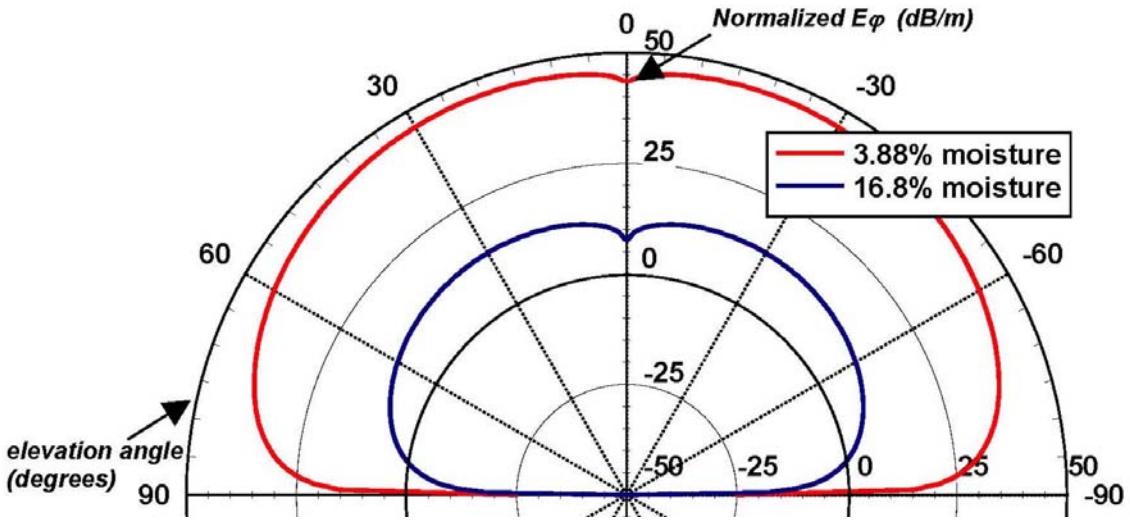

Figure 21. Far-zone H-plane electric field patterns produced in the air region for a horizontal dipole positioned in a hole contained in sand of various moisture contents at 300 MHz ($a = 0.04\ m$).

$$H_\varphi \sim \left[-\frac{j\left(I_0\ell\right)k_2}{4\pi r}e^{-jkr}\cos\theta_2\cos\varphi\right]\left[\frac{2k^2e^{-jh\sqrt{k_2^2-k^2\sin^2\theta}}\cos\theta}{k\sqrt{k_2^2-k^2\sin^2\theta}+k_2^2\cos\theta}\right]$$

where

$$k_2\sin\theta_2 = k\sin\theta$$

$$k_2\cos\theta_2 = \sqrt{k_2^2-k^2\sin^2\theta}$$

To account for the effects of the hole, we recall that the asymptotic form of the field in the lower-half space (found from the analysis in a previous subsection) was given by

$$H_\varphi^{asym} \sim \frac{-j}{\pi\mu_0}\left(\frac{e^{-jk_2r}}{r}\right)C_m\left(k_z^s\right)k_{2\rho}^s\cos\varphi$$

which, in spherical coordinates can be written as

$$H_\varphi^{asym} \sim \left[\frac{-jI_0\ell}{4\pi r}e^{-jk_2r}\cos\varphi\right]\left[\frac{4}{\mu_0 I_0\ell}C_m\left(k_z^s\right)k_{2\rho}^s\right]$$

or, for convenience,

$$H_\varphi^{asym} \sim \left[\frac{-jI_0\ell k_2}{4\pi r}e^{-jk_2r}\cos\theta_2\cos\varphi\right]C_{h,h}^{'}\left(k_z^s\right)$$

where

$$C_{h,h}^{'}\left(k_z^s\right) = \frac{4}{\mu_0 I_0\ell k_2\cos\theta_2}C_m\left(k_z^s\right)k_{2\rho}^s$$

and the coefficients $C_e\left(k_z^s\right)$ and $C_m\left(k_z^s\right)$ have been defined previously. Thus, using the result from the half-space problem and the argument of multipoles (as done previously), the far-zone magnetic field including the effects of the hole can be written as

$$H_\varphi \sim C_{h,h}^{'}\left(k_z^s\right)\left[-\frac{j\left(I_0\ell\right)k_2}{4\pi r}e^{-jkr}\cos\theta_2\cos\varphi\right]\left[\frac{2k^2e^{-jh\sqrt{k_2^2-k^2\sin^2\theta}}\cos\theta}{k\sqrt{k_2^2-k^2\sin^2\theta}+k_2^2\cos\theta}\right] \tag{14}$$

H_φ Results: Using the same parameters as those used in the evaluation of E_φ, the corresponding far-zone H_φ radiation patterns in the air region are shown in Figures 22-24. In this case, the patterns are shown for the $E-$plane and have normalized according to

$$H_\varphi^{norm} = \frac{4\pi r}{\left(I_o\ell\right)e^{-jkr}}\eta H_\varphi$$

As one would expect, we obtain very similar behavior to the previous electric field patterns, with, in fact, the loss in field levels in each of the different cases being approximately the same as the corresponding

case for the azimuthal electric field. Thus, based on the results for the horizontal (as well as the vertical dipole), we conclude that in order to obtain measurable signals in the far-zone of the upper-air half space and, correspondingly not dissipate most of the signal within the sand, it is generally necessary to reduce the frequency. (The exception here is the case of very low-loss dry sand).

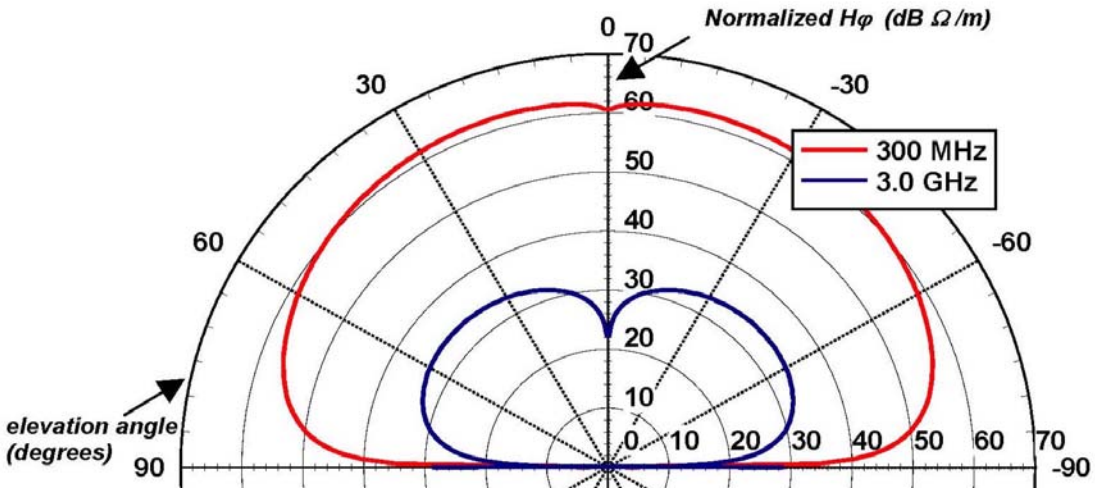

Figure 22. Far-zone E-plane magnetic field patterns produced in the air region by a horizontal dipole positioned in a hole contained in dry sand ($a = 0.04\ m$).

7 Analysis Summary

By examining the upper-half space radiation patterns each characterizing a vertical and horizontal electric dipole located within a hole in the earth, we have found that, in general, simple element factor modifications to the well-known upper-half space result for a dipole in a homogeneous half-space [6] can be made to account for the effects of the hole. The simple closed-form results account for the radiation contribution through the earth and can be easily adjusted to include vertical layering throughout the earth region (although not done so in this analysis).

In the case of the vertical dipole, simple design formulas for the guided-mode attenuation within the hole have been provided. With this formula the attenuation associated with a given frequency and given hole size can be readily obtained and the design tradeoffs can be easily identified (for example, an increase in measured signal level at the top of the hole requires an increase in hole diameter). The same asymptotic methods used to realize the guided-mode attenuation associated with the vertical dipole can be used for the horizontal dipole, although the details are more complicated. At this time, this analysis is left for future work.

8 Conclusions

Relative to a perfectly-electrically conducting waveguide, the diameter of a hole within the earth must be increased to obtain reasonable signals levels at the top of the hole, for the same waveguiding mode of propagation. Furthermore, for the same signal level, the increase in the hole diameter increases as the permittivity of the soil decreases or, equivalently, as the moisture content of the soil decreases.

Due to the high losses associated with propagation through the earth at high frequencies, one solution to obtaining measurable signals at the top of the hole would be to use higher frequencies (e.g. millimeter

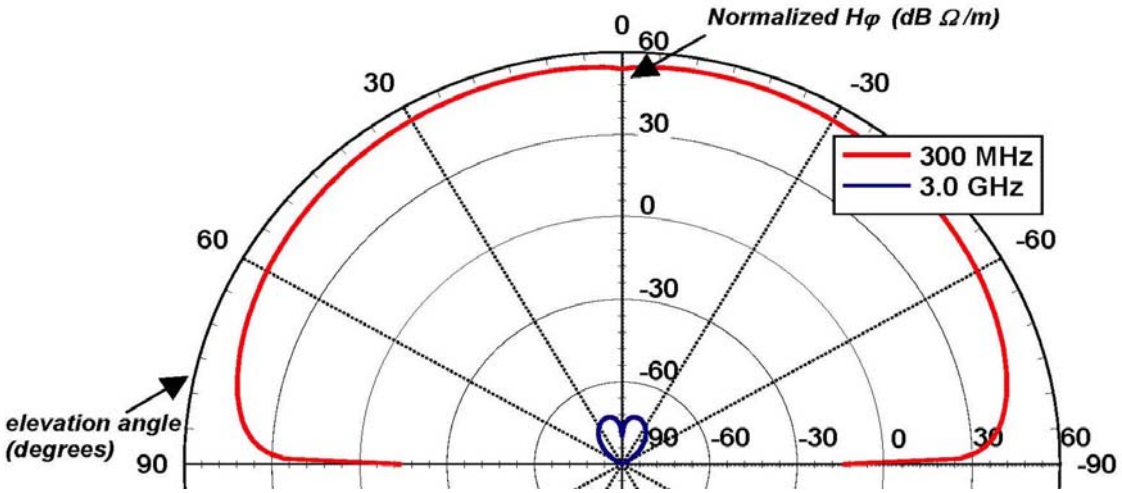

Figure 23. Far-zone E-plane magnetic field patterns produced in the air region for a horizontal dipole positioned in a hole contained in sand of 2.18% moisture content ($a = 0.04\ m$).

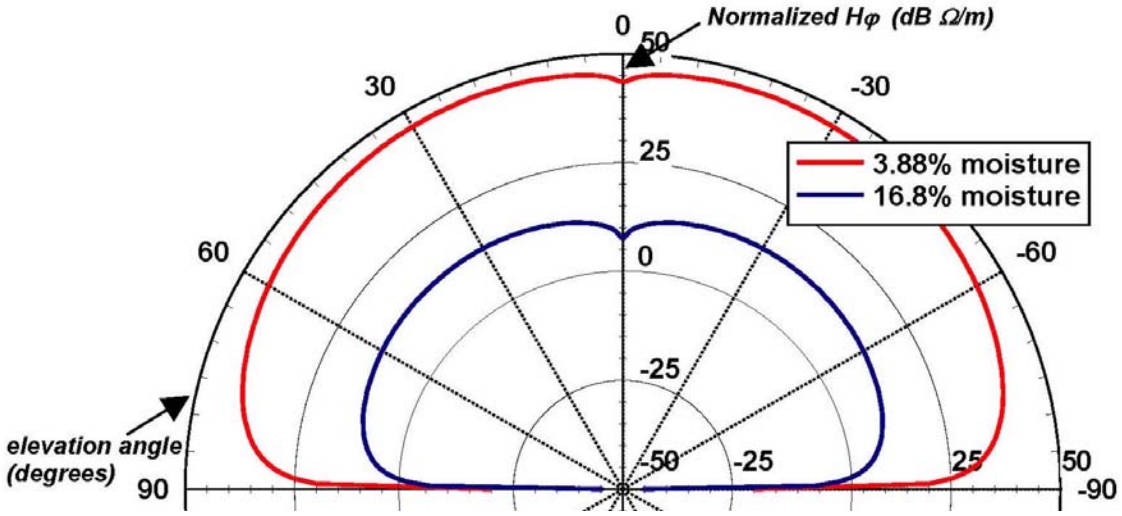

Figure 24. Far-zone E-plane magnetic field patterns produced in the air region for a horizontal dipole positioned in a hole contained in sand of various moisture contents at 300 MHz.

band frequencies) and, correspondingly, a highly directive beam. In this way, the number of reflections off the wall boundary are minimized, less energy is dissipated into the lossy soil, and reasonable signal levels could be measured at the interface. However, we note that this is only a valid solution if no backfill is introduced into the cylindrical hole during the measurement. The case of backfill would lead to extremely large attenuation at these very high frequencies (a much more severe case than when dealing with wavelengths on the order of the hole diameter).

However, instead of relying on the hole as a waveguiding structure, perhaps a better solution would be to use lower frequencies and direct radiation through the earth. In this situation, the electrical dimensions of the hole become negligible and consequently the entire problem can be treated as if the hole does not exist. Here it may be appropriate to use magnetic dipoles or loop antennas for efficiency reasons. As done in this analysis, the magnetic dipoles in the earth-air half space problem can be easily represented by an integral transform solution (which also applies to vertically layered media), which can then be asymptotically evaluated to find the far-zone fields in the air region.

9 Appendix A: Branch Structure

The definition of the branch cuts used throughout this analysis is discussed in this section. First the branch cut from k is given by

$$k_\rho = \sqrt{k^2 - k_z^2} = \sqrt{k - k_z}\sqrt{k + k_z}$$

where

$$\mathrm{Im}\,(k_\rho) \leq 0$$

The complex $k-$plane is shown in Figure 25.

$$k_\rho = \sqrt{|k - k_z|}\sqrt{|k + k_z|}e^{j(\theta_+ + \theta_-)/2}$$

$$-\pi < (\theta_+ + \theta_-)/2 < 0$$

Due to the restricted range of the square root in the cut plane, we do not cross the branch cut of the Hankel function.

In order to use the intrinsic function CSQRT(kz) in the fourth quadrant we must redefine

$$\sqrt{k - k_z} \to e^{-j\pi/2}\sqrt{k_z - k} = -j\sqrt{k_z - k}$$

where

$$-\pi < \arg\,(k_z - k) \leq 0$$

We can use the intrinsic function for $\sqrt{k + k_z}$ in the fourth quadrant without redefining the square root of this factor.

Noting that

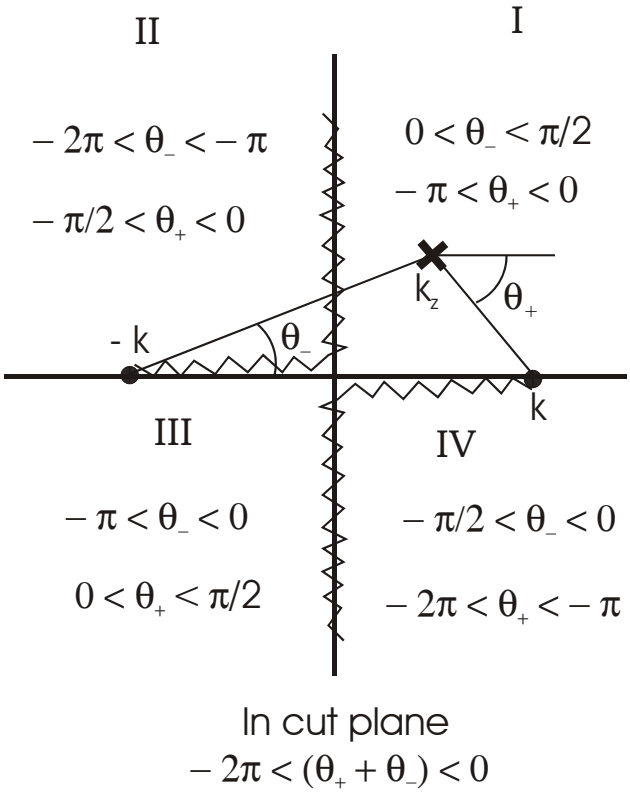

Figure 25. Definition of k_ρ square root function in cut plane.

$$k_2 = k_2' + jk_2'' \ , \ k_2' > 0 \ , \ k_2'' < 0$$

and

$$k_z = k_z' + jk_z''$$

then the square root function

$$k_{2\rho} = \sqrt{k_2^2 - k_z^2}$$

having

$$\mathrm{Im}\,(k_{2\rho}) \leq 0$$

has the deformed branch cuts shown in Figure 25 satisfying

$$k_2' k_2'' = k_z' k_z''$$

The definition above used on the k_2 cut gives

$$\sqrt{k_2 - k_z} \to e^{-j\pi/2}\sqrt{k_z - k_2} = -j\sqrt{k_z - k_2}$$

where

$$-\pi < \arg\,(k_z - k_2) \leq 0$$

Thus this moves the cut so it proceeds to the left of k_2. This definition using CSQRT() is suitable for searching above, to the right of, and below the branch point at k_2. We can rotate the cut so it proceeds downward from the branch point k_2 by writing

$$\sqrt{k_2 - k_z} \to e^{-j\pi/2 + j\pi/4}\sqrt{e^{-j\pi/2}\,(k_z - k_2)} = (1-j)\,\sqrt{-j\,(k_z - k_2)\,/2}$$

This form is suitable for searching to the left of, above, and to the right of the branch point at k_2. Thus, between the two definitions we can search all regions about the branch point in the fourth quadrant. Of course, we must also check where the poles lie with respect to the actual physical cut location. The branch point at $-k_2$ or the function $\sqrt{k_2 + k_z}$ can be implemented directly with the intrinsic FORTRAN function CSQRT() in the fourth quadrant.

10 Appendix B: Magnetic Current Contribution

In this section we consider the contribution of the magnetic current on the interface to the total radiation in the upper-half space region for the case of the horizontal dipole. For this analysis we consider only the low-frequency situation since we have found that very little energy makes it out of the hole and into the air region for the higher frequencies.

Thus, the problem we examine is the 2D static problem of a uniform transverse field $\underline{E}_0 = \underline{e}_x E_0$ in

a medium ε interacting with a cylindrical hole of radius a filled with free space ε_0. The actual far field of the source in the lower medium is propagating along the hole direction with wavenumber k_2 and has a static distribution in the transverse direction. Of course, there will in general be some 3D fringing at the opening of the hole; however, we are neglecting this effect in this simple analysis. The magnetic properties are continuous so it is the electric field perturbation we are concerned with here. Based upon

$$\underline{E} = -\nabla\phi$$

the solution can be found using the potential

$$\phi = -E_0\rho\cos\varphi - \frac{A}{\rho}\cos\varphi\ ,\ \rho > a$$

$$= -B\rho\cos\varphi\ ,\ \rho < a$$

and the displacement vector

$$\underline{D} = \varepsilon\underline{E}$$

Continuity of the potential gives

$$E_0 + A/a^2 = B$$

whereas continuity of the normal displacement gives

$$E_0 - A/a^2 = (\varepsilon_0/\varepsilon)\, B$$

Solving this system of equation, we obtain

$$B = \frac{2\varepsilon}{\varepsilon + \varepsilon_0}E_0$$

$$A/a^2 = \frac{\varepsilon - \varepsilon_0}{\varepsilon + \varepsilon_0}E_0$$

The fields are thus given by

$$E_\rho = E_0\cos\varphi - \frac{a^2}{\rho^2}\frac{\varepsilon - \varepsilon_0}{\varepsilon + \varepsilon_0}E_0\cos\varphi\ ,\ \rho > a$$

$$= \frac{2\varepsilon}{\varepsilon + \varepsilon_0}E_0\cos\varphi\ ,\ \rho < a$$

$$E_\varphi = -E_0\sin\varphi - \frac{a^2}{\rho^2}\frac{\varepsilon - \varepsilon_0}{\varepsilon + \varepsilon_0}E_0\sin\varphi\ ,\ \rho > a$$

$$= -\frac{2\varepsilon}{\varepsilon + \varepsilon_0}E_0\sin\varphi\ ,\ \rho < a$$

Now let us take the difference of these versus the uniform field

$$\Delta E_\rho = -\frac{a^2}{\rho^2}\frac{\varepsilon-\varepsilon_0}{\varepsilon+\varepsilon_0}E_0\cos\varphi\ ,\ \rho > a$$

$$= \frac{\varepsilon-\varepsilon_0}{\varepsilon+\varepsilon_0}E_0\cos\varphi\ ,\ \rho < a$$

$$\Delta E_\varphi = -\frac{a^2}{\rho^2}\frac{\varepsilon-\varepsilon_0}{\varepsilon+\varepsilon_0}E_0\sin\varphi\ ,\ \rho > a$$

$$= -\frac{\varepsilon-\varepsilon_0}{\varepsilon+\varepsilon_0}E_0\sin\varphi\ ,\ \rho < a$$

We define the magnetic currents as twice these values to account for symmetry

$$K_{m\varphi} = 2\frac{a^2}{\rho^2}\frac{\varepsilon-\varepsilon_0}{\varepsilon+\varepsilon_0}E_0\cos\varphi\ ,\ \rho > a$$

$$= -2\frac{\varepsilon-\varepsilon_0}{\varepsilon+\varepsilon_0}E_0\cos\varphi\ ,\ \rho < a$$

$$K_{m\rho} = -2\frac{a^2}{\rho^2}\frac{\varepsilon-\varepsilon_0}{\varepsilon+\varepsilon_0}E_0\sin\varphi\ ,\ \rho > a$$

$$= -2\frac{\varepsilon-\varepsilon_0}{\varepsilon+\varepsilon_0}E_0\sin\varphi\ ,\ \rho < a$$

To determine the amount of radiation produced by this magnetic current, we next find the electric vector potential in the upper half space

$$\underline{D} = -\nabla\times\underline{A}_e$$

$$\varepsilon_0\underline{E} \sim jk\underline{e}_r\times\underline{A}_e$$

$$\underline{A}_e\left(\underline{r}\right) = \frac{\varepsilon_0}{4\pi}\int_V \frac{e^{-jkR}}{R}\underline{J}_m dV'$$

$$= \frac{\varepsilon_0}{4\pi}\int_0^\infty\int_{-\pi}^{\pi}\rho' d\rho' d\varphi'\frac{e^{-jkR}}{R}\underline{K}_m$$

In the far-field, this can be approximated by

$$A_{e\varphi} \sim \frac{\varepsilon}{4\pi}\frac{e^{-jkr}}{r}\int_0^\infty\int_{-\pi}^{\pi}\underline{K}_m e^{jkr'\cdot\hat{r}}\rho' d\rho' d\varphi'$$

where

$$r = \sqrt{\rho^2 + z^2}$$

and

$$r^{'} \cdot \widehat{r} = x^{'} \underline{e}_x + y^{'} \underline{e}_y \cdot \frac{x\underline{e}_x + y\underline{e}_x + z\underline{e}_x}{\sqrt{x^2 + y^2 + z^2}}$$

$$r^{'} \cdot \widehat{r} = \frac{x^{'} x + y^{'} y}{\sqrt{x^2 + y^2 + z^2}}$$

Also

$$r^{'} \cdot \widehat{r} = x^{'} \sin\theta \cos\varphi + y^{'} \sin\theta \sin\varphi$$

or, in cylindrical coordinates,

$$r^{'} \cdot \widehat{r} = \sin\theta \left[\rho' \cos\varphi' \cos\varphi + \rho' \sin\varphi' \sin\varphi\right]$$

$$r^{'} \cdot \widehat{r} = \rho' \sin\theta \cos\left(\varphi - \varphi'\right)$$

Thus

$$\underline{A}_e \left(\underline{r}\right) \sim \frac{\varepsilon_0 e^{-jkr}}{4\pi r} \int_0^{\infty} \int_{-\pi}^{\pi} \rho' d\rho' d\varphi' e^{jk\rho' \sin\theta \cos\left(\varphi - \varphi'\right)} \underline{K}_m$$

where in the far zone

$$\varepsilon_0 \underline{E} \sim jk\underline{e}_r \times \underline{A}_e$$

Substituting,

$$\varepsilon_0 \underline{E} \sim jk \left(\underline{e}_\rho \sin\theta + \underline{e}_z \cos\theta\right) \times \left(A_{e\varphi}\underline{e}_\varphi + A_{e\rho}\underline{e}_\rho\right)$$

where, extracting the magnetic current contribution to the $\varphi-$component of the radiated field (the electric-field component previously calculated for the horizontal dipole case), we obtain

$$\varepsilon_0 E_\varphi \sim jk\underline{e}_z \cos\theta \times A_{e\rho}\underline{e}_\rho$$

$$E_\varphi \sim j\frac{k}{\varepsilon_0} A_{e\rho} \cos\theta$$

where

$$A_{e\rho} \sim \frac{\varepsilon_0 e^{-jkr}}{4\pi r} \int_0^{\infty} \int_{-\pi}^{\pi} \rho' d\rho' d\varphi' K_{m\rho}\ e^{jk\rho' \sin\theta \cos\left(\varphi - \varphi'\right)}$$

Substituting,

$$A_{e\rho} \sim -\frac{\varepsilon_0 e^{-jkr}}{4\pi r}\int_0^a\int_{-\pi}^{\pi} 2\frac{\varepsilon-\varepsilon_0}{\varepsilon+\varepsilon_0}E_0\sin\varphi'\ \rho' d\rho' d\varphi' e^{jk\rho'\sin\theta\cos(\varphi-\varphi')}$$

$$-\frac{\varepsilon_0 e^{-jkr}}{4\pi r}\int_a^{\infty}\int_{-\pi}^{\pi} 2\frac{a^2}{(\rho')^2}\frac{\varepsilon-\varepsilon_0}{\varepsilon+\varepsilon_0}E_0\sin\varphi'\ \rho' d\rho' d\varphi' e^{jk\rho'\sin\theta\cos(\varphi-\varphi')}$$

$$A_{e\rho} \sim -\frac{\varepsilon_0 e^{-jkr}}{4\pi r}2\frac{\varepsilon-\varepsilon_0}{\varepsilon+\varepsilon_0}E_0\left[\int_0^a\int_{-\pi}^{\pi}\sin\varphi'\rho' d\rho' d\varphi' e^{jk\rho'\sin\theta\cos(\varphi-\varphi')}\right.$$

$$\left.+\int_a^{\infty}\int_{-\pi}^{\pi}\frac{a^2}{\rho'}\ \sin\varphi' d\rho' d\varphi' e^{jk\rho'\sin\theta\cos(\varphi-\varphi')}\right]$$

Note that for the integral in φ', we have

$$\int_{-\pi}^{\pi}\sin\varphi' e^{jk\rho'\sin\theta\cos(\varphi-\varphi')}d\varphi' = j2\pi J_1\left(k\rho'\sin\theta\right)\sin\varphi$$

and $A_{e\rho}$ becomes

$$A_{e\rho} \sim -j\frac{\varepsilon_0 e^{-jkr}}{r}\frac{\varepsilon-\varepsilon_0}{\varepsilon+\varepsilon_0}E_0\sin\varphi\left[\int_0^a J_1\left(k\rho'\sin\theta\right)\rho' d\rho'\right.$$

$$\left.+a^2\int_a^{\infty} J_1\left(k\rho'\sin\theta\right)\frac{1}{\rho'}\ d\rho'\right]$$

In order to compute the ρ' integrals, we rewrite $A_{e\rho}$ as

$$A_{e\rho} \sim -j\frac{\varepsilon_0 e^{-jkr}}{r}\frac{\varepsilon-\varepsilon_0}{\varepsilon+\varepsilon_0}E_0\sin\varphi\left[\frac{1}{(k\sin\theta)^2}\int_0^{ka\sin\theta} J_1\left(u\right)u\ du\right.$$

$$\left.+a^2\int_{ka\sin\theta}^{\infty} J_1\left(u\right)\frac{1}{u}\ du\right]$$

or, equivalently,

$$A_{e\rho} \sim -j\frac{\varepsilon_0 e^{-jkr}}{r}\frac{\varepsilon-\varepsilon_0}{\varepsilon+\varepsilon_0}E_0\sin\varphi\left[\frac{1}{(k\sin\theta)^2}\int_0^{ka\sin\theta} J_1\left(u\right)u\ du\right.$$

$$\left.+a^2\left\{\int_0^{\infty} J_1\left(u\right)\frac{1}{u}\ du-\int_0^{ka\sin\theta} J_1\left(u\right)\frac{1}{u}\ du\right\}\right]$$

where we let

$$u = k\rho'\sin\theta$$

$$du = k\sin\theta\ d\rho'$$

This form is convenient for using [4]. Thus,

$$A_{e\rho} \sim -j\frac{\varepsilon_0 e^{-jkr}}{r}\frac{\varepsilon-\varepsilon_0}{\varepsilon+\varepsilon_0}E_0\sin\varphi\left[\frac{1}{(k\sin\theta)^2}\int_0^{ka\sin\theta} J_1(u)\,u\,du\right.$$

$$\left.+a^2\left\{1-\int_0^{ka\sin\theta} J_1(u)\frac{1}{u}\,du\right\}\right]$$

and

$$A_{e\rho} \sim -j\frac{\varepsilon_0 e^{-jkr}}{r}\frac{\varepsilon-\varepsilon_0}{\varepsilon+\varepsilon_0}E_0\sin\varphi\cdot$$

$$\left[\frac{1}{(k\sin\theta)^2}\left\{ka\sin\theta\frac{\Gamma\left(\frac{3}{2}\right)}{\Gamma\left(\frac{1}{2}\right)}\sum_{k=0}^{\infty}\frac{(2+2k)\,\Gamma\left(\frac{1}{2}+k\right)}{\Gamma\left(\frac{5}{2}+k\right)}J_{(2+2k)}(ka\sin\theta)\right\}\right.$$

$$\left.+a^2\left\{1-\frac{1}{ka\sin\theta}\frac{\Gamma\left(\frac{1}{2}\right)}{\Gamma\left(\frac{3}{2}\right)}\sum_{k=0}^{\infty}\frac{(2+2k)\,\Gamma\left(\frac{3}{2}+k\right)}{\Gamma\left(\frac{3}{2}+k\right)}J_{(2+2k)}(ka\sin\theta)\right\}\right]$$

Simplifying,

$$A_{e\rho} \sim -j\frac{\varepsilon_0 e^{-jkr}}{r}\frac{\varepsilon-\varepsilon_0}{\varepsilon+\varepsilon_0}E_0\sin\varphi\cdot$$

$$\left[\frac{1}{(k\sin\theta)^2}\left\{\frac{ka\sin\theta}{2}\sum_{k=0}^{\infty}\frac{(2+2k)\,\Gamma\left(\frac{1}{2}+k\right)}{\Gamma\left(\frac{5}{2}+k\right)}J_{(2+2k)}(ka\sin\theta)\right\}\right.$$

$$\left.+a^2\left\{1-\left\{\frac{2}{ka\sin\theta}\sum_{k=0}^{\infty}(2+2k)\,J_{(2+2k)}(ka\sin\theta)\right\}\right\}\right]$$

$$A_{e\rho} \sim -j\frac{\varepsilon_0 e^{-jkr}}{r}\frac{\varepsilon-\varepsilon_0}{\varepsilon+\varepsilon_0}E_0\sin\varphi\cdot\frac{a}{k\sin\theta}$$

$$\left\{ka\sin\theta+\sum_{k=0}^{\infty}\left[\frac{\Gamma\left(\frac{1}{2}+k\right)}{\Gamma\left(\frac{5}{2}+k\right)}-4\right](1+k)\,J_{(2+2k)}(ka\sin\theta)\right\}$$

Thus, the magnetic current contribution to E_φ is therefore given by

$$E_\varphi^{K_m} \sim \left[E_0 a\frac{e^{-jkr}}{r}\left(\frac{\varepsilon-\varepsilon_0}{\varepsilon+\varepsilon_0}\right)\cot\theta\sin\varphi\right]\cdot$$

$$\left\{ka\sin\theta+\sum_{k=0}^{\infty}\left[\frac{\Gamma\left(\frac{1}{2}+k\right)}{\Gamma\left(\frac{5}{2}+k\right)}-4\right](1+k)\,J_{(2+2k)}(ka\sin\theta)\right\}$$

Also in the far-field

$$\mathbf{H} = -j\omega \mathbf{A}_e$$

so that for the $\varphi-$component of the magnetic field (again the previously calculated component used in evaluating the direct radiation of the horizontal dipole) we have

$$H_\varphi = -j\omega A_{e\varphi}$$

The component of the electric vector potential is given by

$$A_{e\varphi} \sim \frac{\varepsilon_0 e^{-jkr}}{4\pi r} \int_0^\infty \int_{-\pi}^{\pi} K_{m\varphi} \rho' d\rho' d\varphi' e^{jk\rho' \sin\theta \cos(\varphi - \varphi')}$$

where substituting we obtain

$$A_{e\varphi} \sim -E_0 \frac{\varepsilon_0 e^{-jkr}}{2\pi r} \frac{\varepsilon - \varepsilon_0}{\varepsilon + \varepsilon_0} \left[\int_0^a \int_{-\pi}^{\pi} \cos\varphi' \rho' d\rho' d\varphi' e^{jk\rho' \sin\theta \cos(\varphi - \varphi')} \right.$$

$$\left. -a^2 \int_a^\infty \int_{-\pi}^{\pi} \frac{1}{\rho'} \cos\varphi' d\rho' d\varphi' e^{jk\rho' \sin\theta \cos(\varphi - \varphi')} \right]$$

For the φ' integration , we have

$$\int_{-\pi}^{\pi} \cos\varphi' e^{jk\rho' \sin\theta \cos(\varphi - \varphi')} d\varphi' = j2\pi J_1 (k\rho' \sin\theta) \cos\varphi$$

so

$$A_{e\varphi} \sim -j \frac{\varepsilon_0 e^{-jkr}}{r} \frac{\varepsilon - \varepsilon_0}{\varepsilon + \varepsilon_0} E_0 \cos\varphi \left[\int_0^a \rho' J_1 (k\rho' \sin\theta) \, d\rho' \right.$$

$$\left. -a^2 \int_a^\infty \frac{1}{\rho'} J_1 (k\rho' \sin\theta) \, d\rho' \right]$$

Again letting

$$u = k\rho' \sin\theta$$

$$du = k \sin\theta \; d\rho'$$

we have

$$A_{e\varphi} \sim -jE_0 \frac{\varepsilon_0 e^{-jkr}}{r} \frac{\varepsilon - \varepsilon_0}{\varepsilon + \varepsilon_0} \cos\varphi \left[\frac{1}{(k \sin\theta)^2} \int_0^{ka \sin\theta} u J_1 (u) \, du \right.$$

$$\left. -a^2 \int_{ka \sin\theta}^\infty \frac{1}{u} J_1 (u) \, du \right]$$

Using a similar method used to evaluate $A_{e\rho}$, $A_{e\varphi}$becomes

$$A_{e\varphi} \sim -jE_0 \frac{\varepsilon_0 e^{-jkr}}{r} \frac{\varepsilon - \varepsilon_0}{\varepsilon + \varepsilon_0} \cos\varphi \cdot \frac{a}{k \sin\theta}$$

$$\left[-ka \sin\theta + \sum_{k=0}^{\infty} \left[\frac{\Gamma\left(\frac{1}{2} + k\right)}{\Gamma\left(\frac{5}{2} + k\right)} + 4 \right] (1+k) \, J_{(2+2k)} \left(ka \sin\theta\right) \right]$$

Thus,

$$H_{\varphi}^{K_m} = E_0 \omega a \frac{\varepsilon_0 e^{-jkr}}{r} \frac{\varepsilon - \varepsilon_0}{\varepsilon + \varepsilon_0} \cos\varphi \frac{1}{k \sin\theta} \cdot$$

$$\left[ka \sin\theta - \sum_{k=0}^{\infty} \left[\frac{\Gamma\left(\frac{1}{2} + k\right)}{\Gamma\left(\frac{5}{2} + k\right)} + 4 \right] (1+k) \, J_{(2+2k)} \left(ka \sin\theta\right) \right]$$

Here we note that the magnetic current contribution to both the electric and magnetic field is presented in terms of a normalization constant E_0. For this analysis, E_0 is taken as the field in the lower half space region (evaluated at the interface) modified by the Fresnel reflection coefficient to account for the mismatch at the air/conducting half-space boundary. Thus,

$$E_0 = \left[\frac{2\sqrt{\varepsilon}}{\sqrt{\varepsilon} + \sqrt{\varepsilon_0}} \right] E_x|_{z=h, \rho=a}$$

where E_x can be found through Maxwell's equations and the magnetic field analysis for H_φ presented in *Section 4.1.* We recall that in this section both saddle-point and numerical results were presented, with the most discrepancy in the lower-half space fields occurring at $\rho = a$. For the determination of E_0 we choose to normalize with respect to the saddle-point fields, which have higher levels at the hole boundary, and thereby, if anything, *overestimate* the effects of the magnetic current contribution. Thus, in the results that follow, it is important to keep in mind that a very conservative approach has been taken so as not to weaken the effects of the magnetic current at the interface.

In order to demonstrate the dominance of the direct dipole radiation relative to the magnetic current contribution, the normalized azimuthal component of the electric and magnetic field are shown in Figs. 26 and 27. Here two cases of sand moisture content are included (dry and 3.88% moisture) at 300 MHz. Thus, it is evident that the upper half-space radiation accounting for the discontinuity in the electric field at the interface is nearly indistinguishable from the results including only the direct dipole radiation and, for practical purposes, the magnetic current at the interface can be neglected. This same behavior is observed at 3.0 GHz, as shown in Figs. 28 and 29. Here only the case of dry sand is examined, since the levels of radiation in the upper half-space region at this high of a frequency are extremely low in the more conductive sand situations.

References

[1] A. Von Hippel, **Dielectric Materials and Applications**, Cambridge: Technology Press of MIT, 1954, p. 314.

[2] B.K. Singaraju, D.B. Giri, C.E. Baum, Air Force Weapons Lab Notes #42, March 1976.

[3] W.L. Weeks, Electromagnetic Theory for Engineering Applications, Wiley & Sons, New York, 1964, pp. 246-258.

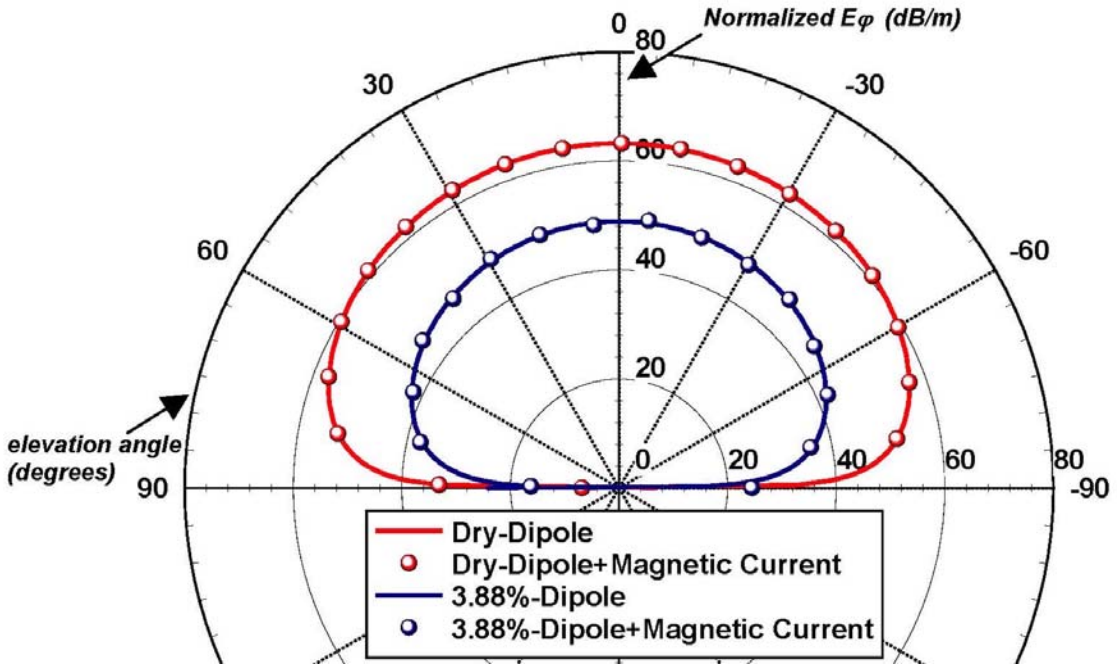

Figure 26. Far-zone E-plane electric field patterns produced in the air region by a horizontal dipole positioned in a hole of 0.04 m radius (300 MHz).

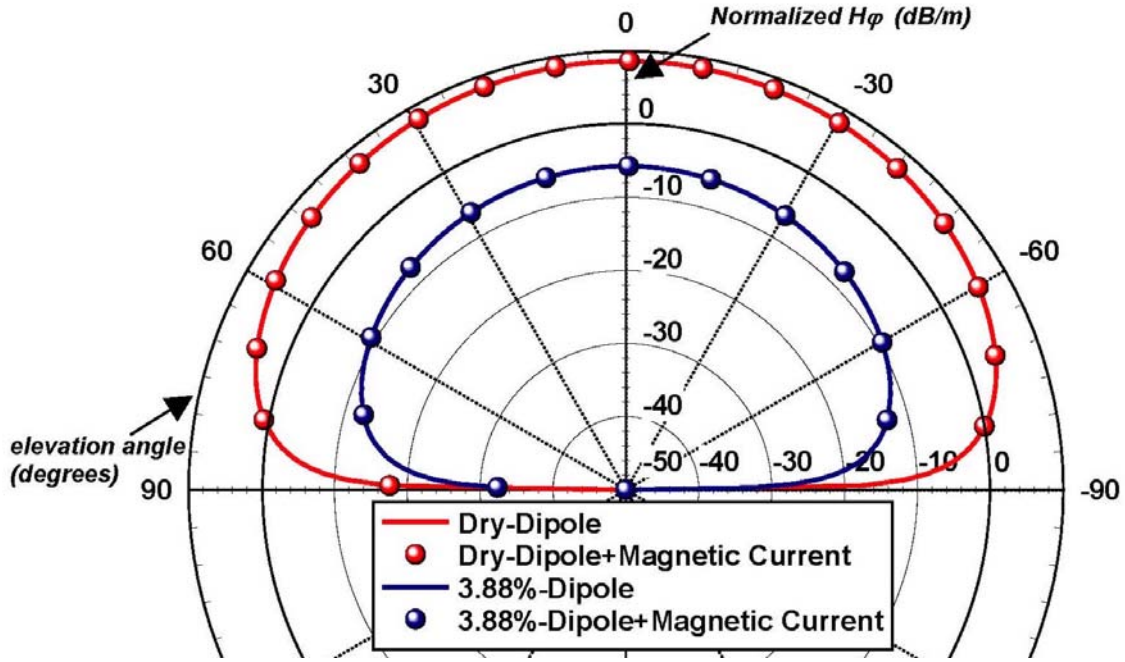

Figure 27. Far-zone E-plane magnetic field patterns produced in the air region by a horizontal dipole positioned in a hole of 0.04 m radius (300 MHz).

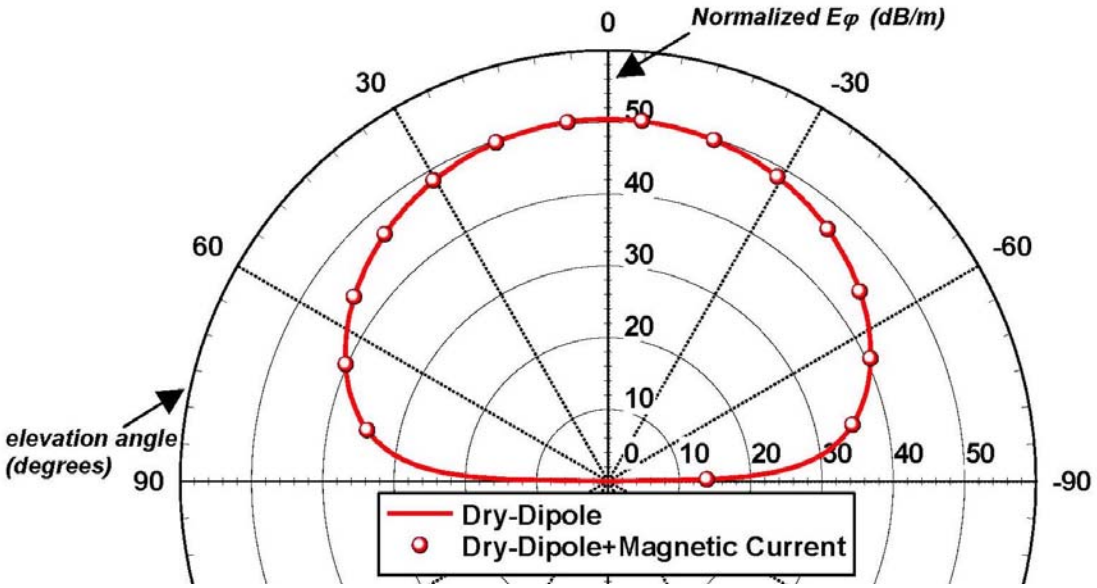

Figure 28. Far-zone E-plane magnetic field patterns produced in the air region by a horizontal dipole positioned in a hole of radius 0.04 m (3.0 GHz).

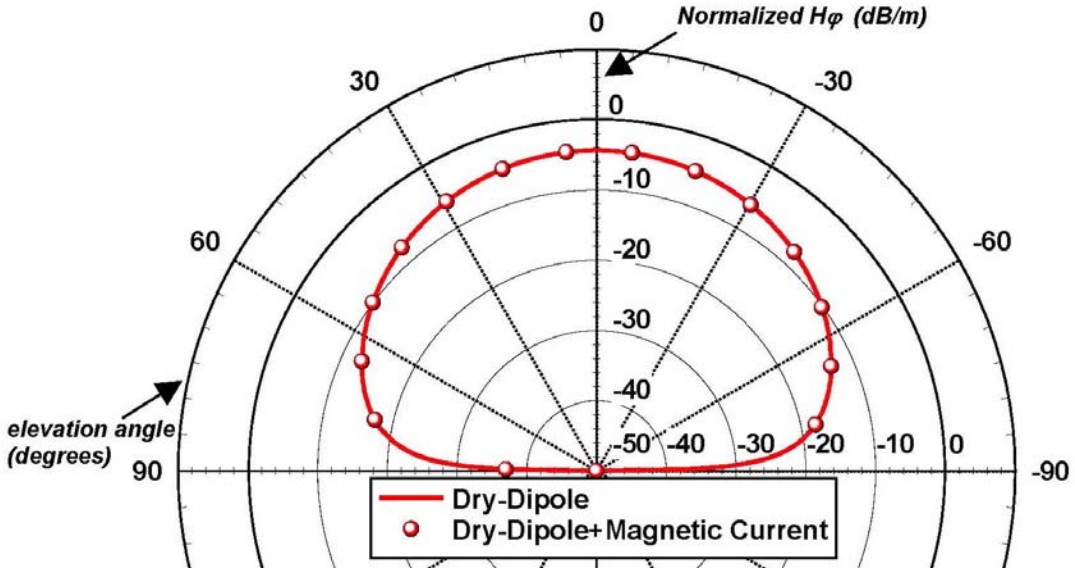

Figure 29. Far-zone E-plane magnetic field patterns produced in the air region by a horizontal dipole positioned in a hole of 0.04 m radius (3.0 GHz).

[4] M. Abramowitz and I.A. Stegun, **Handbook of Mathematical Functions with Formulas, Graphs, and Mathematical Tables**, New York, Dover Publications, 1965.

[5] G.B. Arfken and H.J. Weber, **Mathematical Methods for Physicists**, San Diego, Ca: Academic Press, 1995.

[6] A. Baños, Jr., **Dipole Radiation in the Presence of a Conducting Half-Space**, New York: Pergamon Press, 1966.

[7] R. W. P. King, G. S. Smith, M. Owens, and T. T. Wu, **Antennas in Matter**, Cambridge, MA: MIT Press, 1981.

[8] R. W. P. King, M. Owens, and T. T. Wu, **Lateral Electromagnetic Waves**, New York: Springer-Verlag, 1992.

[9] A. Sommerfeld, **Partial Differential Equations in Physics**, New York: Academic Press, 1949.

Distribution:

1 ITT Industries/AES
Attn: K. S. H. Lee
1033 Gayley Avenue
Suite 215
Los Angeles, CA 90024

10	MS1152	L. I. Basilio, 01652
10	MS1152	L. K. Warne, 01642
10	MS1152	W. A. Johnson, 01652
1	MS1152	R. J. Mariano, 09042
1	MS1152	M. T. Oswald, 02621
1	MS1152	R. J. Punnoose, 08235
1	MS1152	M. A. Foreman, 08774
1	MS1152	M. L. Kiefer, 01642
1	MS1152	R. E. Jorgenson, 01652
1	MS1194	L. X. Schneider, 01643
1	MS1194	M. E. Morris, 01642
1	MS0405	K. O. Merewether, 12333
1	MS0492	K. C. Chen, 12332
1	MS9018	Central Technical Files, 8945-1
2	MS0899	Technical Library, 09616